International Journal of Photoenergy

Solar Energy in Local Energy Communities: Transition to a Sustainable Energy System

Lead Guest Editor: Anna Pinnarelli
Guest Editors: Marialaura Di Somma and Angel A. Bayod-Rújula

Solar Energy in Local Energy Communities: Transition to a Sustainable Energy System

International Journal of Photoenergy

Solar Energy in Local Energy Communities: Transition to a Sustainable Energy System

Lead Guest Editor: Anna Pinnarelli
Guest Editors: Marialaura Di Somma and Angel A. Bayod-Rújula

Chief Editor

Academic Editors

Contents

Analysis of the Power Cloud Framework Benefits and the Role of the City Energy Provider in the New Italian Electricity Tariff Scenario
D. Menniti, A. Pinnarelli, N. Sorrentino, G. Brusco, L. Mendicino, and M. Mercuri
Research Article (14 pages), Article ID 3605498, Volume 2020 (2020)

An Advanced Multicarrier Residential Energy Hub System Based on Mixed Integer Linear Programming
Yue Yuan, Angel A. Bayod-Rújula, Huanxin Chen, Amaya Martínez-Gracia, Jiangyu Wang, and Anna Pinnarelli
Research Article (12 pages), Article ID 1384985, Volume 2019 (2019)

Development of a Daily Databank of Solar Radiation Components for Moroccan Territory
Mohammed Benchrifa, Hajar Essalhi, Rachid Tadili, Mohammed N. Bargach, and Abdellah Mechaqrane
Research Article (20 pages), Article ID 6067539, Volume 2019 (2019)

Line-End Voltage and Voltage Profile along Power Distribution Line with Large-Power Photovoltaic Generation System
Toshiro Matsumura, Masumi Tsukamoto, Akihiro Tsusaka, Kazuto Yukita, Yasuyuki Goto, Yasunobu Yokomizu, Kento Tatewaki, Daisuke Iioka, Hirotaka Shimizu, Yuuki Kanazawa, Hiroyuki Ishikawa, Akimori Matsuo, and Hideki Iwatsuki
Research Article (8 pages), Article ID 1263480, Volume 2019 (2019)

Hindawi
International Journal of Photoenergy
Volume 2020, Article ID 3605498, 14 pages
https://doi.org/10.1155/2020/3605498

Research Article

Analysis of the Power Cloud Framework Benefits and the Role of the City Energy Provider in the New Italian Electricity Tariff Scenario

D. Menniti, A. Pinnarelli, N. Sorrentino, G. Brusco, L. Mendicino, and M. Mercuri

Department of Mechanical, Energy and Management Engineering (DIMEG), University of Calabria, Via Bucci 42C, Arcavacata di Rende-CS, Italy

Correspondence should be addressed to L. Mendicino; luca.mendicino@unical.it

Received 2 April 2019; Revised 12 September 2019; Accepted 29 November 2019; Published 18 January 2020

Academic Editor: Fabio Bisegna

The need to consume less and better energy pushes more and more to find efficient solutions at the individual end-user and community levels. The concept of an energy community is becoming increasingly popular, and recently, many studies try to demonstrate how an aggregation of end-users, which produces energy according to a distributed generation concept, is a mechanism able to overcome the increasingly tight constraints imposed by the electricity market, both for the end-user and for the network and market operators. In this context, the paper is aimed at verifying the convenience for both end-user and aggregator sides to operate in an aggregate form considering the new tariff scenario imposed in some European countries like Italy.

1. Introduction

It is well known that new technologies have obvious benefits on electricity consumption and savings achieved by the end-users. In particular, it has been analysed in [1] how the end-users with enabling technologies such as a nanogrid for home application (nGfHA) have the possibility to interconnect domestic loads, renewable energy source (RES) plant, and storage systems obtaining a double benefit. On the one hand, the savings achievable in the annual electricity bill result from decreased consumption; on the other hand, the social advantage results from participation in a possible energy community managed by an entity who covers the role of an aggregator defined as a *community energy provider* (CEP) [2].

The recent reforms undertaken by the Italian Authority (AEEGSI), such as the reform of the electrical dispatching (RDE) which started with the deliberation 393/2012/R/eel, put as its central topic the full integration of renewable sources in the energy service market, the changes to the electrical dispatching [3], the regulation of energy imbalances [4], and the new tariff (DT) for end-users, as reported in [5, 6]. It has undoubtedly influenced the electricity market, the operators, and the actual technologies and also the introduction of new operators as the *aggregators*.

This redefinition of the electricity market has influenced both the possible activities performed by these new operators and the economic convenience for the end-users to install technologies able to reduce the energy consumption. For this reason, in the paper, an aggregation representing an energy community managed by a CEP, defined by the authors as Power Cloud [1], is considered. Several studies have been performed which led to the definition of an optimization model to evaluate the economic convenience of the Power Cloud framework in the view of new regulation changes' introduced in the electricity market. In particular, it has tried to define (if possible) the aggregation size so that there is a convenience for the CEP and for each single end-user who decides to aggregate, comparing the Italian tariff scenario of 2016 with the one of 2017.

The paper is structured as follows.

In the first part, the optimization model proposed for the valuation of the Power Cloud optimal size is illustrated. The second part shows the most significant case studies demonstrating that an economic convenience of adopting the Power Cloud model is still possible even in the new tariff scenario that would not seem to incentivise the self-consumption and so the PV plant installation.

2. The CEP Optimization Model

Different types of users such as the consumer, prosumers, and producers can coexist in an aggregation. In the paper, the aim is to incentivise the increase of renewable energy sources (RES) and enable technologies to improve a better power management of energy resources. It is assumed that all end-users, participating in the Power Cloud, will be equipped with RES plants and enable technology configuring all the aggregated end-users as prosumers [7]. The community energy provider (CEP) manages the aggregation. In addition, it will refer to the Italian electricity market context.

The goal of the CEP optimization model is to evaluate the optimal Power Cloud size that maximizes the economic benefit of all involved actors, CEP and the end-user considered as a customer (a residential domestic user with an installed power equal to 3 kW). In detail, the CEP will achieve an economic profit ($\text{CEP}_{\text{Profit}}$) as the maximum difference between its revenues and operating costs. At the same time, the end-user achieves the maximum profit ($\text{User}_{\text{Profit}}$) as the maximum difference between the amount previously paid for the annual electricity bill (before joining the Power Cloud) and the amount that it will pay in case it is joined in the Power Cloud. The CEP optimization model is so formulated as follows:

$$\text{Max}(\text{Aggregation Economic Benefit}), \tag{1}$$

where $\text{Aggregation Economic Benefit} = \text{CEP}_{\text{Profit}} + \text{User}_{\text{Profit}}$ is the Power Cloud benefit for both, CEP and the end-users; $\text{CEP}_{\text{Profit}} = \text{Revenues}_{\text{CEP}} - \text{Costs}_{\text{CEP}}$ is the CEP profit, and $\text{User}_{\text{Profit}} = \text{Annual electricity bill (not aggregated end-user)} - \text{Annual electricity bill}_{\text{CEP}}(\text{Aggregated end-user})$ is the benefit achieved by the end-user.

In the following, each single quantity will be defined and analysed.

2.1. CEP Profit. Let us start with the analysis of the CEP profit. It is defined as the difference between the management costs ($\text{Costs}_{\text{CEP}}$) and revenues ($\text{Revenues}_{\text{CEP}}$).

$\text{Costs}_{\text{CEP}}$ represents all costs incurred by the CEP for the Power Cloud operating management. These costs are due to the Energy Market Operator (in Italy, GME (Within the Italian electricity market, the GME (Gestore dei Mercati Energetici) is the Energy Market Operator who organizes and manages the wholesale electricity market since the liberalization of the energy sector. On the electricity market managed by GME (also known as Italian Power Exchange (IPEX)), producers and buyers sell and buy electricity wholesale.)) for using the energy exchange platform (PCE) (Exchange energy platform in the Italian electricity market refers to the PCE (Piattaforma Conti Energia) managed by the Energy Market Operator (GME). PCE is used for recording transactions concluded "over the counter." On this platform, parties that have concluded contracts outside IPEX record their commercial obligations and the related electricity input and withdrawal energy programs which they undertake to carry out in compliance with these contracts.), the costs and guarantees owed to the national Transmission System Operator (TSO; in Italy, *Terna* (Terna S.p.A. represents the Transmission System Operator, and it is the owner of the Italian National Transmission Grid. It operates under a natural monopoly regime (so it is the only operator in Italy for the management of the transmission grid) and carries out a public service mission for the transmission and dispatching of electricity across the country. 90% of its activity takes place in the regulated market. The role is essential for the functioning of the entire system and to ensure electricity for citizens and businesses.)), costs for guarantees due to the Distributor System Operator (DSO) and excise duties on electricity due to the Customs Agency Authority [8], and finally operating expenses related to the management service performed by the CEP.

$\text{Costs}_{\text{CEP}}$ is so defined as

$$\text{Costs}_{\text{CEP}} = C_{\text{PowExcOp}} + C_{\text{TSO}} + C_{\text{DSO}} + C_{\text{Taxes}} + C_{\text{ServCEP}}, \tag{2}$$

where C_{PowExcOp} represents the cost to register energy injection and draw of schedule on PCE. C_{PowExcOp} is so defined as

$$C_{\text{PowExcOp}} = C_{\text{Plat}} + \text{Fee}_{\text{Plat}} + \text{CCT}, \tag{3}$$

where C_{Plat} is a fixed cost charged "una tantum"; Fee_{Plat} are the variable fees, which need to be paid according to the electricity schedule registered on PCE; and CCT represents the difference between the single national price defined as PUN, which is a reference for the energy purchase in the Italian electricity market and zonal price (P_z) that is a reference of sale price for the energy sold in the area where a production plant is located. In particular, it has been assumed that

(i) $C_{\text{Plat}} = 1000.00€^{*}$

(ii) $\text{Fee}_{\text{Plat}} = 0.008^{**}\,\text{ExEn}_{\text{Inj}} + 0.008 * \text{ExEn}_{\text{Drw}}$

(iii) $\text{CCT} = (\text{PUN} - P_z) * \text{ExEn}_{\text{Inj}}$

*The access fee in PCE (*una tantum*) is equal to 1000.00€.
**Fee per MWh exchanged and registered amounts to 0.008 €/MWh—http://www.mercatoelettrico.org/It/Mercati/PCE/CorrispettiviPCE.aspx.

where

$$\text{ExEn}_{\text{Inj}} \tag{4}$$

is the quantity of the energy produced and injected which is registered and exchanged in the electricity market, while

$$\text{ExEn}_{\text{Drw}} \tag{5}$$

is the quantity of energy absorbed that is registered and exchanged in the electricity market.

$+C_{TSO}$ represents the costs due to the TSO that includes both the part concerning the energy injection into the grid ($C_{TSO-Inj}$) and the energy drawn from the grid ($C_{TSO-Drw}$), it is so defined as

$$C_{TSO} = C_{TSO-Inj} + C_{TSO-Drw}. \quad (6)$$

$C_{TSO-Inj}$ is composed of the guarantee that needs to be provided towards the TSO for the generation plants in the aggregation and added in the dispatching contract related to the energy injection (C_{WarInj}) (The guarantee to be provided to Terna is a function of the installed power of the production plant added in the dispatching contract for energy injection—Annex A.61: Regulation of the system of guarantees in art. 49 Annex A to resolution 111/06 AEEG-SI—https://www.terna.it/it-it/sistemaelettrico/codicedirete.aspx.), the monthly costs incurred for the actual energy imbalances ($C_{InjEffInba}$) (Analysis performed on some plants assumed that the actual imbalance, i.e., the programming error generated for a photovoltaic plant with a nominal power of 1 MWp, is approximately 1200.00€/year which matches with the total contribution of management to be paid to the GSE in the case of the RID service—http://www.espwr.it/download/espwr_281_SbilanciamentoFV.pdf. This value compared to the equivalent hours of production considered (1400 h/year) has the same cost of 0.85 c€/MWh.), and an adjustment component (defined as *perequativa*) based on the energy imbalance rules adopted ($C_{PerComInj}$) (From analysis performed on some PV plants in the South Italy area, cost due to the adjustment component has been identified that on average in the year 2016 has been equal to 0.215€/MWh registered.). $C_{TSO-Inj}$ is so defined as

$$C_{TSO-Inj} = C_{WarInj} + C_{InjEffInba} + C_{PerComInj}, \quad (7)$$

where

(i) $C_{WarInj} = f(\text{Installed Power})$

(ii) $C_{InjEffInba} = 0.85€/\text{MWh}$

(iii) $C_{PerComInj} = 0.215€/\text{MWh}$

$C_{TSO-Drw}$ is composed of the guarantee (C_{WarDrw}) (The guarantee to be provided to Terna according to the average annual power of the dispatching contract for energy absorbed from the grid—Annex A.61: Regulation of the system of guarantees in art. 49 Annex A to resolution 111/06 AEEG—https://www.terna.it/it-it/sistemaelettrico/codicedirete.aspx. From analysis performed on users, managed for the energy absorption in a dispatching contract, a guarantee requested by Terna of €46.6 per customer with an annual average power of 3.34 kW has been identified, which corresponds to the PMA of household users.) to be provided to the TSO based on the number of point of delivery (POD) managed and on the annual average power absorbed from the grid; the monthly costs incurred for real imbalances on the energy drawn from the grid ($C_{DrwEffInba}$) (From analysis performed on some customers managed by a Supplier in the South Italy area has been identified a cost due to the actual energy imbalance equal to 0.005€/kWh); and nonarbitrage fees (C_{DrwArb}) (From analysis performed on some customers managed by a Supplier in the South Italy area has been identified a cost for non-arbitrage equal to 0.005€/MWh and so 0.0005€/kWh.) which represent a similar cost to the CCT expected in the dispatching contract of energy injection. $C_{TSO-Drw}$ is so defined as

$$C_{TSO-Drw} = C_{WarDrw} + C_{DrwEffInba}, \quad (8)$$

where

(i) $C_{WarDrw} = f(\text{Annual Average Power})$

(ii) $C_{DrwEffInba} = 0.005€/\text{kWh}$

(iii) $C_{DrwArb} = 0.0005€/\text{kWh}$

To complete the charges due to the national TSO, there are other fees in the case of the drawn energy from the grid. Such costs, however, are defined passer-by charges (Fee to cover the costs for the remuneration of the load interruption service (Art. 24.6 Del 107/09 (TIS)), fee to cover the costs for the remuneration of available production capacity (art. 24.5 Del 107/09 (TIS)), fee to cover the costs for Terna's operation (Art. 24.3 Del 107/09 (TIS)), fee to cover the modulation of wind production costs (Art. 24.7 Del 107/09 (TIS)), fee to cover costs of essential units for the system safety (Art. 24.2 Del 107/09 (TIS)), and fee for the resource supply in the MSD (art. of the 24.1 107/09 (TIS)).) and are not included in the CEP profit since they are at the same time a cost and a revenue for the CEP. These charges are costs incurred by the CEP but fully charged to end-users in the electricity bill.

$+C_{DSO}$ represents the guarantee to be provided to the DSO which is equal to three months of the yearly charges ($C_{GridServ}$ discussed in the following) incurred by the end-user and calculated as

$$C_{DSO} = \frac{\text{Annual energy transport charges}}{4}. \quad (9)$$

$+C_{Taxes}$ is the guarantee to be provided to the Customs Agency Authority (in Italy, *Agenzia delle Dogane*), and it is equal to three months of the yearly excises incurred by the end-user and calculated as

$$C_{Taxes} = \frac{\text{Annual Excise duty}}{4}. \quad (10)$$

$+C_{ServCEP}$ are the costs incurred by the CEP corresponding to the sum of depreciation of used facilities (C_{Dpr}), general expenses (C_{GenExp}), Customer Relation Management system (CRM) necessary for the billing process towards the end-users ($C_{BillSist}$), and personnel costs (C_{Empl}) for the staff that manages the end-users and registers the schedule

transactions on PCE. C_{ServCEP} is so defined as

$$C_{\text{ServCEP}} = C_{\text{Dpr}} + C_{\text{GenExp}} + C_{\text{BillSist}} + C_{\text{Empl}}. \quad (11)$$

In the following, the operating revenues of the CEP ($\text{Revenues}_{\text{CEP}}$) are valuated. These revenues can be assessed examining the component related to the marketing and sales operations (PCV). It represents the remuneration to cover all the incurred fixed costs necessary for the commercial management of end-users. Moreover, there is a quota that contributes to the CEP revenues due to the energy supplied to the end-users, evaluated at the price PE_{CEP}. $\text{Revenues}_{\text{CEP}}$ is so defined as

$$\text{Revenues}_{\text{CEP}} = \text{n.users} * \left(\text{PCV} + \left(\text{PE}_{\text{CEP}} * \overline{\text{WDR}}_{\text{SingUserProsumer}}\right)\right) - \text{CE}_{\text{Market}} * \text{AnExEn}_{\text{Market}}, \quad (12)$$

where

$$\overline{\text{WDR}}_{\text{SingUserProsumer}} \quad (13)$$

represents the average annual energy drawn by the end-user from the grid and is considered as energy net of self-consumption (SelfCons);

$$\text{AnExEn}_{\text{Market}} \quad (14)$$

is the amount of energy that the CEP purchases on the market to satisfy the demand related to the end-user consumption which is not satisfied with the energy produced inside the Power Cloud, and $\text{CE}_{\text{Market}}$ is the related cost on the market.

2.2. End-User Profit. Focusing on the end-user side, it is possible to say that the main profit is given by the difference between the amount paid for the annual electricity bill in the case he is *not aggregated* (so, as a single end-user which is in the regulated services defined in the Italian Market "*Maggior Tutela*" and thus not equipped with the enabling technology) and the annual electricity bill that the end-user equipped with the enabling technology would pay if he is aggregated. For this purpose, in the following, the cost of the annual electricity bill for a not aggregated end-user will be analysed and evaluated, considering him as a simple consumer and the case of the end-user aggregated and operating as a prosumer.

2.2.1. Not Aggregated End-User. Taking into account the case of a residential domestic user with a 3 kWp installed power, the cost of the electricity bill consists of four main components [9]: *energy supply*, *energy transport and meter management* (*grid services*), *system charges*, and *taxes* (*excises* and *vat*) [10]. It is remarkable to consider that the year 2016 represented a transition period in Italy by a tariff structure, which persisted from 1970 to a greater flexible tariff structure starting from 2017. This new tariff scenario, with a continuous change until 2025, will encourage the energy consumption from the grid and will eliminate the differences between residential and nonresidential end-users in order to define a single and unique tariff, called *Domestic Tariff* (DT). The occurred changes [5] regard the displacement/changes of fixed components and/or changes of variable quota and some threshold values. Obviously, these components between the previous and new tariff scenario have different values, but the CEP optimization model previously illustrated is still valid. For these reasons, it is possible to evaluate the end-user electricity bill cost as

$$B_{\text{DoUser}} = C_{\text{EnMat}} + C_{\text{GridServ}} + C_{\text{SysCh}} + C_{\text{UsTax}}. \quad (15)$$

$+C_{\text{EnMat}}$ represents the cost of the energy supply that includes the *variable costs* (CV_{EnMat}) of the energy, the *fixed quota* ($\text{FixComp}_{\text{EnMat}}$) and a *power quota* ($\text{PwrComp}_{\text{EnMat}}$), all as defined by the Italian tariff scenario [11]. It includes the amounts related to the various activities carried out by the seller to supply the energy to the end-users.

The total price applied in the bill for CV_{EnMat} is given by the sum of the prices for the following components: energy price (PE), dispatching (PD), adjustment (PPE), and dispatching component (DispBT). The tariff scenario defines the value of all those components. The price of $\text{FixComp}_{\text{EnMat}}$ is given by the price for marketing and sales operations named PCV and by the fixed quota of the dispatching component (DispBT). $\text{PwrComp}_{\text{EnMat}}$ related to the energy supply is currently equal to 0, thus C_{EnMat} is defined as

$$C_{\text{EnMat}} = \left(CV_{\text{EnMat}} * \overline{\text{WDR}}_{\text{SingUser}}\right) + \text{FixComp}_{\text{EnMat}} + \left(\text{PwrComp}_{\text{EnMat}} * \text{InstPower}\right), \quad (16)$$

where

$$\overline{\text{WDR}}_{\text{SingUser}} \quad (17)$$

represents the average annual energy absorbed by the end-user (*the same quantity considered in the following for the prosumer net of self-consumption*) and

$$\text{InstPower} \quad (18)$$

represents the installed power (equal to 3 kW).

$+C_{\text{GridServ}}$ is the cost for the energy transport and the meter management. It is also named *grid services* [12] which include the transmission, distribution, and metering components, respectively, $\tau 1$, $\tau 2$, and $\tau 3$, the components necessary to cover the imbalances of the equalization systems' costs for the energy transport (UC3) and cover a part of the costs incurred by the system to encourage and subsidize the companies that manage the transport and distribution networks for actions that lead an improvement of the service quality (UC6). The total price applied in the bill for the variable quota C_{GridServ} is given by the sum of the prices of the three components $\tau 3$, UC3, and UC6 (variable quota). The price of the fixed component $\text{FixComp}_{\text{GridServ}}$ is exactly the value of component $\tau 1$.

The power component $\text{PwrComp}_{\text{GridServ}}$ is given by the sum between the power quota of $\tau 2$ and the power quota of UC6; thus, C_{GridServ} is defined as

$$C_{\text{GridServ}} = \left(CV_{\text{GridServ}} * \overline{\text{WDR}}_{\text{SingUser}}\right) + \text{FixComp}_{\text{GridServ}} + \left(\text{PwrComp}_{\text{GridServ}} * \text{InstPower}\right). \tag{19}$$

$+C_{\text{SysCh}}$ represents the cost for the end-user due to the general system charges which include amounts billed to cover the costs related to activities of general interest for the whole electricity system [13], paid by all end-users which use the electricity service. The total price includes the components A2 (*nuclear charges*), A3 (*incentives for renewable sources*), A4 (*subsidies for the railway sector*), A5 (*system research*), Ae (*advantages for energy-intensive industries*), As (*costs for the electricity bonus*), UC4 (*smaller electricity companies*), UC7 (*promotion of energy efficiency*), and MCT (*entity that host nuclear plants*). The total price CV_{SysCh} charged into the bill is given by the sum of the variable part of all listed components.

Currently, for the analysed end-user (residential domestic user with an installed power equal to 3 kW), both fixed quota $\text{FixComp}_{\text{SysCh}}$ and variable component $\text{PwrComp}_{\text{SysCh}}$ are equal to 0. C_{SysCh} is so defined as

$$C_{\text{SysCh}} = \left(CV_{\text{SysCh}} * \overline{\text{WDR}}_{\text{SingUser}}\right) + \text{FixComp}_{\text{SysCh}} + \left(\text{PwrComp}_{\text{SysCh}} * \text{InstPower}\right). \tag{20}$$

$+C_{\text{UsTax}}$ represents the excise duties paid by the end-user in the electricity bill that maintains a banded structure and where the reform started in 2017 was not affected because the definition of the excise duties does not concern the Authority AEEGSI [14], and it is calculated according to the relation below:

$$C_{\text{UsTax}} = \left(\overline{\text{WDR}}_{\text{SingUser}} - 4440\right) * 0.0227 + 1800 * 0.0454 + 840 * 0.0227, \tag{21}$$

considering the following thresholds:

(1) 0-1800 kWh/year = 0***

(2) 1800-2640 kWh/year, excises equal to 2.27c€/kWh

(3) 2640-4440 kWh/year, excises equal to 4.54c€/kWh

(4) >4440 kWh/year, excises equal to 2.27c€/kWh

***In case of energy supply with installed power over 1.5 kW and up to 3 kW: if the consumption is up to 220 kWh/month, the excises are not applied to the first 150 kWh; otherwise, the kWh exempted from excise is gradually reduced.

2.2.2. Aggregated End-User. Considering now the same type of end-user (a residential domestic user with an installed power 3 kW) but equipped with a RES plant and enabling technologies, he will be subjected in the electricity bill to the same cost components [9]. However, in this case, the energy cost component related to the energy (PE_{CEP}) is due to a customized price fixed by the CEP and therefore different from the price PE (PE corresponds to the expected cost for the purchase of energy, which is sold to end customers, and it includes network losses, i.e., the cost of energy that does not reach in a useful way the delivery point.) defined by the Authority, as previously shown. The electricity bill cost, in this case, is so defined as

$$B_{\text{DoUserCEP}} = C_{\text{EnMatCEP}} + C_{\text{GridServ}} + C_{\text{SysCh}} + C_{\text{UsTax}} + \text{TechPaym} - \left(\text{PremPrice}_{\text{CEP}} * \overline{\text{INJ}}_{\text{SingUserProsumer}}\right). \tag{22}$$

$+C_{\text{EnMatCEP}}$ represents the cost of the energy supply in the aggregation which includes the *variable costs* of the energy (CV_{EnMatCEP}), the *fixed quota* ($\text{FixComp}_{\text{EnMat}}$) and a *power quota* ($\text{PwrComp}_{\text{EnMat}}$), as defined and illustrated in Section 2.2.1. Contrary to the not aggregated end-user case, in this one, the variable energy component has a different value because of the energy price customization (PE_{CEP}) defined by the CEP and the amount of energy absorbed by the end-user and considering that the self-consumption quota is different. Then, C_{EnMatCEP} is defined as

$$C_{\text{EnMatCEP}} = \left(CV_{\text{EnMatCEP}} * \overline{\text{WDR}}_{\text{SingUserProsumer}}\right) + \text{FixComp}_{\text{EnMat}} + \text{PwrComp}_{\text{EnMat}} * \text{InstPower}. \tag{23}$$

All other components, burdens owed to the grid operators, remain equal as previously shown in Section 2.2.1. The energy consumption from the grid by the single end-user, in this case,

$$\overline{\text{WDR}}_{\text{SingUserProsumer}} \tag{24}$$

is referred to as a prosumer, and therefore, it represents the average annual energy drawn from the grid by the end-user considering the self-consumption quota. The other cost components that define $B_{\text{DoUserCEP}}$ have the same structure of the case in Section 2.2.1 (*see cost items which compose the user's electricity bill in the case in* Section 2.2.1) but consider now $\overline{\text{WDR}}_{\text{SingUserProsumer}}$:

$$\begin{aligned} C_{\text{GridServ}} &= \left(CV_{\text{GridServ}} * \overline{\text{WDR}}_{\text{SingUserProsumer}}\right) + \text{FixComp}_{\text{GridServ}} + \left(\text{PwrComp}_{\text{GridServ}} * \text{InstPower}\right), \\ C_{\text{SysCh}} &= \left(CV_{\text{SysCh}} * \overline{\text{WDR}}_{\text{SingUserProsumer}}\right) + \text{FixComp}_{\text{SysCh}} + \left(\text{PwrComp}_{\text{SysCh}} * \text{InstPower}\right), \\ C_{\text{UsTax}} &= \left(\overline{\text{WDR}}_{\text{SingUserProsumer}} - 4440\right) * 0.0227 + 1\,800 * 0.0454 + 840 * 0.0227. \end{aligned} \tag{25}$$

+TechPaym represents the instalment cost incurred by the end-user in order to install the RES plant and the enabling technologies (nGfHA *including storage system*) to make him a prosumer. The instalment cost is supposed to be calculated using an amortization plan with a flat rate for t time with an interest rate i:

$$\overline{\mathrm{INJ}}_{\mathrm{SingUserProsumer}} \tag{26}$$

represents the average annual energy injected into the grid by the end-user net of the self-consumption and the energy needs to charge the storage system. It will be sold to other end-users of the Power Cloud. Such energy will be remunerated to the end-user according to a tariff $\mathrm{PremPrice}_{\mathrm{CEP}}$ defined by the CEP according his economic convenience limits.

2.3. Energy Balance Constraints. It is possible to define, in the purpose of the CEP, an equation on the annual energy balance. The fundamental constraint has to be considered for the operating of an energy aggregation and so of the Power Cloud. The annual energy balance is

$$\left(\mathrm{AnExEn}_{\mathrm{Drw}} - \mathrm{AnExEn}_{\mathrm{Inj}}\right) - \mathrm{AnExEn}_{\mathrm{Market}} = 0, \tag{27}$$

where

$$\mathrm{AnExEn}_{\mathrm{Inj}} \tag{28}$$

is the average annual energy injected into the grid by all end-user net of the self-consumption, which is the number of end-users multiplied by the average annual energy $\overline{\mathrm{INJ}}_{\mathrm{SingUser}}$ previously defined:

$$\mathrm{AnExEn}_{\mathrm{Inj}} = \mathrm{n.users} * \overline{\mathrm{INJ}}_{\mathrm{SingUser}}, \tag{29}$$

where

$$\mathrm{AnExEn}_{\mathrm{Drw}} \tag{30}$$

is the average annual energy absorbed by all end-users, which is the number of end-users (n.users) multiplied by the average annual energy absorbed from the grid $\overline{\mathrm{WDR}}_{\mathrm{SingUser}}$ for the single end-user (in the case where the end-user is a prosumer, the energy absorbed $\overline{\mathrm{WDR}}_{\mathrm{SingUserProsumer}}$ is considered as energy net of the self-consumption):

$$\mathrm{AnExEn}_{\mathrm{Drw}} = \left(\mathrm{n.users} * \overline{\mathrm{WDR}}_{\mathrm{SingUser}} \text{ or n.users} * \overline{\mathrm{WDR}}_{\mathrm{SingUserProsumer}}\right). \tag{31}$$

$\mathrm{AnExEn}_{\mathrm{Market}}$ is previously defined in Section 2.1.

2.4. Discount Thresholds on Absorbed Energy. The enhancement of the energy component ($\mathrm{PE}_{\mathrm{CEP}}$) with respect to the case of not aggregated end-user can be defined by the CEP according to some economic convenience limits, which correspond to a percentage of discount applied to the energy price defined by the regulated service *Maggior Tutela* (PE) (For the analysis, the PE is considered flat. PE flat is an option of the regulated service Maggior Tutela where the price is always the same at any time.). In detail, the CEP may establish discount thresholds based on the number of end-users of Power Cloud, so

$$\mathrm{PE}_{\mathrm{CEP}} = \mathrm{PE} - x\%, \tag{32}$$

where x depends on n.users.

2.5. Premium Price Thresholds for Produced Energy. The energy produced and injected into the grid because it is not consumed by the end-user can be virtually utilized by the CEP in order to satisfy the energy needs of other end-users. It must be underlined that at this scope, the use of the enabling technology such as the nGfHA is fundamental because by using such system, the CEP, at the aggregation level, can demonstrate that "the energy absorbed from an end-user is exactly the surplus production injected into the grid by another end-user which has sold this energy to the CEP."

The enhancement of this energy injected into the grid for an end-user is a way of participating to the local market as if it was a small producer who sells energy on the market at a price defined with the CEP. Such modality is similar to what is done by the bigger producers that sell energy through "over-the-counter" contracts (bilateral contracts) agreed with the energy wholesalers or the RID (in Italy, *Ritiro dedicato*) of the GSE [15]. An additional example for small users can be the energy exchange named in Italy *Scambio Sul Posto* (SSP), which provides the enhancement of the energy injected into the grid. Being the RID, the enhancement of the energy at the average hourly zonal price (P_z) (The zonal price (P_z) is defined as a reference of the valuation price of the sales offers accepted on the day-ahead market in the relevant period, in the area where the production unit is located.), the *premium price*, is defined as the additional percentage on the RID:

$$\mathrm{PremPrice}_{\mathrm{CEP}} = \mathrm{RID} + y\%, \tag{33}$$

where y is defined by the CEP according to the economic convenience of the aggregation and based on n.users.

2.6. End-User Billing System. The billing system to end-users is the core of the end-user management service for the CEP. The unit management cost per end-user of a CRM system that is able to provide data aggregation, data transmission, and billing for energy consumption has been examined for the analysis. Such a system involves start-up costs related to the installation which includes a small number of end-users that can be managed. After that, for a group of 500 PODs (*point of delivery*), the cost is €6 per user/year. Based on these considerations, it has been possible to define cost thresholds for groups of end-users as shown in the following:

$$C_{\mathrm{BillSist}} = C_{\mathrm{BillUser}} * \mathrm{n.users}, \tag{34}$$

where

$$C_{\text{BillUser}} \tag{35}$$

depends on n.users according to the following scheme:

$$\begin{cases} 1-3000, & \text{end-users} \rightarrow 12.5€/\text{year}, \\ 3001-4000, & \text{end-users} \rightarrow 11€/\text{year}, \\ 4001-5000, & \text{end-users} \rightarrow 10€/\text{year}, \\ 5001-6000, & \text{end-users} \rightarrow 9€/\text{year}, \\ >6000, & \text{end-users} \rightarrow 8€/\text{year}, \end{cases} \tag{36}$$

3. Simulations and Case Study

Once the CEP optimization model was defined, the numerical results will be reported considering the most significant cases of study after making specific hypothesis on both the end-user side (i.e., consumption, RES plant size) and CEP side.

3.1. Hypothesis on the End-User Side

(i) The single end-user, so the prosumer, has an annual total consumption of 5620 kWh

(ii) The PV plant has a peak power equal to 3 kWp

(iii) The estimated annual production of the PV plant supposing to be located in South Italy is set equal to 1430 kWh/kWp

(iv) The PV plant production per year is approximately 4288 kWh/year

(v) Each nGfHA is equipped with a storage system having a capacity equal to 3 kWh

(vi) For each end-user, *demand response* (DR) software in coordination with the storage management system is installed. It allows to achieve a higher level of self-consumption (referring to the produced energy) equal to approximately 70% and so 3037 kWh/year

(vii) The additional annual energy required by the end-user according to the management model of the Power Cloud will be satisfied through the energy surplus produced by other end-users or the energy that the CEP buys from the electricity market

3.2. Hypothesis on the CEP Side

(i) The kWp cost of the PV plants is considered equal to 1200.00€/kWp. Consequently, the overall PV plant cost is equal to €3600.00

(ii) The cost of nGfHA equipped with storage system is considered equal to €3500.00. So, the overall cost for the end-user enabling technology is equal to €7100.00

(iii) The useful life of technological equipment is assumed to be 25 years

(iv) The guarantee to be provided to Terna is a function of installed PV power added in the dispatching contract. From empirical analysis and data processing, for the year 2016, a guarantee amount of €4803.00 per MWp has been considered

(v) For 2017, it has resulted that because of new Terna's *Annex A.61* for a new end-user that applies to a new dispatching contract, the calculus of the first guarantee on a 1 MWp PV plant is approximately about €138000.00. It can be reduced by a correction factor (CF) equal to 20 times lower, only if it results in a balanced energy program after six months with minimum energy imbalance. For the analysis, being this value so excessive, it has been considered the already reduced value and equal to 6932.00€/MWp. It corresponds to an increase of about 44% compared to 2016 scenario for which the value is considered 4803.00€/MWp

3.3. Simulations. The main changes between 2016 tariff scenario and the amendments starting from 2017 mainly consist of three items as shown in Table 1:

(i) The estimated change in the CCT value, based on the price changes (*average PUN and average*P_z)

(ii) The effect of the new imbalance regulation scenario, due to the application of the new dual mechanism on the small production plants [4] which will result in a higher cost ($C_{\text{InjEffInba}}$)

(iii) The amendment of Terna's Annex A.61 related to the 111/06 deliberation on dispatching which results in a higher guarantee amount (C_{WarInj})

In the following, the numerical results of the main case studies are shown in order to evaluate the aggregation size in terms of n.users that guarantees the balance between costs and revenues for the CEP and maximizes the end-user profit.

3.4. Case Study. First of all, in this case study, any discount percentage or incentive to production is considered to understand how, in the two tariff scenarios (2016 *vs.* 2017), the above-mentioned changes have impacted in the two different years from the CEP point of view. Moreover, the purpose is to find the minimum number of end-users so that there is a balance between costs and revenues for the CEP.

It is worth to underline that, between the prices and profit margins, it is possible to see a greater value of PCV component and a higher profit margin due to the difference between the PUN and PE of 2017 scenario compared to those of 2016 (*this difference represents the profit margin between purchasing electricity in the day-ahead market, MGP in Italy, and the sale to the end-user*). In Table 2, some of the price data used in the analysis are reported.

Table 1: Main changes 2016 vs. 2017.

Hypothesis	2016	2017	Considerations
CCT* (€/MWh)	5	6	Increase of +1€ for the difference PUN and P_z SUD.
$C_{\text{InjEffInba}}$ (€/MWh)	0.85	2.55	The new energy imbalance rules ("dual price") that affect the cost in +300%.
C_{WarInj} (€/MWp)	4 803	6 932	Increase the first guarantee for the dispatching contract of 44%.

∗ refers to an estimate based on the analysis performed.

Table 2: Market prices 2016 vs. 2017.

Hypothesis	2016	2017	Considerations
Average PUN (€/MWh)	42.74	47.44	It has been considered the average PUN of the last four quarters of 2016
Average P_z SUD (€/MWh)	40.34	44.17	It has been considered the average PUN of the last 4 quarters, thus three quarters of 2016 and the first quarter of 2017 to assess the price changes
PE (€/MWh)	47.08	53.16	Value related to the PE component established by the Authority for the quarter under analysis (IV 2016 vs. I 2017)
RID (€/MWh)	39.00	39.00	It has been considered the minimum remuneration of the GSE for the production plants ("*Ritiro dedicato*," (RID))
PCV (€/year)	28.38	34.04	Value related to the market and sales component established for the energy suppliers necessary to cover its costs. The PCV is yearly paid by the user

Table 3: Numerical results for 2016 tariff scenario.

Break-even point		n.users	% SelfCons	% energy discount	% premium price
$\text{Costs}_{\text{CEP}}$	-€764027	18069	71% of production (3037 kWh)	0%	0%
$\text{Revenues}_{\text{CEP}}$	€764027				
n.users	$\overline{\text{WDR}}_{\text{SingUser}}$ (kWh)	$\overline{\text{WDR}}_{\text{SingUser Prosumer}}$ (kWh)	SelfCons (kWh)	$\overline{\text{INJ}}_{\text{SingUser}}$ (kWh)	$\text{AnExEn}_{\text{Drw}}$ (kWh)
18069	5620 (100%)	2583 (46%)	3037 (54%)	1061	46643438
$\text{Revenues}_{\text{CEP}}$ (e. supply)	Total energy cost	$\text{Revenues}_{\text{CEP}}$ (e. supply per user)*	$\text{Revenues}_{\text{CEP}}$ (PCV per user)	Total profit (e. supply + PCV)	
€2195973	€1583982	€33.87	€28.38	€1124861	
$\text{AnExEn}_{\text{Inj}}$ (e. sold in the market)				€386697	
$\text{PremPrice}_{\text{CEP}}$ (premium price for producers)				-€747532	
Total				€764027	

*Such revenue depends on the reused energy, provided by the prosumer injection into the grid, used to cover a part of the total energy needed. Otherwise, the energy profit would be lower as shown in Table 4.

In the following, the numerical results for each tariff scenario are illustrated.

3.4.1. Case 1: Analysis with 2016 Tariff Scenario. Despite a series of costs charged on the CEP, which have been lower if compared to 2017 (see Table 1), a lower profit margin between the market prices has been found (PE, Average PUN, and Average P_z, see Table 2). This leads to the results reported in Table 3. The minimum number of end-users that guarantees the financial balance between CEP costs and revenues is 18069 users.

The margins occurring in the energy sales are shown in Table 4.

It is possible to see that the consumption of the 2583 kWh from the grid of the single end-user returns a 4.34€/MWh CEP profit (0.434c€/kWh) for a total amount of about €11.20 per year to which is added a yearly fixed component, received by the energy supplier, the PCV of €28.38 per year. In addition, a minimum margin is obtained on the surplus energy that the end-user yields to the CEP (*that provides to resell to other end-users or in the energy market at the price*P_z); it returns a profit margin of about €41 per user per year.

In Table 5, it is reported how the Power Cloud cost change depend on the number of users and the related balancing point (*break-even point* (BEP)).

Graphic representation of Table 5 is illustrated in Figure 1.

3.4.2. Case 2: Analysis with Tariff Scenario 2017. In the following, a simulation with the same hypothesis of Case 1 is shown, considering the 2017 tariff scenario.

Table 4: Yearly CEP profit for single end-user (2016).

Absorption (kWh)	PE-PUN (€/MWh)	Energy quota (€/year)	PCV (€/year)	Total (€/year)
2583	4.34	11.20	28.38	39.58
e. injection (kWh)	P_z-RID (€/MWh)	Profit for e. injection (€/year)	—	—
1061	1.34	1.43	—	1.43
Profit (€/year per user)				41.00

Table 5: CEP costs and revenues per users—2016.

n.users	1000	5000	10000	15000	20000
Costs	€176202	€320510	€484020	€657530	€831040
Revenues	€42284	€211420	€422840	€634261	€845681

Although CEP costs are greater if comparing the 2017 tariff scenario with that of 2016 (see Table 1), the solution of the CEP optimization model leads to a balance situation in the Power Cloud with a lower number of users of approximately 50% as shown in Table 6. This is due to an increase of the possible profit margins in the market prices applicable on the market due to the increased gap between prices (see Table 7).

In this second case, the consumption of 2583 kWh from the grid of the single end-user determines return of 5.71 €/MWh CEP profit (0.571c€/kWh) for a total amount of about €14.75 per year to which is added a yearly fixed component (net PCV) received by the energy supplier increasing to €34.04 per year (*significant increase with respect to 2016*). In addition, taking into account the profit margin on the excess energy that the end-user yields to the CEP (*which have a greater value with respect to 2016*), it returns a profit margin of about €54 per user per year. This significant increase in the CEP profit margins determines a recovery of the CEP costs with a smaller number of users equal to 7868 (*see* Table 6). On the contrary, it was expected that the tariff scenario 2017 (*which implies an increase in the management costs*) would make an increase of the users' number for the balance condition between CEP costs and revenues. This would be true if the profit margin conditions had remained the same; however, changes in the nature of expenses are necessary to take into account the changes of the possible revenues. In this case, it is shown how the CEP costs change depending on the number of users involved, as reported in Table 8.

Graphic representation of Table 8 is illustrated in Figure 2.

It must be said in fact that for an increase in the costs has been observed a more than proportional increase in profit margins that can be generated from the energy supply (see Tables 4 and 7) and as a consequence a reduction in the user number needed for the economic balance.

In such a situation, the main problem remains the economic advantage of the end-user compared with the standard situation that he would have if he did not participate in an energy community. The situation shown above is certainly useful and makes advantages for the CEP who manages the Power Cloud but shows a drawback from the end-user side.

As it is possible to see below, the break-even situation shown with the current market margins leads to an economic balance for the CEP but not for the end-user that if it is compared to the previous tariff scenario 2016, he pays for the electricity an annual amount slightly higher due to the instalment costs of the enabling technologies (see Table 9).

At this point, it has been decided to evaluate the end-user profit, applying firstly the maximum possible discount on the energy component (PE_{CEP}) by the CEP and secondly applying the maximum premium price on the energy injected into the grid by the end-user. The constraint is placed that the end-users could not exceed the number of end-users expected for 2016 tariff scenario (that is, 18069). Finally, in the same conditions, a third case has been evaluated, applying the maximum discount value and premium price simultaneously so that the end-user would get the maximum savings.

Observing the results in Table 10, it is relevant that, in any case, the annual electricity bill paid by the end-user is less convenient comparing with the case of the absorption from the grid (end-user not aggregated, see Table 9). Therefore, a better solution is needed to improve the situation and get a real convenience for the end-user.

4. Observations

The numerical results demonstrate that by *also trying to facilitate the end-user in a better way according to the CEP economic constraints*, *the end-user with high electricity consumption has a reduced convenience to participate in the Power Cloud with the tariff scenario of 2017*. Such a situation is due to the decrease in average cost per kWh when the electricity consumption increases. This situation is well clear in Figures 3 and 4 considering the annual electricity bill for an end-user not aggregated in terms of his annual electricity consumption.

In the 2016 tariff scenario, for greater electricity consumption, the introduction of a RES plant is more convenient because it cuts the highest cost due to the cost progressivity in dependence of consumption. With the 2017 tariff scenario, the higher consumption is not so penalized (*being the new tariff a nonprogressive tariff*) having an average kWh cost lower than that of 2016 [5]. For a better understanding, it is possible to see Table 11 where the annual electricity bill (*with a flat* PE) of an end-user is calculated comparing the 2016 tariff scenario with that of 2017 and considering several annual electricity consumption cases.

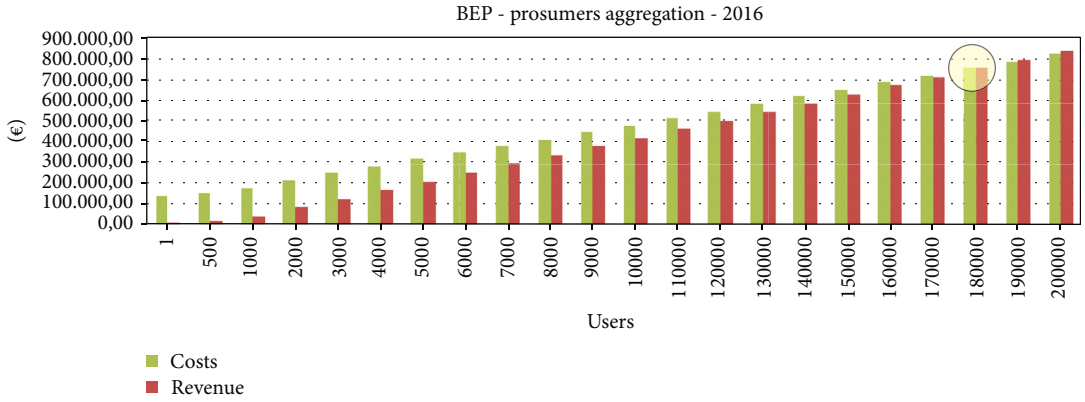

Figure 1: CEP costs, revenues, and break-even point 2016.

Table 6: Cost, revenues, and users' distribution—2017 (a).

Break-even point		n.users	% SelfCons	% energy discount	% premium price
$Costs_{CEP}$	-€440760	7868	71% of production	0%	0%
$Revenues_{CEP}$	€440760				
n.users	$\overline{WDR}_{SingUser}$ (kWh)	$\overline{WDR}_{SingUser}$ (kWh) Prosumer	SelfCons (kWh)	$\overline{INJ}_{SingUser}$ (kWh)	$AnExEn_{Drw}$ (kWh)
7868	5620 (100%)	2583 (46%)	3037 (54%)	1061	20310397
$Revenues_{CEP}$ (e. supply)	Total energy cost	$Revenues_{CEP}$ (e. supply per user)	$Revenues_{CEP}$ (PCV per user)	Total profit (e. supply + PCV)	
€1079700	€765634	€39.92	€34.04	€581909	
$AnExEn_{Inj}$ (e. sold in the market)				€184356	
$PremPrice_{CEP}$ (premium price for producers)				-€325505	
Total				€440760	

Table 7: Yearly CEP profit for single end-user (2017).

Absorption (kWh)	PE-PUN (€/MWh)	Energy quota (€/year)	PCV (€/year)	Total (€/year)
2583	5.71	14.75	34.04	48.79
e. injection (kWh)	P_z-RID (€/MWh)	Profit for e. injection (€/year)	—	—
1061	5.17	5.49	—	5.49
Profit (€/year per user)				54.28

Table 8: CEP costs and revenues per user number—2017.

n.users	1000	5000	10000	15000
Costs	€180107	€340037	€523075	€716113
Revenues	€56020	€280100	€560200	€840300

Considering EU's 2050 goal (to increase the production from renewable sources [16] to 80%-90% and improve the load management [17]), in the analysis, a 100% of self-consumption of the production capacity of RES plant (*thanks to new home automation technologies, storage systems, and demand response software*) (corresponding to a 76% of the total annual electricity consumption) can be assumed for an end-user with enabling technology (*prosumer*) and aggregated. In this case, the end-user will not have an annual electricity bill more expensive than the one that it would pay in the 2017 tariff scenario if it was not equipped with enabling technology (see Table 12) and not aggregated.

In Table 12, the annual electricity bill is reported, comparing the case of the simple consumer, a prosumer with a consumption of 70% with respect to the production capacity of RES plant, and a prosumer with 100%.

From the results of Table 12, it is evident that the main effort of the enabling technologies must be addressed to maximization of the electricity self-consumption percentage.

In the 2017 tariff scenario, only under the hypothesis of a 100% electricity self-consumption, the end-user achieves convenience in the installation of a RES plant and enabling

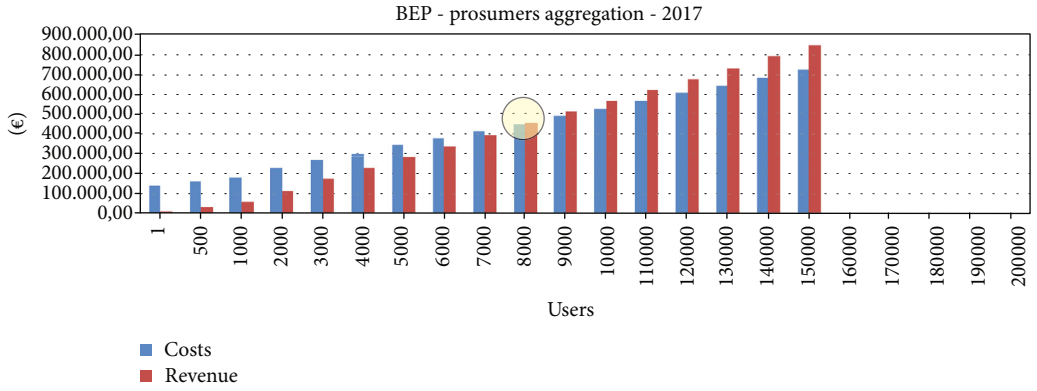

Figure 2: CEP costs and revenues 2017.

Table 9: Yearly electricity bill 2016 vs. 2017 for the end-user not aggregated and aggregated.

Year	$\overline{WDR}_{SingUser}$	Annual e. bill for end-user not aggregated	Annual e. bill for end-user aggregated	Savings	Savings with premium price
2016	5620 kWh	€1381.45	€1255.62	€125.82 (9%)	€167.20 (12%)
2017	5620 kWh	€1073.78	€1268.25	-€194.47 (-18%)	-€153.10 (-14%)

Table 10: Annual electricity bill 2017 with advantages.

	%	Annual e. bill for end-user not aggregated	Annual e. bill (CEP)	Savings with premium price
(1) max discount	7.16	€1073.78	€1216.06	-€142.28 (-13%)
(2) max premium	23.7		€1217.04	-€143.26 (-13%)
(3) max discount & premium	5.5 + 5.5		€1216.29	-€142.51 (-13%)

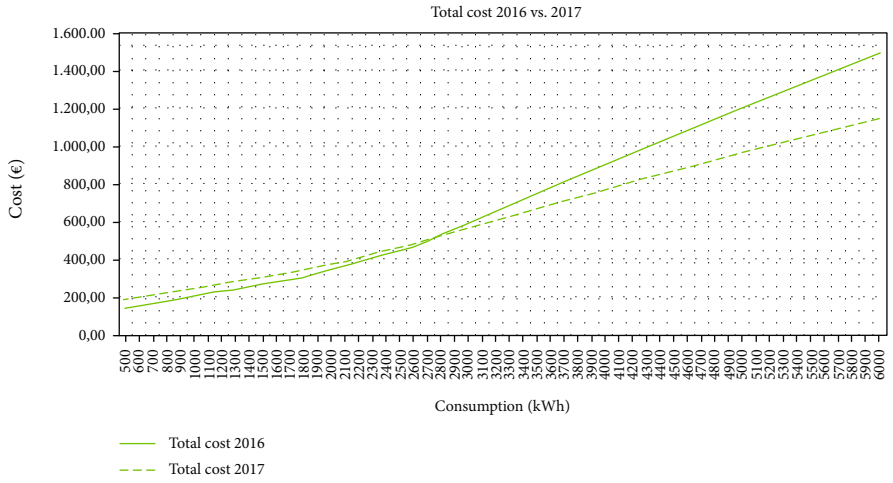

Figure 3: Annual electricity bill cost 2016-2017.

technologies, and at the same time, the CEP reaches an economic balance between costs and revenues. From the CEP view point, this situation implies that there will not be a dispatching management being the energy produced by each end-user entirely self-consumed.

Naturally, under that hypothesis, the number of end-users that guarantees the balance between the CEP costs and revenues changes as reported in Table 13.

It can be observed that the number of end-users is less than the previous case (see Table 6) because the energy to

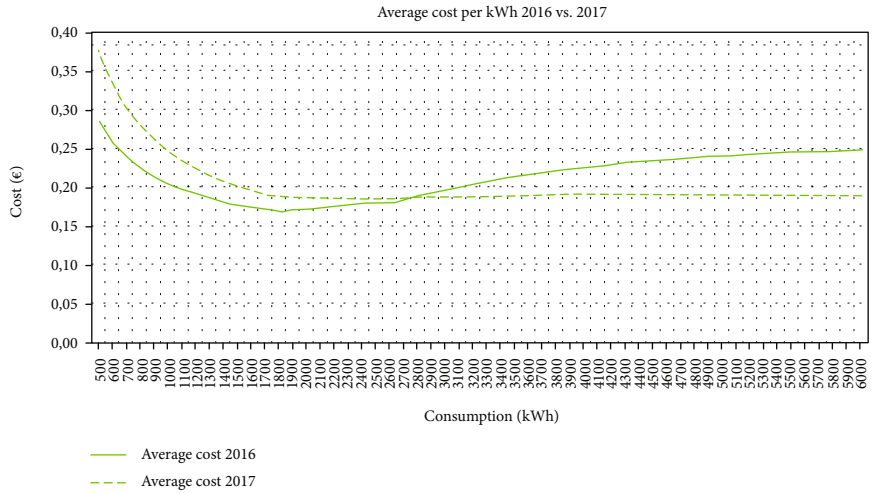

Figure 4: Average cost 2016-2017.

Table 11: Energy bills 2016 vs. 2017 and average costs.

Annual energy consumption (kWh)	2016 annual e. bill (€)	2017 annual e. bill (€)	Delta (€)	2016 average cost	2017 average cost
500	142.66	188.02	-45.35	0.2853	0.3760
900	192.74	234.54	-41.80	0.2142	0.2606
1800	305.40	339.20	-33.80	0.1697	0.1884
2700	498.33	503.14	-4.81	*0.1846*	*0.1863*
3600	779.47	688.05	91.42	0.2165	0.1911
4500	1059.12	871.47	187.65	0.2354	0.1937
5400	1317.78	1033.91	283.87	0.2440	0.1915
5620	1381.45	1073.78	307.67	0.2458	0.1911

be purchased on the market is less due to the higher electricity self-consumption percentage.

Also, for this case, it has been taken into consideration the possibility of applying an additional discount on PE. In Table 14, it is illustrated how the number of end-users changes with increasing of the PE discount quadrupling with a PE discount of 20%.

A significant increase of the number of end-users is necessary to compensate for the discount on PE (*consequent savings in the bill despite the difficulties of the nonprogressive tariff*) and to reach the balance between CEP costs and revenues simultaneously.

5. Conclusions

In the paper, the authors tried to prove that there is still the possibility to create aggregation forms of end-users maintaining a common benefit (CEP *and end-users*) despite the new electricity tariff scenario like the Italian 2017 tariff scenario, which from the analysis reported in [18] does not seem to incentivise the electricity self-consumption. At this scope, a CEP optimization model has been formulated suitable to each type of end-user (*consumer*, *producer*, *and prosumer*).

In the paper, the case of prosumer end-users equipped with enabling technologies has been considered. In this case, it can be observed that

(i) aggregation forms are more advantageous in terms of the number of end-users considering the 2017 tariff scenario with respect to the 2016 one. This is because with the 2017 tariff scenario, despite the increase in the CEP management costs, at the same time, an increase of the profit margin in energy supply has been observed

(ii) the advantage for the aggregated end-user becomes positive only in the case of self-consumption, which is almost equal to the production capacity of RES plant. This can be assumed realistic with the growing of new technologies, efficient storage systems, and smart building systems. As reported in [19], in the short term, the expected and progressive decrease in storage system costs will support the situation that will allow to achieve higher electricity self-consumption percentage and to make more competitive the energy cost of the self-consumption with respect to the cost of energy purchased from the grid [20]

(iii) in such a context, there is a lot of space for other possible configurations of new energy production systems defined in the Italian electricity market, efficient system for users (in Italian, SEU) where the end-user does not pay the RES plant but he pays

Table 12: The annual electricity bill in terms of electricity self-consumption percentage.

	Consumer	Prosumer (70%)	Prosumer (100%)
$\overline{WDR}_{SingUser}$ total per year (kWh)	5620 kWh	5620 kWh	5620 kWh
$\overline{WDR}_{SingUser}$ from grid (kWh)	5620 kWh	2583 kWh	1340 kWh
Annual SelfCons (kWh)	0 kWh	3037 kWh	4280 kWh
Electricity cost (€)	€1073.78	€480.24	€285.77
Technology instalment (€)	0	€788.00	€788.00
Average cost (grid) (€/kWh)	€0.19	€0.19	€0.21
Average cost (self-consumption) (€/kWh)	—	€0.26	€0.185
Annual electricity bill 2017 (€)	€1073.78	€1268.25	€1073.78

Table 13: Cost revenues and users' distribution—2017 (b).

Break-even point		n.users	% SelfCons	% energy discount	% premium price
$Costs_{CEP}$	-€297648	7128	99% of production	0%	0%
$Revenues_{CEP}$	€297648				
n.users	$\overline{WDR}_{SingUser}$ (kWh)	$\overline{WDR}_{SingUser}$ (kWh) Prosumer	SelfCons (kWh)	$\overline{INJ}_{SingUser}$ (kWh)	$AnExEn_{Drw}$ (kWh)
7128	5620 (100%)	1340 (24%)	4280 (76%)	8	9555716
$Revenues_{CEP}$ (e. supply)	Total energy cost	$Revenues_{CEP}$ (e. supply per user)	$Revenues_{CEP}$ (PCV per user)	Total profit (e. supply + PCV)	
€507981	€452030	€7.85	€34.04	€298604	
$AnExEn_{Inj}$ (e. sold in the market)				€1249	
$PremPrice_{CEP}$ (premium price for producers)				-€2205	
Total				€297648	

Table 14: Discount thresholds—2017.

% PE discount	n.users prosumers	Savings	$Costs_{CEP}$	$Revenues_{CEP}$
0%	7128	—	€297648	€297648
5%	8750	€3.92	€334210	€334210
10%	11328	€7.84	€392317	€392317
15%	16061	€11.76	€498971	€498971
20%	27583	€15.68	€758656	€758656
PE = 53.16 (€/MWh)		PUN = 47.44 (€/MWh)		P_z SUD = 44.18 (€/MWh)

the electricity self-consumption at a price equal or less than the price applied to the energy purchased from the grid. In this case, however, other problems arise, such as the huge initial investments needed to provide the enabling technology to the end-users. It requires a high level of participation by the end-users towards a new energy business model

(iv) last but not the least, a certain stability of the electricity market regulation is required. The 2017 tariff scenario is in an ever-changing situation, as demonstrated by the evolution of the electricity tariff and market regulations that tries to find solutions less expensive to manage the grid despite the significant development of the distributed generation

Data Availability

The energy platform and imbalance costs' data used to support the findings of this study are included within the article as reported in the notes. Others as billing system's costs have been provided from the national service provider based on specific quotation (https://www.terranovasoftware.eu/it/). The national market energy price data used to support the findings of this study were supplied by the national market operator (GME) and freely available at (http://www.mercatoelettrico.org/en/) the section "Result&Statistics." The standard tariff data for the domestic consumer were supplied by the national Authority (AREA) and freely available at (https://www.arera.it/it/prezzi.htm) the section

"Prices&Tariffs." All other data used during the study have been obtained as calculations and analysis.

Conflicts of Interest

The authors declare that they have no conflicts of interest.

Acknowledgments

This work has been funded by the Italian Ministry of the Economic Development (MISE) and the Ministry of Education, University and Research (MIUR), through the National Operational Program for Business and Competitiveness 2014-2020, PON F/050159/03/X32.

References

[1] D. Menniti, A. Pinnarelli, N. Sorrentino et al., "Nanogrids for home application in a power cloud framework," in *AEIT International Annual Conference (AEIT)*, Capri, Italy, 2016.

[2] B. P. Koirala, E. Koliou, J. Friege, R. A. Hakvoort, and P. M. Herder, "Energetic communities for community energy: a review of key issues and trends shaping integrated community energy systems," *Renewable and Sustainable Energy Reviews*, vol. 56, article S1364032115013477, pp. 722–744, 2016.

[3] AEEGSI-Terna, "268/2016/R/eel-Avvio di procedimento in tema di garanzie ai fini dell'accesso al servizio di dispacciamento dell'energia elettrica e verifica di conformità degli allegati A.61 e A.26 al Codice di trasmissione, dispacciamento, sviluppo e sicurezza," May 2016, http://www.autorita.energia.it/it/docs/16/268-16.htm.

[4] AEEGSI-Terna, "444/2016/R/eel-Interventi prioritari in materia di valorizzazione degli sbilanciamenti effettivi nell'ambito del dispacciamento elettrico," July 2016, http://www.autorita.energia.it/it/docs/16/444-16.htm.

[5] AEEGSI, "293/2015/R/eel - Riforma delle tariffe di rete e delle componenti tariffarie a copertura degli oneri generali di sistema per i clienti domestici di energia elettrica," June 2015, http://www.autorita.energia.it/it/docs/dc/15/293-15.jsp.

[6] AEEGSI, "582/2015/R/eel-Riforma delle tariffe di rete e delle componenti tariffarie a copertura degli oneri generali di sistema per i clienti domestici di energia elettrica," December 2015, http://www.autorita.energia.it/it/docs/15/582-15.htm.

[7] M. Lawrence, J. Vrins, R. Elberg et al., "Navigating the energy transformation. Building a competitive advantage for energy cloud 2.0," *Navigant*, vol. 3, 2016.

[8] AEEGSI, "Agenzia delle Dogane," http://www.autorita.energia.it/it/dati/eep38.htm.

[9] AEEGSI, "BOLLETTA 2.0 - Guida alla lettura delle voci di spesa per i clienti serviti in regime di tutela," January 2017, https://bolletta.autorita.energia.it/bolletta20/index.php/guida-voci-di-spesa/elettricita.

[10] AEEGSI, "Condizioni economiche per i clienti del mercato tutelato," 2016-2017, http://www.autorita.energia.it/allegati/dati_documenti/prezzi/elettricita-domestici.xls.

[11] AEEGSI, *818/2016/R/eel-Aggiornamento, per il trimestre 1 gennaio - 31 marzo 2017, delle condizioni economiche del servizio di vendita dell'energia elettrica in maggior tutela*, 2016.

[12] AEEGSI, "Tariffe trasmissione, distribuzione e misura - clienti domestici," 2017, http://www.autorita.energia.it/it/elettricita/d2d3.htm.

[13] AEEGSI, "814/2016/R/com-Aggiornamento, dal 1 gennaio 2017, delle componenti tariffarie destinate alla copertura degli oneri generali e di ulteriori componenti del settore elettrico e gas," December 2016, http://www.autorita.energia.it/it/docs/16/814-16.htm.

[14] S. Maggiore and M. Gallanti, "Analisi della spesa energetica di un'abitazione avente un impianto fotovoltaico alla luce delle recenti proposte tariffarie dell'Autorità," *L'Energia Elettrica*, vol. 92, no. 6, p. 38, 2015.

[15] Gestore dei Servizi Energetici (GSE), "Ritiro dedicato," 2016-2017, https://www.arera.it/allegati/elettricita/PMGvalori.xlsx.

[16] A. Wilson, "Briefing - new deal for energy consumers," 2016, http://www.europarl.europa.eu/RegData/etudes/BRIE/2016/573896/EPRS_BRI(2016)573896_EN.pdf.

[17] B. Nordman and K. Christensen, *DC Local Power Distribution with Microgrids and Nanogrids*, ICDCM, Atlantic City, NJ, USA, 2015.

[18] S. Maggiore and M. Gallanti, "Analisi della bolletta elettrica di un'abitazione con impianto fotovoltaico e nuove tariffe domestiche," *L'Energia Elettrica*, vol. 93, no. 1/2, pp. 35–50, 2016.

[19] V. Canazza, G. Ciapponi, M. DAlena, and G. Perico, "Le potenzialità Tecnologiche," *L'Energia Elettrica*, vol. 93, no. 4, p. 30, 2016.

[20] P. D'Aprile, J. Newman, and D. PinnerAugust 2016, http://www.mckinsey.com/business-functions/sustainability-and-resource-productivity/our-insights/the-new-economics-of-energy-storage.

Hindawi
International Journal of Photoenergy
Volume 2019, Article ID 1384985, 12 pages
https://doi.org/10.1155/2019/1384985

Research Article

An Advanced Multicarrier Residential Energy Hub System Based on Mixed Integer Linear Programming

Yue Yuan,[1] Angel A. Bayod-Rújula,[2] Huanxin Chen,[3] Amaya Martínez-Gracia,[4] Jiangyu Wang,[3] and Anna Pinnarelli[5]

[1]*China-Eu Institute for Clean and Renewable Energy, Huazhong University of Science and Technology, Wuhan 430074, China*
[2]*Department of Electrical Engineering, University of Zaragoza, Spain*
[3]*Department of Refrigeration & Cryogenics, Huazhong University of Science and Technology, 1037 Luoyu Road, 430074 Wuhan, China*
[4]*Department of Mechanical Engineering, University of Zaragoza, Spain*
[5]*Department of Mechanical, Energy and Management Engineering, University of Calabria, Arcavacata of Rende-Cosenza 87036, Italy*

Correspondence should be addressed to Angel A. Bayod-Rújula; aabayod@unizar.es

Received 27 February 2019; Accepted 14 May 2019; Published 9 June 2019

Academic Editor: Francesco Riganti-Fulginei

This work proposes a multicarrier energy hub system with the objective of minimizing the economy cost and the CO_2 emissions of a residential building without sacrificing the household comfort and increasing the exploitation of renewable energy in daily life. The energy hub combines the electrical grid and natural gas network, a gas boiler, a heat pump, a photovoltaic plant, and a photovoltaic/thermal (PV/T) system. In addition, to increase the overall performance of the system, a battery-based energy storage system is integrated. To evaluate the optimal capacity of each energy hub component, an optimization scheduling process and the optimization problem have been solved with the YALMIP platform in the MATLAB environment. The result showed that this advanced system not only can decrease the economic cost and CO_2 emissions but also reduce the impact to electrical grid.

1. Introduction

As the climate becomes increasingly polarized today, the demand for electricity and heating load of buildings also increases daily, sometimes even accounting for half of the total building energy consumption. Relying only on the electrical grid and natural gas network input to meet customer demand, energy utilization efficiency will be extremely low. Not only can the grid meet a huge pressure during peak load period, but it will also produce large amounts of CO_2 which will aggravate urban heat island effect, which makes the demand of polarization phenomenon more serious. In recent years, although renewable energy generation has been greatly developed, the constraint in terms of transport capacity of the electrical grid still becomes a bottleneck of its participation in energy supply. In last years, in order to provide a solution to these limits, a large number of small renewable energy generators have been connected to the distribution networks [1].

An energy hub is a multicarrier energy system consisting of multiple energy conversion, storage, and/or network technologies and is characterized by some degree of local control. Conception of an energy hub (EH) system has been first proposed on the research project "Vision of Future Energy Network" by ETH, Zurich, in 2007 [2]. In this future vision of energy networks, an energy hub system is a highly abstract unit structure, providing a great opportunity for system schedulers and operation workers to create a more efficient system [3]. An energy hub is an initial part of a multienergy

system, which can accommodate various forms of energy input and diversified load types [4]. Because of this diversified form of energy carrier, the energy hub system can realize collaborative optimization for various forms of energy [5]. In order to ensure that the energy hub is operated under a secure and economic and environmentally friendly condition, the research for energy hub systems mainly focuses on the component type or the capacity of an energy hub and the energy hub optimal dispatch [6–9]. Different from using traditional flat traffic, Le Blond et al. [10] introduced "dynamic traffic" to drive energy storage system operation to control energy hub system operation under minimum cost and CO_2 emissions. Beigvand et al. [11] proposed a new algorithm named SAL-TVAC-GSA to dispatch energy hub economic cost. In [9], Setlhaolo et al. present a residential energy hub model for a smart home as a modified framework of conventional energy hubs in a smart grid with consideration of heat pump water heater, coordination of sources, and carbon emission. Lingang Industrial Park is an engineering example [12], whose results provide a technical support for the construction of a resource-saving and environment-friendly harbour. In [13], a residential building and its electrical equipment are modelled as an energy hub system, including washing machine, dryer, HVAC system, refrigerator, and lighting equipment, to minimize energy cost, carbon emission, and peak load for optimal scheduling under the premise of maintaining the comfort of the users. In addition, a cloud computing framework is present to achieve the effective management of data and information. Ma et al. [8] presented a community micro energy grid in four different scenarios on a typical summer day, and the roles of renewable energy, energy storage devices, and demand response are discussed separately.

Due to the fact that an energy hub is an efficient means for the optimal exploitation of renewable energy generation, research focuses are generally concentrated on variable kinds of energy inputs [14–16]. Sharif et al. [17] presented a simulation model for an energy hub which major energy source is renewable energy (wind and solar energy) and natural gas. Ha et al. [18] proposed an energy hub system for residential buildings with solar energy and battery-based energy storage systems, and the results showed that this energy system structure conforms to the characteristics of residential buildings' energy consumption. Furthermore, it can reduce costs and save energy consumption at the same time. However, little research considers the integration of PV/T systems into an energy hub. PV/T can generate water heating and electricity at the same time [19], being an ideal component for residential energy hub system. This paper proposes a multicarrier energy hub (EH) system based on solar PV and PVT systems and a battery-based energy storage system. Moreover, an optimal scheduling strategy is proposed to calculate the optimum capacity of each component in order to minimize the energy cost and the CO_2 emission. The optimization problem has been solved with the YALMIP platform in the MATLAB environment. The proposed EH system is tested for a residential application according to the characteristics of buildings of apartments in Zaragoza, Spain.

2. Description of the Building Simulation Model and Optimization Process

A residential building located in Zaragoza, in the centre of Spain, with a simple but typical architecture as shown in Figure 1 has been simulated in EnergyPlus software. Climatic parameters, including ambient temperature, solar irradiation, and wind speed, have been taken from the Zaragoza local dataset. The simulation building is a 3-storey residential building, 1660.73 m^2, with five 3-bedroom apartments per floor. It has been considered that 4 people live in each apartment.

Solar irradiation in Zaragoza is abundant (see Figure 2), so it is reasonable to introduce photovoltaic (PV) systems or PV/T systems into energy hubs to decrease the energy costs and the CO_2 emissions.

The electricity price has been calculated from hourly local real-time price in Spain in 2017, as it is shown in Figure 3. The considered gas prices were 0.0667 euro/kWh and 0.0865 euro/kWh according to Spain gas prices for household consumers, all taxes and levies included in the first and second semester of 2017, respectively [20].

The daily energy consumption of the simulation building for four seasons is shown in Figure 4; blue bars represent electricity (including air conditioning) consumption and red curve represents heating demand (including heating and hot water demand). The highest electricity demand can approach 220 kWh per day (sum of the blue bar in Figure 4 for summer) and the highest heating demand is approximately 55 kWh per day (sum of grey values in Figure 4, winter).

Relying only on the electrical grid and natural gas network to satisfy electricity and heating demands of this building, the economic cost is 11713 euro/year and the CO_2 emission is 21711 kg/year (see Table 1).

An EH system has been so developed with the aim to minimize the energy cost and the CO_2 emissions but also for relief grid's pressure. Firstly, in accordance with the building's energy consumption pattern, an EH system with only a gas boiler (GB), a heat pump (HP), a PV plant (PV), and a PV/T system has been designed. A capital cost of 800 euro/kW has been considered for the GB and 1000 euro/kW for the HP, both with an estimated lifetime of 20 years. In the case of the PV plant, a capital cost of 1500 euro/kWp has been considered (including inverter, wire, and protections) and 700 euro/m^2 for the PVT systems and their lifetime has been considered to be 30 years. Later, the EH system has been improved with the integration of a BESS. The EH system design has been optimized by the optimization scheduling process as shown in Figure 5. The optimization problem is solved by using Mixed Integer Linear Programming (MILP) on the YALMIP platform in the MATLAB environment. Since there are too many elements included in the EH system, it is difficult to get the optimal solution directly through a single-layer optimization process. Therefore, the EH system design is threefold. Firstly, only the HP and the PV (with variable efficiency) are considered as elements involved in the operation of the EH system and for this configuration their optimum capacity is obtained. Then, operating the EH system under this optimum capacity, a PV/T (with variable

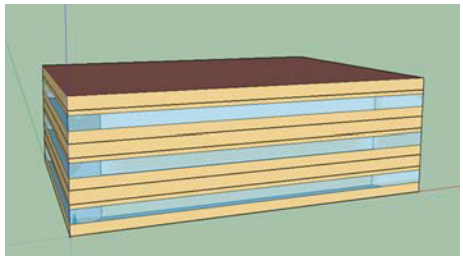

Figure 1: Building structure simulated in EnergyPlus software.

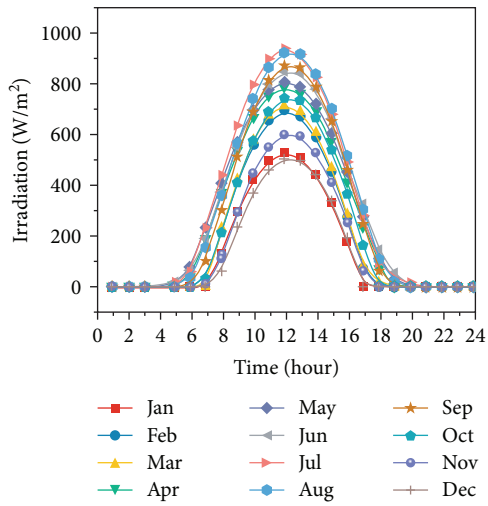

Figure 2: Average daily solar irradiation in Zaragoza for each month.

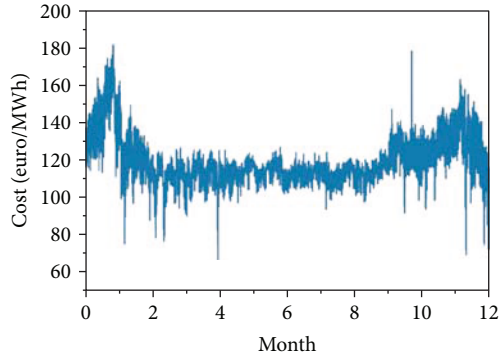

Figure 3: Actual hourly real-time electricity price in 2007.

thermal efficiency) is introduced into the EH system and the optimization schedule is solved again to calculate the optimal PV/T capacity. Finally, the BESS is integrated and the final optimal capacity of each element of the EH system is obtained. The entire process is modelled taking into account the dynamic price of electricity and natural gas.

The optimal operation model is formulated with the multiple objective of minimizing the entire cost, CO_2 emission, and peak load:

$$\begin{cases} \min \sum_{t-1}^{T-8760} \left[P_{\text{ele}}(t) p_{\text{ele}}(t) \Delta t + P_{\text{gas}}(t) \times p_{\text{gas}}(t) \Delta t \right] + F_{\text{install}} + f_{\text{O\&M}}, \\ \min \sum_{t-1}^{T-8760} P_{\text{ele}}(t) E_{\text{ele}}(t) \Delta t + \sum_{t-1}^{T} P_{\text{gas}}(t) E_{\text{gas}}(t) \Delta t, \\ \min P_{\text{ele}}^{\max}(t), \end{cases} \tag{1}$$

where $P_{\text{ele}}(t)$ and $P_{\text{gas}}(t)$ represent the price of electricity and gas from the main grid, respectively. $E_{\text{ele}}(t)$ and $E_{\text{gas}}(t)$ represent the CO_2 emission index of electricity and gas, respectively. F_{install} represents the installation fee of all components, and $F_{\text{O\&M}}$ represents the operation and management fee of all components.

Electricity balance constraints and heat balance constraints can be formulated as equations (2) and (4), respectively.

$$L_{\text{ele}}(t) = e_{\text{ele,grid}}(t) + e_{\text{ele,PV}}(t) + e_{\text{ele,PV/T}}(t) - e_{\text{ele,hp}}(t) - S_{\text{ele,B}}(t), \tag{2}$$

$$\begin{cases} e_{\text{ele,grid}}(t) = P_{\text{ele,grid}}(t) \eta_{\text{ele,grid}}(t), \\ e_{\text{ele,PV}}(t) = A_{\text{PV}} G(t) \eta_{\text{ele,PV}}(t), \\ e_{\text{ele,PV/T}}(t) = A_{\text{PV/T}} G(t) \eta_{\text{ele,PV/T}}(t), \end{cases} \tag{3}$$

where $e_{\text{ele,grid}}(t)$ is the electricity supplied from the main grid, $e_{\text{ele,PV}}(t)$ is the electricity supplied from the PV panel, and $e_{\text{ele,PV/T}}(t)$ is the electricity supplied from the PV/T panel; A_{PV} and $A_{\text{PV/T}}$ are the surface areas of the PV panel and the PV/T panels. $G(t)$ is the solar irradiance. $e_{\text{ele,hp}}(t)$ represents the electrical input of the heat pump at time, which is determined by heating balance constraints. And $S_{\text{ele,B}}(t)$ is the energy input or output from the battery.

$$L_{\text{heat}}(t) = h_{\text{heat,grid}}(t) + h_{\text{heat,PV/T}}(t) + h_{\text{ele,hp}}(t), \tag{4}$$

$$\begin{cases} h_{\text{heat,grid}}(t) = P_{\text{heat,grid}}(t) \eta_{\text{heat,grid}}(t), \\ h_{\text{heat,hp}}(t) = \text{COP}_{\text{hp}}(t) e_{\text{ele,hp}}(t), \end{cases} \tag{5}$$

where $h_{\text{heat,grid}}(t)$ and $h_{\text{heat,hp}}(t)$ represent the heating supplied from natural gas net and heat pump, respectively, and $h_{\text{heat,PV/T}}(t)$ is the heat supplied from the PV/T panel.

Solving the layer-by-layer optimization is helpful to know the impact of each element on the EH system and simplify the solving process at the same time. The building performance throughout the year is valuated with all the components at its optimum capacity.

3. The EH Structure and Matrix Representation

The first structure of the EH system proposed for the building is shown in Figure 6. Initially, a gas boiler (GB), a heat pump (HP), a PV plant (PV), and a PV/T system are considered besides the electrical grid and the natural gas network.

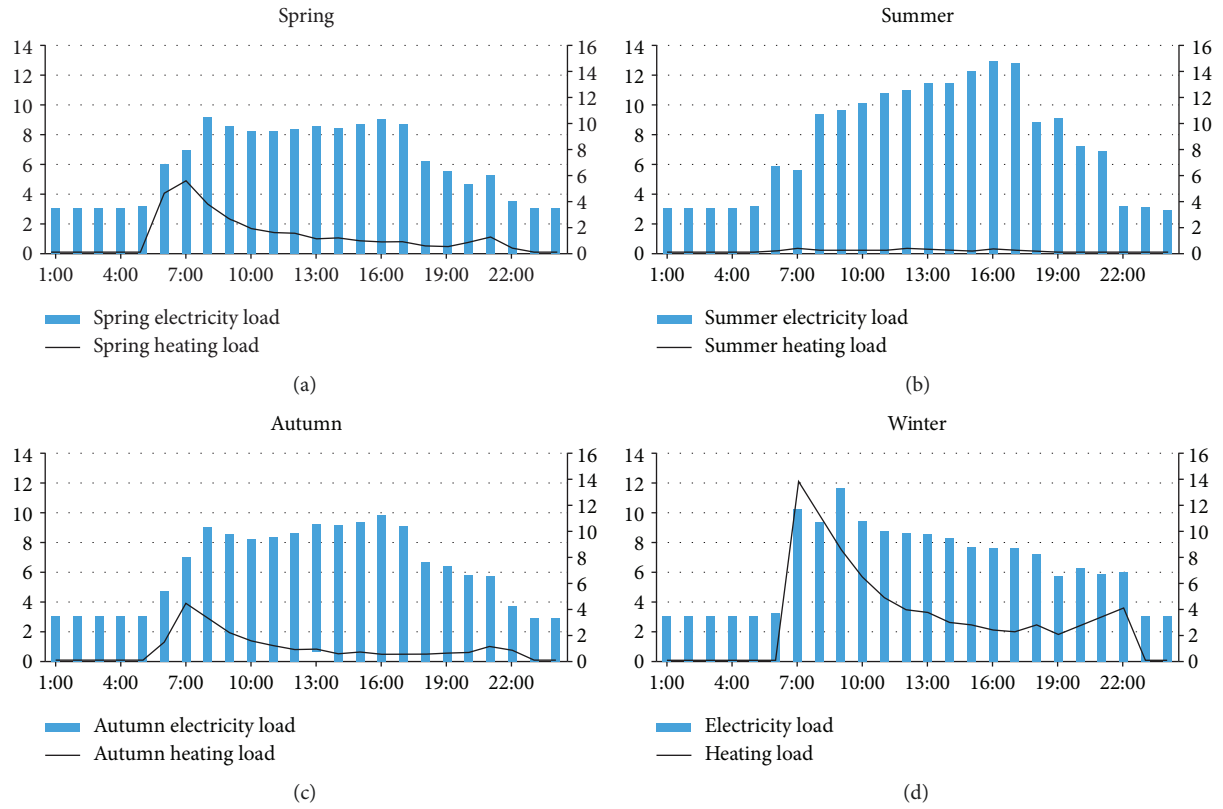

Figure 4: Daily energy consumption of the simulation building for different seasons.

Table 1: Cost, energy consumption, and CO_2 emissions for the traditional supply.

Cost (euro/year)	CO_2 emission (kg/year)	Gas consumption (kWh/year)	Electricity consumption (kWh/year)
11713	21711	20518	62589

The basic mathematical model of the EH system is [21]

$$L = f(P), \tag{6}$$

where L expresses the energy (electricity and heating) demand and considers the power supply.

The basic matrix function of the EH system can be written as

$$\begin{bmatrix} L_1 \\ L_2 \\ \vdots \\ L_n \end{bmatrix}_{n\times 1} = \begin{bmatrix} c_{11} & c_{12} \cdots c_{1m} \\ c_{21} & c_{22} \cdots c_{2m} \\ & \cdots \\ c_{n1} & c_{n2} \cdots c_{nm} \end{bmatrix}_{n\times m} \begin{bmatrix} P_1 \\ P_2 \\ \vdots \\ P_m \end{bmatrix}_{m\times 1}. \tag{7}$$

In this function, $c_{ij}{}^{\text{th}}$ is the coupling factor, which represents the conversion efficiency between the i^{th} energy input and the j^{th} energy output.

In this framework, the relationship between the demand side and the supply side of the EH system is formulated with a coupling matrix indicated as follows:

$$L = [C_1\ C_2] \begin{bmatrix} P \\ R \end{bmatrix}, \tag{8}$$

$$L = C_1 P + C_2 R. \tag{9}$$

Energy demand matrix L is equal to coupling matrix C times the installed generating capacity of P and the renewable energy R.

$C_1 P$ can be developed as

$$C_1 P = \begin{bmatrix} \eta_{\text{grid}} & \eta_{\text{heatpump}} & \eta_{\text{boiler}} \end{bmatrix} \begin{bmatrix} P_{\text{grid}} \\ P_{\text{heatpump}} \\ P_{\text{boiler}} \end{bmatrix}, \tag{10}$$

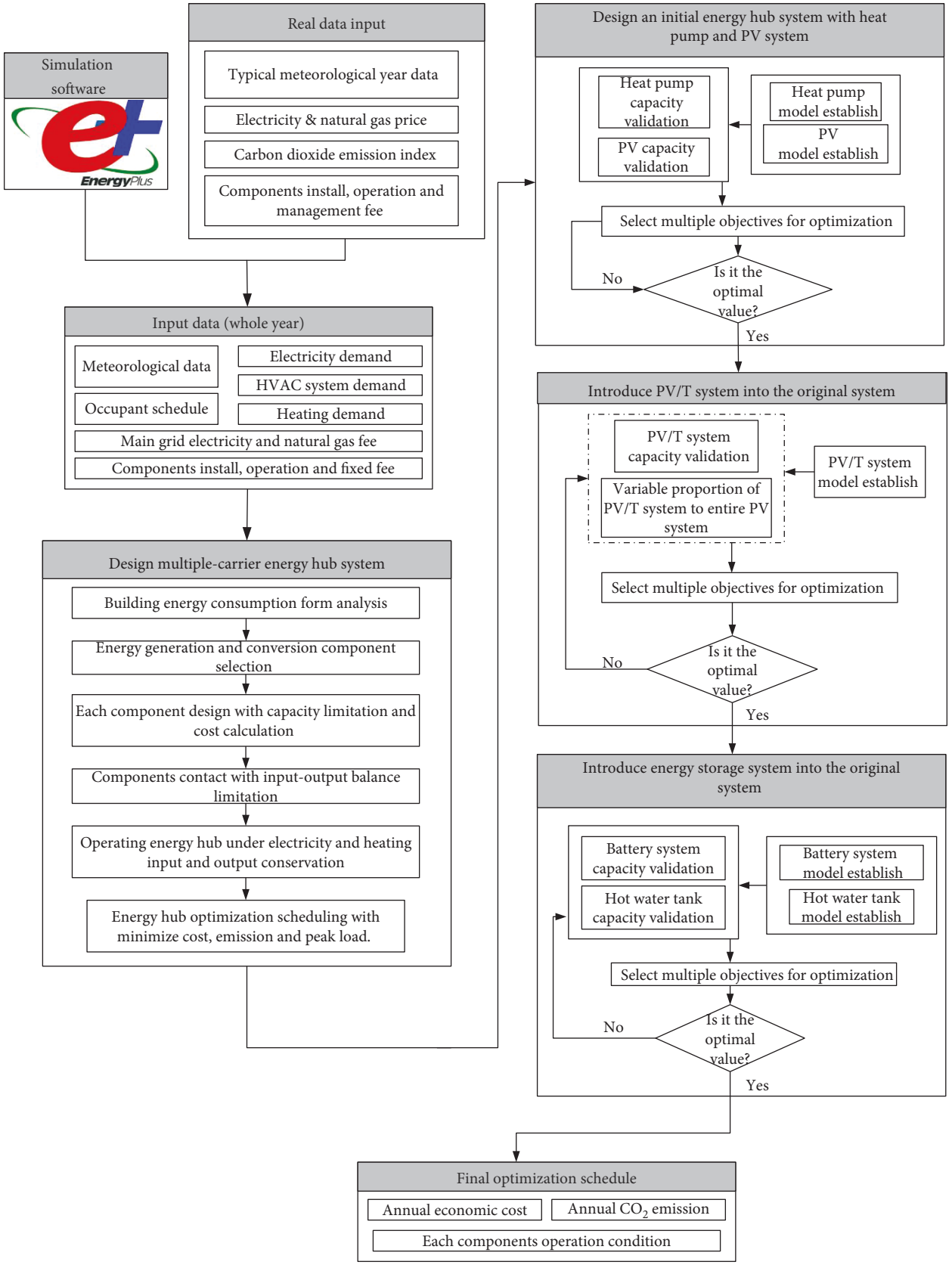

Figure 5: EH system optimization scheduling process.

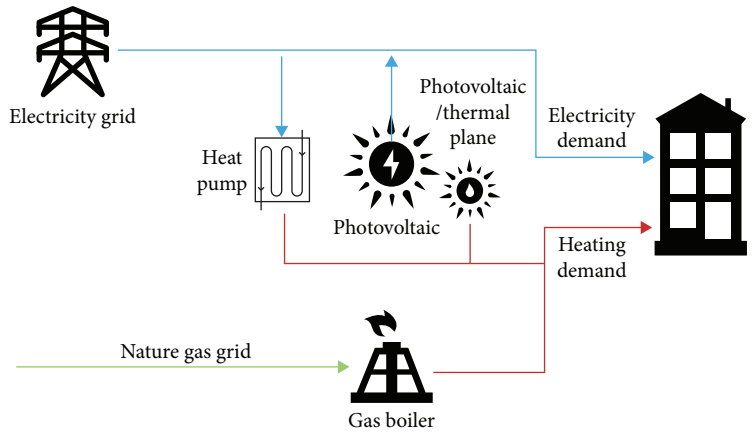

Figure 6: EH system structure for the building.

$$C_1P = \left[\eta_{\text{grid}}P_{\text{grid}} + \eta_{\text{heatpump}}P_{\text{heatpump}} + \eta_{\text{boiler}}P_{\text{boiler}}\right], \quad (11)$$

$$\begin{cases} \eta_{\text{grid}}P_{\text{grid}} = \begin{bmatrix} \eta_{\text{grid,ele}} \\ \eta_{\text{grid,heat}} \end{bmatrix} \begin{bmatrix} P_{\text{grid,ele}} \\ P_{\text{grid,heat}} \end{bmatrix}, \\ \eta_{\text{heatpump}}P_{\text{heatpump}} = \begin{bmatrix} \eta_{\text{heatpump,ele}} \\ \eta_{\text{heatpump,heat}} \end{bmatrix} \begin{bmatrix} P_{\text{heatpump,ele}} \\ P_{\text{heatpump,heat}} \end{bmatrix}, \\ \eta_{\text{boiler}}P_{\text{boiler}} = \begin{bmatrix} \eta_{\text{boiler,ele}} \\ \eta_{\text{boiler,heat}} \end{bmatrix} \begin{bmatrix} P_{\text{boiler,ele}} \\ P_{\text{boiler,heat}} \end{bmatrix}. \end{cases} \quad (12)$$

In (7), due to the value of $\eta_{\text{boiler,ele}}P_{\text{boiler,ele}}$ which is equal to 0, the equation can be represented as

$$C_1P = \begin{bmatrix} \eta_{\text{grid,ele}}P_{\text{grid,ele}} + \eta_{\text{heatpump,ele}}P_{\text{heatpump,ele}} \\ \eta_{\text{grid,heat}}P_{\text{grid,heat}} + \eta_{\text{heatpump,heat}}P_{\text{heatpump,heat}} + \eta_{\text{boiler,heat}}P_{\text{boiler,heat}} \end{bmatrix}. \quad (13)$$

C_2R can be represented as

$$C_2R = \begin{bmatrix} \eta_{\text{PV}} \\ \eta_{\text{PV/T}} \end{bmatrix} \begin{bmatrix} P_{\text{PV}} \\ P_{\text{PV/T}} \end{bmatrix}, \quad (14)$$

$$C_2R = \begin{bmatrix} \eta_{\text{PV,ele}}P_{\text{PV,ele}} + \eta_{\text{PV/T,ele}}P_{\text{PV/T,ele}} \\ \eta_{\text{PV,heat}}P_{\text{PV,heat}} + \eta_{\text{PV/T,heat}}P_{\text{PV/T,heat}} \end{bmatrix}. \quad (15)$$

Because the value of $\eta_{\text{PV,heat}}P_{\text{PV,heat}}$ is equal to 0, C_2R can be represented as

$$C_2R = \begin{bmatrix} \eta_{\text{PV,ele}}P_{\text{PV,ele}} + \eta_{\text{PV/T,ele}}P_{\text{PV/T,ele}} \\ \eta_{\text{PV/T,heat}}P_{\text{PV/T,heat}} \end{bmatrix}. \quad (16)$$

For each EH system component, the following parameters are included: capacity, efficiency, capital cost, fixed cost, variable cost, and lifetime as reported in Table 2. The electricity net emission factor considered is 0.28 kg/kWh and 0.204 kg/kWh for natural gas [22].

In real-life application, the PV efficiency is not a constant value; it varies with such parameters as solar irradiation, environmental temperature, and PV panel surface temperature. The working temperature of the cells (T_c) depends exclusively on the solar irradiation G and the ambient temperature (T_a) according to the linear function

$$T_c - T_a = C_2G, \quad (17)$$

where C_2 is represented by

$$C_2 = \frac{\text{NOCT}(^\circ\text{C}) - 20}{800\ \text{W/m}^2}. \quad (18)$$

NOCT in equation (18) is the nominal operating cell temperature defined as the temperature reached by open circuited cells in a module under 800 W/m^2 cell surface irradiance and ambient temperature of 20°C and so on. NOCT of a typical commercial module is approximately 45 ± 2°C, accordingly, C_2 is approximately equal to 0.3°C/(W/m^2).

Therefore, if the PV nominal power value under STC condition (P_n) is known, it will be possible to figure out the PV power value at any time via

$$P_m = P_n\frac{G}{G_{\text{STC}}}[1 - \gamma(T_c - 25)], \quad (19)$$

where G_{STC} is the irradiation under standard test conditions (STC), which is equal to 1000 W/m^2.

In a conventional PV plant of crystalline silicon, the conversion efficiency is in the range 15%-20% so 75% to 80% of the solar energy is not being used effectively [22]. Besides, the unused solar energy will heat up the panel, causing a decrease in the efficiency of the electricity generation.

Transferring the thermal energy to a heat transfer fluid, we obtain useful thermal energy and refrigerate the photovoltaic cells at the same time. This system, which can make use of solar light and thermal simultaneously, is called photovoltaic/thermal integrated system (PV/T system) (Figure 7).

Table 2: EH system component parameters.

Component name	Efficiency (%)	Capital cost (€/kW or €/m^2)	Fixed cost (€/kW)	Variable cost (€/kWh)	Lifetime (years)
Gas boiler	70	800	10	0.02	20
Heat pump	3.2 (COP)	1000	8.7	0	20
PV	Variable	250	2	0	30
PV/T	Variable	700	10	0	30

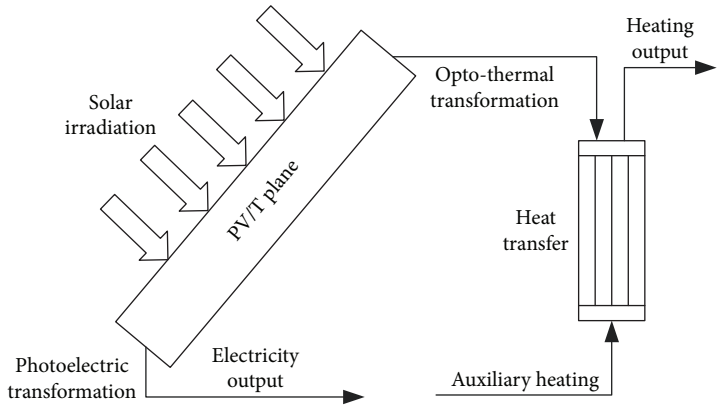

Figure 7: The schematic of the PV/T system.

The calculation about the thermal part of the PV/T system is shown as follows:

$$Q_S = G \times A_C, \tag{20}$$

$$Q_C = \eta_h \times Q_S, \tag{21}$$

$$Q_C = \text{cpw} \times \text{mw}_\text{C} \times (t_{\text{we\_c}} - t_{\text{ws\_c}}), \tag{22}$$

$$Q_d = A_C \times U_d \times (t_{\text{we\_c}} - t_0), \tag{23}$$

$$Q_{\text{cons}} = \text{cpw} \times m_r \times \left(t_{\text{d\_ini}} - t_{\text{pipe}}\right), \tag{24}$$

$$\begin{aligned} \int_0^{\text{inct}} (Q_C - Q_d - Q_{\text{cons}}) &= \text{cpw} \times \text{mw}_\text{d} \times (t_{\text{d\_fin}} - t_{\text{d\_ini}}) \\ &= \text{cpw} \times m_r \times \left(t_{\text{consig}} - t_{\text{d\_fin}}\right). \end{aligned} \tag{25}$$

Q_S represents the radiation projected onto the PV plane, Q_C is the heat absorbed by the panel, η_h is the heating efficiency of the PV/T systems, mw_C is the fluid mass under the panel, $t_{\text{we\_c}}$ and $t_{\text{ws\_c}}$ are output and input temperature of under panel fluid, respectively, Q_d is the heat loss of natural convection heat transfer between the tube and the environment, and t_0 represents the ambient temperature. Q_{cons} refers to the heat loss of direct heat transfer between the fluid in the pipe and the pipe wall. $t_{\text{d\_ini}}$ and $t_{\text{d\_fin}}$ are fluid input and output pipe temperature, respectively. t_{pipe} is the temperature of pipe shall and t_{consig} is the final demand fluid temperature. Q_a is the auxiliary energy supply. The thermodynamic relationship characterizing the PV/T is shown in Figure 8.

In addition, the thermal part of the PV/T system efficiency η_h is influenced by many factors, such as solar irradiation and pipe fluid temperature, as represented in

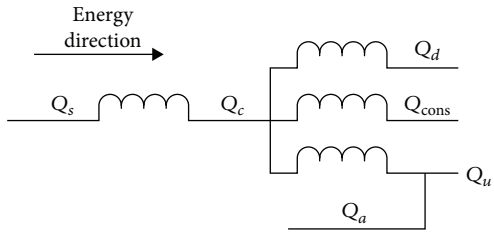

Figure 8: Thermodynamic relationship in the PV/T systems.

$$\eta_h = \eta_0 - a_1 \times \frac{(T_e - T_a)}{G} - a_2 \times \frac{(T_e - T_a)}{G}. \tag{26}$$

In this equation, η_0 means the optical performance of the PV/T system, a_1 and a_2 are the thermal loss coefficients, in this paper set as 3.3 (W/m^2)/K and 0.018 (W/m^2)/K^2, respectively, and I represents solar irradiation. T_e is the average value of pipe fluid temperature and T_a is the ambient temperature.

First of all, the scale of the PV/T system water tank is shown in Table 3.

$$V_d = \pi \left(\frac{D_d}{2}\right)^2 H_d, \tag{27}$$

$$A_d = 2\pi \left(\frac{D_d}{2}\right)^2 + \pi D_d H_d. \tag{28}$$

The temperature of the PV and PV/T panels is shown in Figure 9. Obviously, the PV/T surface temperature is higher

Table 3: Hot water tank dimension.

Name	Signal	Value	Unit
Tank volume	V_d	0.326	m^3
Panel surface area	A_c	3.26	m^2
Tank height	H_d	0.744	m
Tank bottom diameter	D_d	0.744	m
Tank surface area	A_d	5.22	m^2

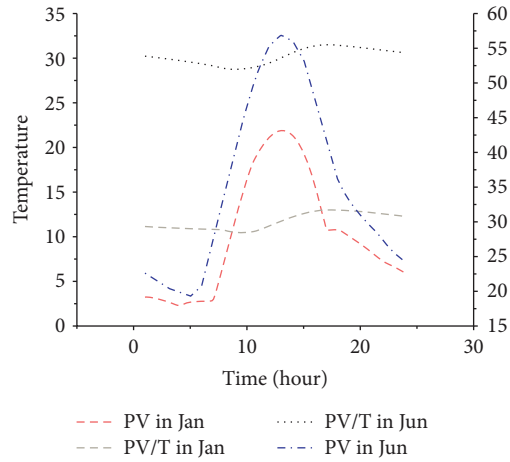

Figure 9: Panel temperature comparison between the PV and PV/T systems.

than the PV panel in summer season. In order to decrease the PV/T surface temperature, the hot water tank size should be enlarged. In this case, the hot water tank size is related to panel area, when V_d/A_c value is increased from 0.1 to 0.2, the hot water tank will become bigger gradually. Figure 9 presents the panel temperatures for $V_d/A_c = 0.2$.

The thermal efficiency of the PV/T system is shown in Figure 10.

The average daily electricity generation for 1 m^2 PV and PV/T panel with an 18% efficiency is shown in Figure 11 for every month. A PV/T system can generate more electricity in winter months and part of spring and autumn.

4. Energy Hub Results

The optimum values of the EH system components' capacity for the building under analysis were calculated in a previous paper [22] for a 20 kW HP and 65 m^2 of PV systems. With the combination of PV+PVT, the best results were obtained for a HP of 20 kW, 36 m^2 of PV modules, and 30 m^2 of PV/T. With the operating condition of 20 kW HP and 65 m^2 of PV systems, the cost reaches the minimum value 10727 euro/year. The CO_2 emission achieved 13560 kg/year at the meantime. Comparing these values with the total supply of electricity and heat from the electrical grid and natural gas network, respectively (see Table 1), a reduction of 8.42% in cost was obtained with a reduction of 37.54% in CO_2 emission. Otherwise, the results considering the optimal capacity of PV/T and PV systems (36 m^2 of PV and 30 m^2 of PV/T) are shown in Table 4. Compared with the result shown in Table 1, a great improvement is reached. A decrease of 10.61% in cost with a reduction of 30.02% in electricity consumption and 60.07% in gas consumption is achieved. A reduction of 39.66% in CO_2 emissions is also obtained.

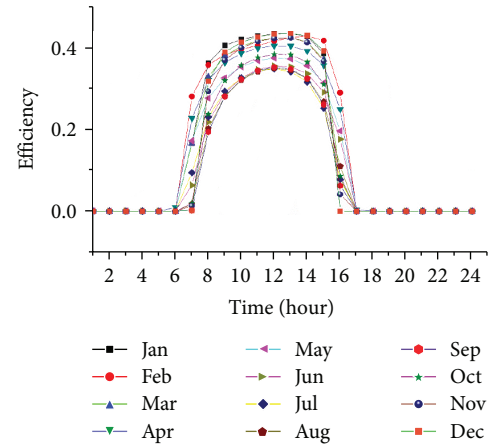

Figure 10: Daily efficiency for different months.

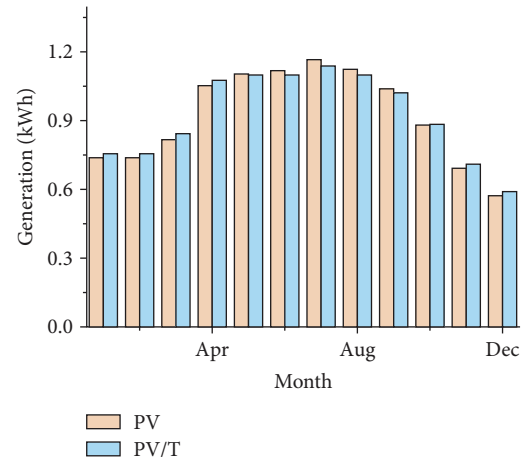

Figure 11: Average daily electricity generation for 1 m^2 of PV and PV/T panel for every month.

Table 4: Cost, electricity and gas consumption, and CO_2 emissions for the optimal sizing (20 kW of HP, 36 m^2 of PV, and 30 m^2 of PV/T).

Cost (euro/year)	Electricity consumption (kWh/year)	Gas consumption (kWh/year)	CO_2 emission (kg/year)
10470	43800	4419	13100

5. Energy Hub with a Battery-Based ESS

The renewable generation is sometimes greater than customer's demand and part of electricity generated from a

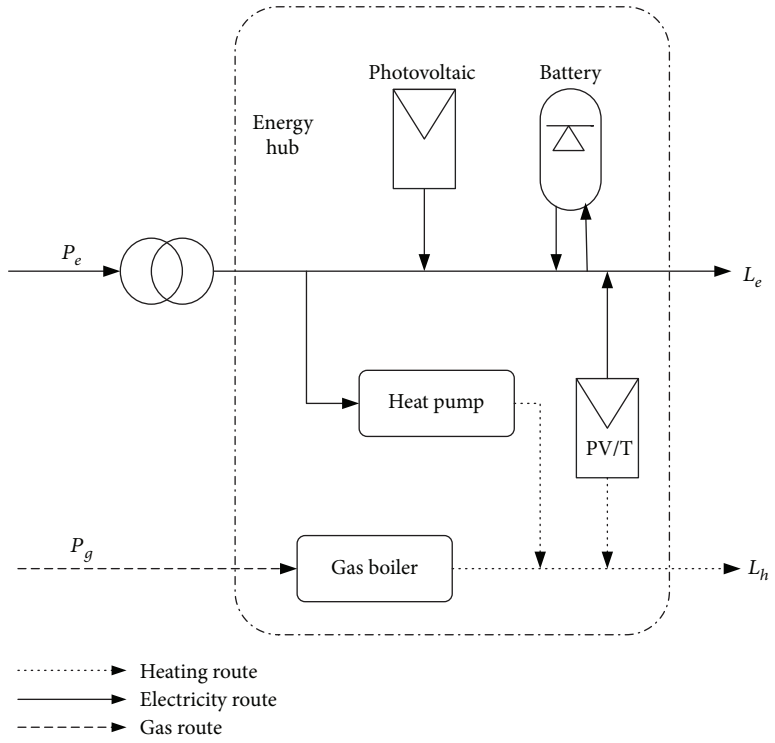

Figure 12: Ultimate energy hub structure for a building.

Table 5: Advanced EH system performance for several BESS sizes.

Battery capacity (kWh)	Cost (euro/year)	Electricity consumption (kWh/year)	CO_2 emission (kWh/year)
1	10211	41690	12520
2	10205	41650	12510
3	10200	41620	12500
4	10195	41590	12500
5	10190	41560	12490
6	10185	41530	12480
7	10179	41500	12470
10	10165	41410	12450
12	10214	41340	12430
15	10230	41280	12410

PV plant must be injected into the electrical grid or wasted. In order to improve the EH system performance, a BESS is integrated. The BESS provides a solution in case the renewable energy cannot be injected due to the regulation code (zero-injection schemes) or due to technical restrictions at that time. It is even able to provide voltage and frequency support and contribute to demand response procedures such as peak shaving. So, the advanced EH system structure is shown in Figure 12 with the BESS integrated.

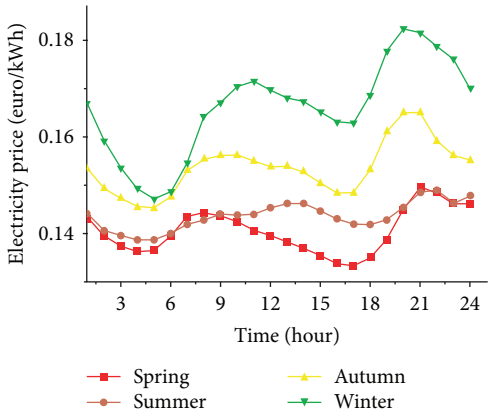

Figure 13: Daily electricity price for different seasons.

In this work, the battery is optimally charged and discharged to compensate the generation fluctuation of the PV and PV/T. The BESS dynamic model used is

$$E \times \mathrm{SOC}_t = E \times \mathrm{SOC}_0 + t_s \sum_{\gamma=1}^{t} \left\{ \eta_c P_{b,\gamma} - \frac{\bar{P}_{b,\gamma}}{\eta_d} \right\}, \quad 1 \le t \le N. \tag{29}$$

E is the BESS capacity, SOC_0 is the initial SOC of the BESS, SOC_t is the SOC at the given time t, $P_{b,\gamma}$ and $\bar{P}_{b,\gamma}$ are the continuous variables at time step γ, and $t_s \sum_{\gamma=1}^{t} \eta_c P_{b,\gamma}$

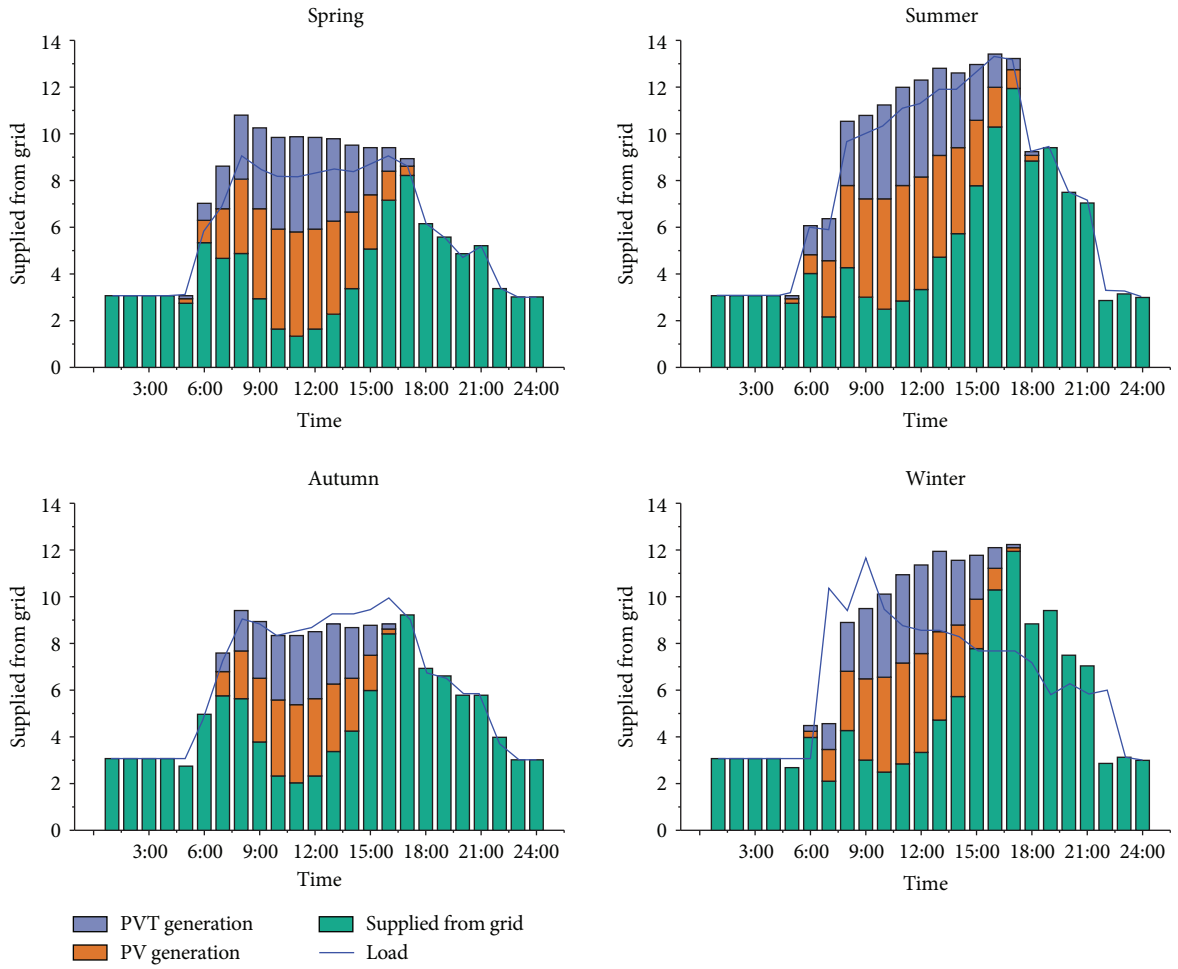

Figure 14: Energy structure in the proposed energy hub for different days of the four seasons.

and $t_s\sum_{\gamma=1}^{t}(\bar{P}_{b,\gamma}/\eta_d)$ are the BESS energy during the charging and discharging period, respectively.

BESS constraints are applied to the model:

$$0.2 \le SOC_t \le 0.8, \quad t = 1, \cdots, N, \tag{30}$$

$$P_{b,t} \times \bar{P}_{b,t} = 0, \quad t = 1, \cdots, N. \tag{31}$$

N is the number of sampling intervals; in this case, it is 8760.

The capacity limits are given in equations (30) and (31), which does not allow the BESS to charge and discharge at the same time. This constraint also permits the idle state of BESS.

The BESS involved here is an ideal model, which has a linear charge state and a SOC around 0.2 to 0.8. The optimization objective of BESS is the same as the previous system, minimum cost and minimum CO_2 emission. Due to the economic goal of the whole system, the BESS will be charged during the low electricity price period, and when the electricity price is high, it will discharge energy to satisfy the demand.

Now the matrix of this advanced EH system is shown as follows; S is the storage coupling matrix and E is the storage energy.

$$L = C_1 P + C_2 R - SE. \tag{32}$$

Table 5 shows the results of the simulation for different sizes of battery. The lowest cost is obtained for a battery of 10 kWh of capacity. Comparing with the results of Table 4, 2.91% cost and 5.46% CO_2 emission will be saved. Comparing with the results of Tables 1, 13% cost, 42.7% CO_2 emission, and 33.8% will be saved. Therefore, the simulation results confirm that adopting the proposed advanced EH system and the related optimization scheduling process not only significantly promotes efficiency and cost savings but also provides relief from the global pressure of greenhouse effect.

Four representative days for the four seasons of the year have been selected. Daily electricity prices for these days are presented in Figure 13. In Figure 14, the energy absorbed from PV, PV/T, and electrical grid for these representative days is shown.

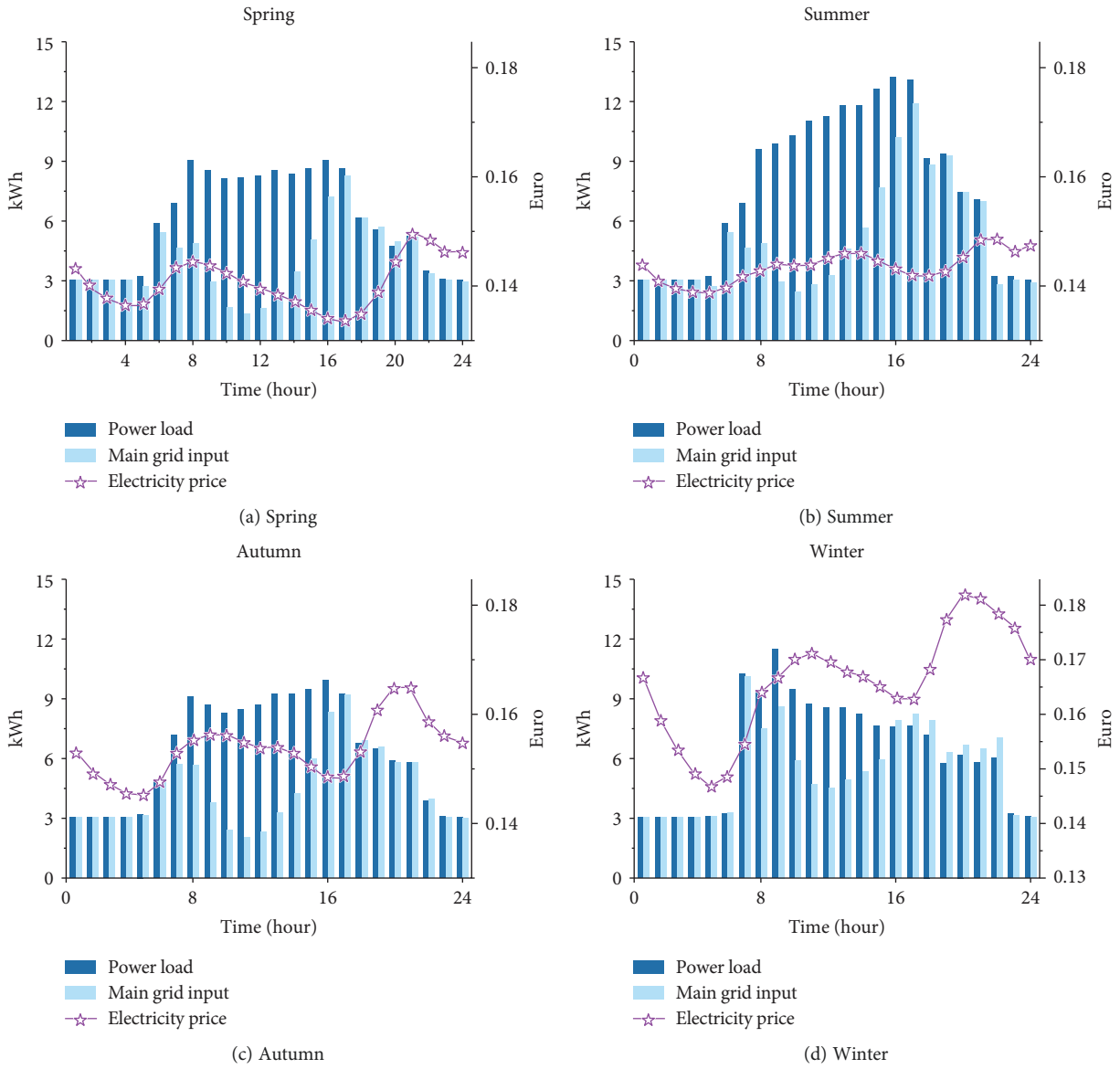

Figure 15: Comparison between electrical grid supply without the EH system and with the advanced EH system for different representative days for the four seasons.

Sometimes the supply is not totally equal to the demand due to the presence of BESS. When electricity price is high, the EH system avoids the supply of electricity from the electrical grid. In Figure 14, it is easy to find out that the EH system generates more electricity than the demand in autumn and winter which is related to the fact that electricity price is higher in these two seasons; indeed, the EH system chooses discharging via BESS to meet the customers' demand.

During the high demand hours, the EH system showed an outstanding performance for reduction of the absorption of energy from the electrical grid (Figure 15). Calculating according to that high demand hours from 8:00 a.m. to 16:00 p.m., the EH system can reduce 65.3%, 61.6%, 57.9%, and 33.9% absorption from the electrical grid. Meanwhile, during this period, 6.21 euro, 7.95 euro, 6.37 euro, and 4.14 euro are saved per day, respectively, for this building. Besides, due to the function of BESS, the electrical grid will supply more electricity when the price is relatively low.

6. Conclusions

This paper proposes an advanced multicarrier energy hub integrating not only generation components such as PV and PV/T systems but also a battery-based energy storage system to improve the performance. The optimal capacity of each component of the multicarrier energy hub in order to minimize the energy cost and the CO_2 emissions is based on the use of an optimization scheduling process solved on the YALMIP platform in the MATLAB environment. The simulation results confirm that large-scale utilization of the proposed approach will lead to significant cost and CO_2 savings.

Data Availability

The data used to support the findings of this study are included within the article.

Conflicts of Interest

The authors declare that there is no conflict of interest regarding the publication of this paper.

Acknowledgments

The authors gratefully acknowledge the support of National Natural Science Foundation of China (Grant 51876070) and (Grant 51576074).

References

[1] A. A. Bayod-Rújula, "Future development of the electricity systems with distributed generation," *Energy*, vol. 34, no. 3, pp. 377–383, 2009.

[2] H. X. Zhao and F. Magoulès, "A review on the prediction of building energy consumption," *Renewable and Sustainable Energy Reviews*, vol. 16, no. 6, pp. 3586–3592, 2012.

[3] P. Favre-Perrod, "A vision of future energy networks," in *Power engineering society inaugural conference and exposition in Africa*, pp. 13–17, Durban, South Africa, 2006.

[4] G. T. Ayele, P. Haurant, B. Laumert, and B. Lacarrière, "An extended energy hub approach for load flow analysis of highly coupled district energy networks: illustration with electricity and heating," *Applied Energy*, vol. 212, pp. 850–867, 2018.

[5] P. Cui, J. Shi, F. Wen et al., "Optimal energy hub configuration considering integrated demand response," *Dianli Zidonghua Shebei/Electric Power Automation Equipment*, vol. 37, pp. 101–109, 2017.

[6] M. Moeini-Aghtaie, A. Abbaspour, M. Fotuhi-Firuzabad, and E. Hajipour, "A decomposed solution to multiple-energy carriers optimal power flow," *IEEE Transactions on Power Systems*, vol. 29, no. 2, pp. 707–716, 2014.

[7] A. Sheikhi, M. Rayati, S. Bahrami, and A. Mohammad Ranjbar, "Integrated demand side management game in smart energy hubs," *IEEE Transactions on Smart Grid*, vol. 6, no. 2, pp. 675–683, 2015.

[8] T. Ma, J. Wu, and L. Hao, "Energy flow modeling and optimal operation analysis of the micro energy grid based on energy hub," *Energy Conversion and Management*, vol. 133, pp. 292–306, 2017.

[9] D. Setlhaolo, S. Sichilalu, and J. Zhang, "Residential load management in an energy hub with heat pump water heater," *Applied Energy*, vol. 208, pp. 551–560, 2017.

[10] S. Le Blond, R. Li, F. Li, and Z. Wang, "Cost and emission savings from the deployment of variable electricity tariffs and advanced domestic energy hub storage management," in *2014 IEEE Pes General Meeting | Conference & Exposition*, pp. 1–5, National Harbor, MD, USA, July 2014.

[11] S. D. Beigvand, H. Abdi, and M. La Scala, "A general model for energy hub economic dispatch," *Applied Energy*, vol. 190, pp. 1090–1111, 2017.

[12] X. Tian and R. Zhao, "Energy network flow model and optimization based on energy hub for big harbor industrial park," *Journal of Coastal Research*, vol. 73, pp. 298–303, 2015.

[13] M. C. Bozchalui, S. A. Hashmi, H. Hassen, C. A. Canizares, and K. Bhattacharya, "Optimal operation of residential energy hubs in smart grids," *IEEE Transactions on Smart Grid*, vol. 3, no. 4, pp. 1755–1766, 2012.

[14] M. Rastegar and M. Fotuhi-Firuzabad, "Load management in a residential energy hub with renewable distributed energy resources," *Energy and Buildings*, vol. 107, pp. 234–242, 2015.

[15] K. Orehounig, R. Evins, V. Dorer, and J. Carmeliet, "Assessment of renewable energy integration for a village using the energy hub concept," *Energy Procedia*, vol. 57, pp. 940–949, 2014.

[16] M. Sepponen and I. Heimonen, "Business concepts for districts' energy hub systems with maximised share of renewable energy," *Energy and Buildings*, vol. 124, pp. 273–280, 2016.

[17] A. Sharif, A. Almansoori, M. Fowler, A. Elkamel, and K. Alrafea, "Design of an energy hub based on natural gas and renewable energy sources," *International Journal of Energy Research*, vol. 38, no. 3, pp. 363–373, 2014.

[18] T. Ha, Y. Zhang, V. V. Thang, and J. Huang, "Energy hub modeling to minimize residential energy costs considering solar energy and BESS," *Journal of Modern Power Systems and Clean Energy*, vol. 5, no. 3, pp. 389–399, 2017.

[19] P. G. Charalambous, G. G. Maidment, S. A. Kalogirou, and K. Yiakoumetti, "Photovoltaic thermal (PV/T) collectors: a review," *Applied Thermal Engineering*, vol. 27, no. 2-3, pp. 275–286, 2007.

[20] Eurostat, https://ec.europa.eu/eurostat/statistics-explained/index.php/Natural_gas_price_statistics#Natural_gas_prices_for_household_consumers.

[21] A. Parisio, C. del Vecchio, and A. Vaccaro, "A robust optimization approach to energy hub management," *International Journal of Electrical Power & Energy Systems*, vol. 42, no. 1, pp. 98–104, 2012.

[22] A. A. Bayod-Rújula, Y. Yuan, A. Martínez-Gracia, J. Wang, J. Uche, and H. Chen, "Modelling and simulation of a building energy hub," *Proceedings*, vol. 2, no. 23, article 1431, 2018.

Hindawi
International Journal of Photoenergy
Volume 2019, Article ID 6067539, 20 pages
https://doi.org/10.1155/2019/6067539

Research Article

Development of a Daily Databank of Solar Radiation Components for Moroccan Territory

Mohammed Benchrifa,[1] **Hajar Essalhi**,[1] **Rachid Tadili**,[1] **Mohammed N. Bargach**,[1] **and Abdellah Mechaqrane**[2]

[1]*Mohammed V University of Rabat, Faculty of Science, B. P 1014 Rabat, Morocco*
[2]*Sidi Mohamed Ben Abdellah University, Faculty of Science and Technology, B. P, Fez, Morocco*

Correspondence should be addressed to Mohammed Benchrifa; simobenchrifa@gmail.com

Received 6 December 2018; Revised 4 March 2019; Accepted 26 March 2019; Published 16 May 2019

Guest Editor: Angel A. Bayod-Rújula

The main objective of this work is to create a daily updated database that includes all components of solar radiation, either energetic or spectral radiation. This will lead us to quantify the Moroccan solar potential and to determine the dimensions of all types of solar thermal and photovoltaic systems. Consequently, the obtained database will be the fundamental support for engineers, designers, and all organizations interested in developing solar systems, in different regions throughout Morocco. It will also be a basic tool for researchers in modelling and simulating the new solar systems. Firstly, we used one year's worth of measurements of the different components of the solar radiation, provided by the National Meteorological Department, to establish the extrapolation equations between the global radiation at the reference site and the global radiation of twenty-eight other sites. As well as with the same measurements, we developed the correlation equations between the global solar radiation and the other solar radiation components. Secondly, from ten years of Fez station's daily global radiation measurements and through the extrapolation equations, we were able to estimate the global radiation of all Moroccan cities. Then, by using the obtained global radiation data and the correlation equations, we predicted the other components of solar radiation. Subsequently, with a new measurement campaign carried out on several sites, we validated the estimation models by using the usual statistical indicators. In addition, we compared our results with those obtained by other estimation models. The resulting differences for each solar component display the advantage of our model with errors under 6%. To facilitate the use of our results, we compiled them into maps representing the spread of solar radiation across Morocco.

1. Introduction

The various applications of solar energy developed in recent years have increased the need for solar radiation component data. However, in most cases, there are not enough stations covering the entire country, and the existing stations do not measure all energetic and spectral components of solar radiation.

To remedy this problem, several works using different prediction models have been developed to estimate these solar components around the world. Among these models, we can cite physical models, empirical models [1–3], artificial neural network models [4–7], hybrid models using a combination of several methods [8, 9], and the models based on the satellite images data [10, 11]. Thus, the physical models are based on physical parameters, which estimates the global radiation from insolation duration [12, 13], meteorological variables [14, 15], and spatial variables [16] in different sky conditions [17, 18]. Also, this model predicts the diffuse solar radiation [19] from the global radiation [20], the insolation duration [21], or the clarity index [22, 23] in different climatic zones [21] and in different sky conditions [24, 25]. However, the same parameters have been used to predict the direct [26], inclined [27] solar radiation and spectral solar components [28, 29].

Table 1: Linear models for estimating daily global solar radiation.

Estimation models	Equations	R	Regions
Lemmini's model [32]	$K_t = 0.25 + 0.49\,\sigma$	0.92	Beni-Mellal, Morocco
Bargach's model [31]	$K_t = 0.27 + 0.5\,\sigma$	0.9	Rabat, Morocco
Nfaoui's model [33]	$K_t = 0.26 + 0.52\,\sigma$	0.93	Rabat, Morocco
Zou et al.'s model [7]	$K_t = 0.208 + 0.559\,\sigma$	0.91	Tengchong, China

Table 2: Quadratic and cubic models for estimating daily global solar radiation.

Estimation models	Equations	R	Region
Ben Kaddour's model [34]	$K_t = 0.18 + 0.83\,\sigma$ - $0.31\,\sigma^2$	0.93	Casablanca, Morocco
Zou et al.'s model [7]	$K_t = 0.185 + 0.587\sigma + 0.037\,\sigma^2$ - $0.032\,\sigma^3$	0.93	Aletai, China

This work aims at establishing a solar data bank of energetic components (H_j, H_{bj}, H_{dj}, and $H_{\beta j}$) and spectral components (H_{UVT}, H_{PAR}, and H_{IR}) all over Morocco. However, this work will be completed in two main steps as follows:

(i) First step: we will establish the extrapolation equations to estimate the global solar radiation. Then, we will develop the correlation equations to estimate the other solar radiation components

(ii) Second step: we will use the obtained extrapolation equations to generate the global solar radiation for twenty-eight sites from reference station data. Then, we will bring together the correlation equations and the estimated global radiation to generate the solar energetic and solar spectral component

The obtained results will be subject to a validity test, by comparing them with the measurements collected in available stations. In addition, we will compare our results with those obtained by other estimation models [7, 30–34].

Finally, all results will be presented in maps [35–38] showing all over Morocco.

2. Review of Solar Component Estimation Models

All solar energy conversion systems require knowledge of the solar radiation component measurements. However, in most cases, these measures are not available. For this reason, several studies have been carried out for estimating the components of solar radiation from different variables such as the duration of insolation, the fraction of insolation, and the coefficient of clarity.

2.1. Global Solar Radiation Estimation Models. The simplest model for estimating solar radiation is the linear model developed by Angstrom and after revised by Prescott. This model establishes a direct relationship between the global solar radiation and the insolation fraction [39].

The Angstrom-Prescott model is as follows:

$$K_t = a + b\,\sigma, \tag{1}$$

where a and b are empirically determined regression constants.

Based on the linear model, several studies have been performed to predict global solar radiation. Among these models, we can cite the models in Table 1.

Other models have been developed such as the quadratic model and cubic model. Among these models, we can mention the models in Table 2.

2.2. Diffuse Solar Radiation Estimation Models. The value of diffuse solar radiation constitute an important data in the study of solar conversion systems. However, several works have focused on the prediction of this component and this by using different variables such as the clarity index K_t. Among these works, we found the following:

(i) Ben Kaddour's model [34]

$$K_d = 0.961 + 0.456\,K_t - 3.344\,K_t^2 + 1.67\,K_t^3 \tag{2}$$

(ii) Nfaoui's model [33]

$$K_d = \begin{cases} 0.98, & K_t < 0.1, \\ -1.48K_t^2 + 0.15k_t + 0.98, & K_t \geq 0.1, \end{cases} \qquad R = 0.93 \tag{3}$$

(iii) Wang et al.'s model, Injinagaui, China [25]

$$K_d = 14.7924\,K_t^4 - 23.95\,K_t^3 + 11.1612\,K_t^2 - 2.4767\,K_t + 1.1665, \qquad R = 0.88 \tag{4}$$

3. Data Description

3.1. Used Data. The Laboratory of Solar Energy and the Environment (LESE) of Mohammed V University of Rabat, Morocco, has, since 2008, a network of five

Table 3: The geographical data of the measuring stations' locations [40].

Measuring station	Latitude (°) Φ	Longitude (°) λ	Altitude (m)
Agadir	30.38	-9.57	18
Al-Hoceima	35.18	-3.83	12
Beni-Mellal	32.37	-6.4	468
Bouarfa	32.52	-1.95	1100
Casa	33.57	-7.67	56
Dakhla	23.77	-15.93	10
El Jadida	33.23	-8.52	27
Essaouira	31.52	-9.78	7
Ifran	33.5	-5.17	1663
Kenitra	34.3	-6.6	5
Laayoun	27.17	-13.22	63
Larache	35.18	-6.13	46
Marrakech	31.62	-8.03	463
Meknes	33.88	-5.53	548
Midelt	32.68	-4.73	1508
Nador	35.15	-2.92	7
Nousar	33.37	-7.57	200
Ouarzazate	30.93	-6.9	1136
Oujda	34.78	-1.93	465
Errachidia	31.93	-4.4	1037
Safi	32.28	-9.23	43
Sidi Ifni	29.37	-10.18	49
Sidi Sliman	34.23	-6.05	51
Tangier	35.72	-5.75	15
Tantan	28.6	-11.08	229
Taza	34.22	-4	509
Tetouan	35.57	-5.33	5
Rabat	34	-6.83	75

measuring stations installed in Rabat, Fez, Tangier, Tetouan, and Marrakech. These stations measure all components of solar radiation and climatic variables such as the following:

(i) Energy components: global, diffuse, and direct solar radiation, as well as the overall inclined plane

(ii) Spectral components: ultraviolet, infrared, and synthetically active light solar radiation

(iii) Climatic variables: ambient temperature, relative humidity, wind speed, wind direction, and precipitation

In addition to these measures, the National Meteorological Department has made available to us one year of climatic variables and solar component measurements for 29 stations of the national network.

Table 3 represents the geographical data of the measuring stations' locations.

3.2. Acquisition of Data. For each station, the following instruments record the measurements of the different components of the solar radiation [41]:

(i) The Kipp & Zonen brand SP-Lite pyranometer for global solar radiation measurements (2% accuracy). The same type of instrument was used to measure the diffuse radiation, but with a sun visor strip to hide the direct radiation

(ii) Pyrheliometer mounted on a follower type Eppley model NIP 31820 E6 to measure direct solar radiation (accuracy 0.5%)

(iii) Total Ultraviolet Radiometer (TUVR) model, type Eppley for measuring the total solar ultraviolet radiation (accuracy 2%)

(iv) Radiometer model NIP 31820 E6, type Eppley, for the measurement of radiation infrared (precision 0.5%)

(v) Quantum sensor SKP215, type Campbell Scientific for the measurement of photosynthetically active radiation PAR (accuracy 0.5%)

(vi) Anemometer equipped with a wind vane model wind monitor 05103, type Campbell Scientific, for the measurement of wind speed and direction (accuracy 0.25%)

(vii) Temperature and relative Humidity Probe HMP45C, manufactured for Campbell Scientific by Vaisala (temperature accuracy 0.2%, humidity accuracy 1%)

(viii) Rain Gauge ARG100, manufactured by Environmental Measurements for Campbell Scientific, to measure precipitation (accuracy 4%)

3.3. Storing Data. All instruments mentioned before are connected to a data acquisition unit (CR10X) with a storage module. Using a computer program, we integrate the measurements collected every 5 seconds over an hour. The obtained hourly values are stored in the raw data files. Then the raw data files are processed and tested to detect and eliminate erroneous values and replace some missing values. In the end, the hourly values are integrated to obtain the daily values.

3.4. Characteristics and Description of the Reference Site. The Fez station has been selected as a reference site because of its central geographical location. This city is known as the cultural capital of Morocco (33° 56′N, Longitude 4° 99′W, elevation 579 m) characterized by a seasonal climate, cold and rainy during winter, dry and warm during summer, and mild during spring and autumn [42].

The radiometric station was placed at the top of the Faculty of Science and Technology of Fez's building. The site of the station is completely clear of any shadow effect.

Statistical analysis of this station's data shows a very small percentage of missing or erroneous data (15 erroneous or

Table 4: The equations used for the global radiation extrapolation in Morocco.

Site	a_{site}	b_{site}	R^2
Agadir	0.79	994	0.89
Al-Hoceima	0.94	-181	0.85
Beni-Mellal	0.94	409	0.8
Bouarfa	0.81	780	0.8
Casa	0.91	322	0.82
Dakhla	0.7	1907	0.84
El Jadida	0.95	50	0.89
Essaouira	0.89	539	0.83
Ifran	0.97	-52	0.83
Kenitra	0.97	-15	0.83
Laayoun	0.8	1285	0.85
Larache	1.01	-383	0.87
Marrakech	0.9	672	0.84
Meknes	0.95	-14	0.85
Midelt	0.85	740	0.81
Nador	0.95	-214	0.85
Nousar	0.95	92	0.86
Ouarzazate	0.85	1151	0.83
Oujda	0.96	-81	0.79
Errachidia	0.76	1372	0.78
Safi	0.96	214	0.78
Sidi Ifni	0.63	1341	0.78
Sidi Sliman	0.96	-75	0.85
Tangier	0.97	-114	0.81
Tantan	0.65	1534	0.77
Taza	0.94	-29	0.85
Tetouan	1	429	0.83
Rabat	1.03	-317	0.93

missing values over 250 390 measured values or 0.006%) throughout the 10-year measurement period (2009-2018).

4. Presentation of the Method

This work aims at establishing a solar data bank of energetic components (H_j, H_{bj}, H_{dj}, and $H_{\beta j}$) and spectral components (H_{UVT}, H_{PAR}, and H_{IR}) all over Morocco. However, this work will be completed in two main steps: firstly, we used one year's worth of measurements of the different components of the solar radiation, provided by the National Meteorological Department, to establish the extrapolation equations between Fez's global radiation and the global radiation of twenty-eight other sites. As well as with the same measurements, for each sites, we developed the correlation equations between the global solar radiation and the other solar radiation components. Secondly, from ten years of Fez station's daily global radiation measurements and through the extrapolation equations, we were able to estimate the global radiation of all Moroccan cities. Then, by using the obtained global radiation data and the correlation equations, we predicted the other components of solar radiation (H_j, H_{bj}, H_{dj}, $H_{\beta j}$, H_{UVT}, H_{PAR}, and H_{IR}).

Thus, we have been able to build a database of different components of solar radiation over ten years for the 29 Moroccan sites. In the end, all the obtained results were tested and validated by using a new series of measurements carried out on the five mentioned stations.

Table 5: Correlation equations for the daily values of the spectral components of solar radiation (Wh/m^2) in function of global solar radiation H (Wh/m^2) for the three sky conditions.

Clarity index intervals	Correlation equations	R^2
$K_t \leq 0.35$	$H_{uv} = 0.048\,H$	0.97
	$H_{PAR} = 0.488\,H$	0.99
	$H_{IR} = 0.46\,H$	0.99
$0.35 < K_t \leq 0.65$	$H_{uv} = 0.044\,H$	0.97
	$H_{PAR} = 0.484\,H$	0.99
	$H_{IR} = 0.471\,H$	0.99
$K_t > 0.65$	$H_{uv} = 0.04\,H$	0.98
	$H_{PAR} = 0.478\,H$	0.99
	$H_{IR} = 0.478\,H$	0.99

Table 6: The performance of models used to estimate daily solar irradiation for the Rabat site.

	RMBE	Mean difference	MAPE	RMSE	Number of values
Global radiation	5.42	252	12.14	14.88	290
Diffuse radiation	-3.63	-77	12.71	15.82	257
Direct radiation	1.45	21.6	14.68	17.52	234
Inclined radiation	-6.21	-365	6.35	7.46	323

5. Extrapolation and Correlation Equations for Daily Solar Components

5.1. Extrapolation of the Daily Global Solar Irradiation. The estimation of global solar radiation can be effected by using several methods, such as the empirical model, ANN model, and satellite imagery. However, the use of these models requires knowledge of several variables and the availability of a database that spans several years. On the other hand, databases are not often available, especially for isolated sites. As a result, to remedy this problem, we developed, as part of this work, an extrapolation method to estimate the global solar radiation. Primarily, this method consists of estimating the global radiation at site where we do not have measurements, from the global radiation measured at another site.

In the first step of this method, from one year of measurements of global radiation for all Moroccan sites, we looked for to establish correlation equations between the global radiation of the different sites and the global radiation of

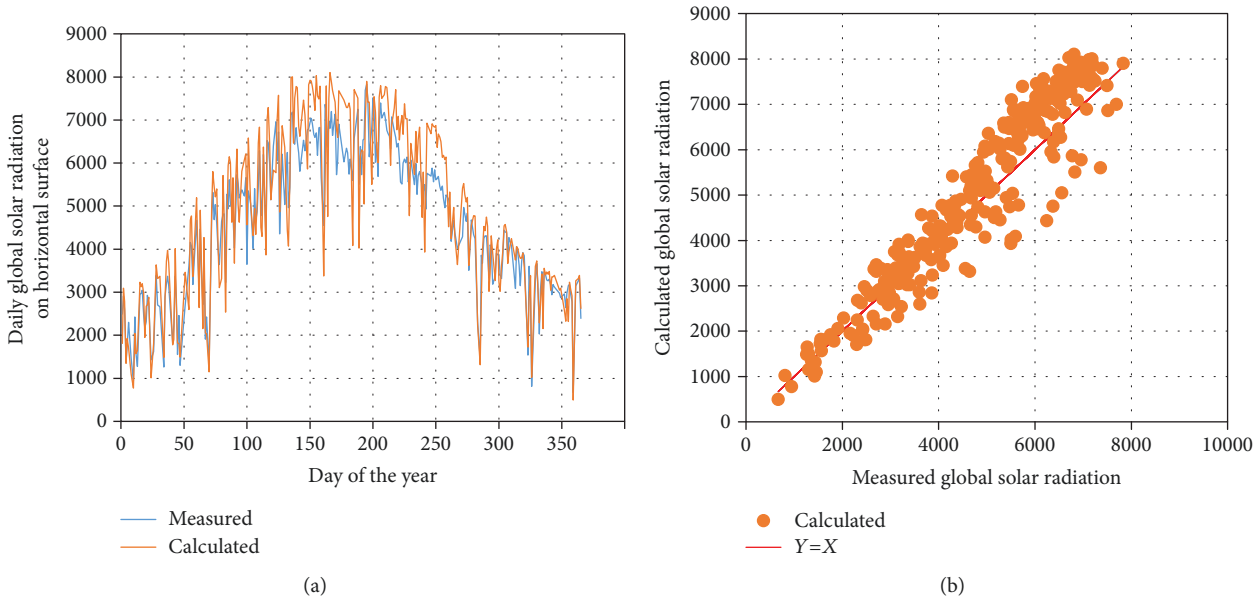

Figure 1: Comparison between measured and estimated values of global radiation.

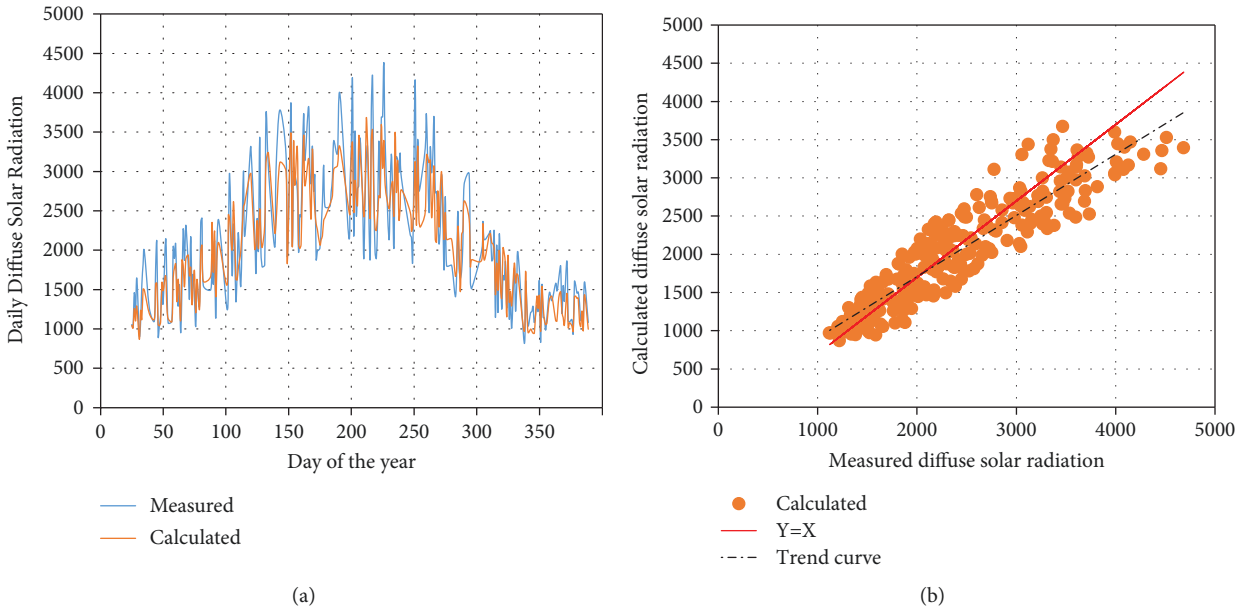

Figure 2: Comparison between measured and estimated values of diffuse radiation using the Collares-Pereira and Rabl's model.

the reference site. For this, we plotted the global radiation values for each site (H_j) according to the global radiation values of Fez's site (H_f), chosen as a reference site.

The obtained shape of the cloud point led us to linear correlations of the type:

$$H_j = a_{\text{site}} H_f + b_{\text{site}}. \quad (5)$$

The coefficients of correlations a_{site} and b_{site} depend strongly on the geographical coordinates of the site and the status of the atmosphere [43]. Table 4 gathers the obtained values from these coefficients for all Moroccan sites.

5.2. Daily Diffuse Solar Irradiation Estimation. The diffuse component is an important factor for evaluating the performance of solar thermal or solar photovoltaic systems. However, several models, involving the clearness index $K_t = (H_j/H_0)$ [44], have been made to estimate this component. Among these models, we can cite the Ruth and Chant's model, the Collares-Pereira and Rabl's model, and the Liu and Jordan model [45].

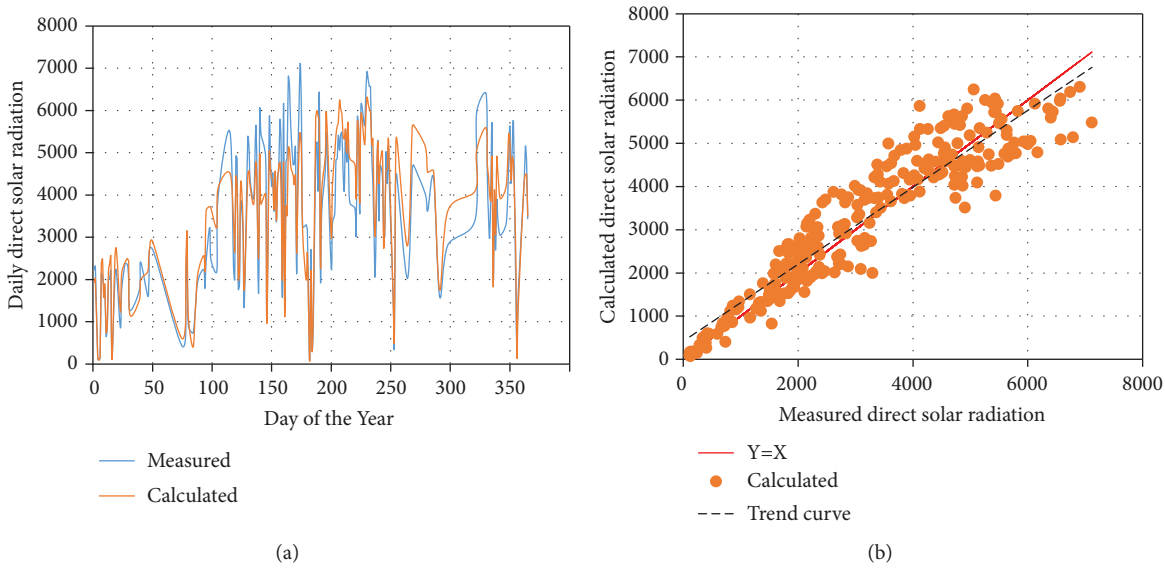

Figure 3: Comparison between measured and estimated direct radiation values.

To find the valid model for Morocco, we compared the estimated diffuse by the mentioned models with the measured diffuse. Then we concluded that the Collares-Pereira and Rabl's model is the most adequate because it produces a minimal error that does not exceed 5%. This model is illustrated by the following equations [42]:

$$K_d = \begin{cases} 0.99\,; K_t < 0.17, \\ 14.648\,K_t^4 - 21.856\,K_t^3 + 9.473\,K_t^2 - 2.272\,K_t + 1.188\,; 0.17 \le K_t \le 0.8. \end{cases} \quad (6)$$

Knowing the diffuse solar irradiation, the direct solar irradiation can easily be inferred by the following equation [46]:

$$H_{bj} = H_j - H_{dj}. \quad (7)$$

5.3. Estimation of Daily Global Solar Irradiations on an Inclined Plane. The solar flux received by an inclined surface consists of three components: a direct component from the solar disk, a diffuse component from the entire celestial vault, and a component reflected by the surrounding soil.

The estimation of the direct component is completed by simple geometric transposition of the direct irradiation of a horizontal plane H_{bj}. On the other hand, for the diffuse component, several models have been proposed for its estimation [45, 47, 48]. Consequently, an earlier study showed that the isotropic model of Liu and Jordan is the most valid for our sites [49]. Most of the cases, the reflected component is the lowest of the three components, and it is generally assumed isotropic.

Table 7: Errors obtained according to clarity index using Rabat measurements.

	H_{UVT} relative error (%)	H_{PAR} relative error (%)	H_{IR} relative error (%)
$K_t < 0.35$	3.8	2.4	2.2
$0.35 < K_t \le 0.65$	1.0	1.8	2.1
$K_t > 0.65$	1.0	1.1	1.1

The general expression of the inclined daily global solar irradiation with an angle β is given by [49]:

$$H_{\beta j} = \underbrace{R_b H_{bj}}_{\text{direct}} + \underbrace{H_{dj}\frac{1+\cos(\beta)}{2}}_{\text{diffuse}} + \underbrace{\rho H \frac{1-\cos(\beta)}{2}}_{\text{reflected}}. \quad (8)$$

R_b is the transposition factor of the direct radiation from a horizontal plane to an inclined plane. It was calculated for a south-oriented plane, by the equation as follows:

$$R_b = \frac{\cos(\delta_j)\cdot\cos(\varphi-\beta)\cdot\sin(\omega_{j\beta}) + \omega_{j\beta}\cdot\sin(\delta_j)\cdot\sin(\varphi-\beta)}{\cos(\delta_j)\cdot\cos(\varphi\varphi\cdot\sin(\omega_j) + \omega_j\cdot\sin(\delta_j)\cdot\sin(\varphi)},$$
$$\omega_{j\beta} = \min\left\{\text{ar cos}\left(-\tan(\delta_j)\cdot\tan(\phi)\right), \text{ar cos}\left(-\tan(\delta_j)\cdot\tan(\phi-\beta)\right\}\right., \quad (9)$$

where $\omega_{j\beta}$ is the time angle of the sunset on the inclined plane.

The values taken by the tilt angle β, correspond to the characteristic inclinations relative to the latitude of each site: $\beta = \varphi$, $\beta = \varphi + 20$, $\beta = \varphi$-20, and $\beta = 90$ corresponding to the vertical facades.

5.4. Estimation of the Spectral Components of Solar Radiation. Some applications of solar energy require knowledge of the

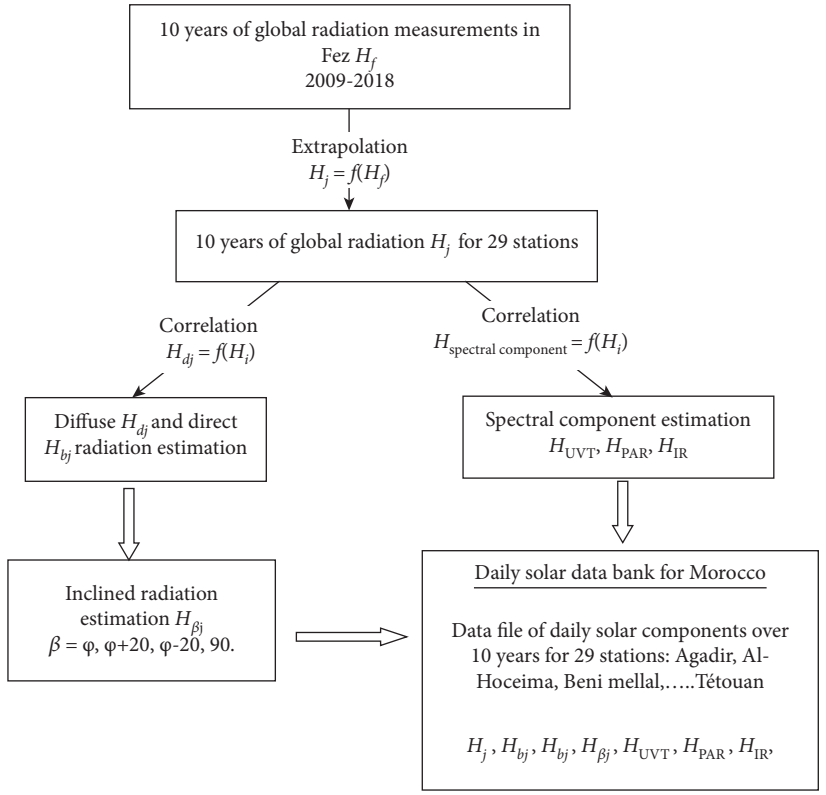

Figure 4: Flowchart of the building steps of the daily solar data bank for Morocco.

Table 8: Sample data file resulting from different estimations.

Year	Nj (day)	Global	Diffuse	Direct	Inclined (φ+20)	Inclined (φ-20)	Inclined (φ)	Inclined (90)	H_{UVT}	H_{PAR}	H_{IR}
2011	1	2808.4	1164.7	1643.7	4683.6	3552.5	4375	4171.9	123.6	1359.3	1322.8
2011	2	2766.6	1202.5	1564.1	4526.3	3470.8	4246.2	4015.1	121.7	1339	1303.1
2011	3	2435.5	1396.1	1039.4	3499.8	2894.4	3383.5	3018.3	107.2	1178.8	1147.1
2011	4	2515.6	1368.7	1146.9	3710.5	3021.7	3565.1	3217.8	110.7	1217.6	1184.8
2011	5	2629.9	1318.1	1311.8	4028	3208.8	3836.5	3520.3	115.7	1272.9	1238.7
2011	6	2844.2	1192.5	1651.7	4669	3574.9	4378.7	4136.5	125.1	1376.6	1339.6
2011	7	2396	1444.7	951.3	3314.2	2805.5	3235.5	2827.6	105.4	1159.7	1128.5
2011	8	2797.1	1250	1547.1	4458.7	3472.3	4209.8	3922.6	123.1	1353.8	1317.4
2011	9	2608.6	1375	1233.6	3860	3139.2	3708	3341.1	114.8	1262.6	1228.7
2011	10	3083.6	1077.5	2006.1	5291.3	3954.6	4918.1	4715.2	135.7	1492.5	1452.4
2011	11	3201.2	1010.7	2190.5	5617.9	4147.9	5198.1	5022.8	128	1530.2	1530.2
2011	12	2695.6	1368.1	1327.5	4022.1	3256.3	3857.7	3480.8	118.6	1304.7	1269.6
2011	13	3228.4	1024.4	2204	5613.5	4167.3	5206	5002.4	129.1	1543.2	1543.2
2011	14	3130.4	1110.8	2019.6	5265.8	3982.2	4918.6	4660.2	137.7	1515.1	1474.4
2011	15	3253.6	1042.2	2211.4	5595.9	4181	5203.6	4967.9	130.1	1555.2	1555.2
2011	16	3160.8	1126.4	2034.4	5264.7	4005	4930	4642.1	139.1	1529.8	1488.7
2011	17	2880.3	1341.1	1539.2	4373.3	3507.7	4181.2	3783.1	126.7	1394.1	1356.6
2011	18	3239.3	1114.8	2124.5	5395.9	4106.4	5055	4748.2	142.5	1567.8	1525.7
2011	19	2272.2	1593.9	678.3	2748	2531.8	2782.5	2248.4	100	1099.7	1070.2
2011	20	3094.1	1268.5	1825.6	4850.4	3821.8	4606.8	4210.1	136.1	1497.5	1457.3
2011	21	3321.7	1132	2189.7	5464.3	4190.8	5136.6	4781.2	146.2	1607.7	1564.5

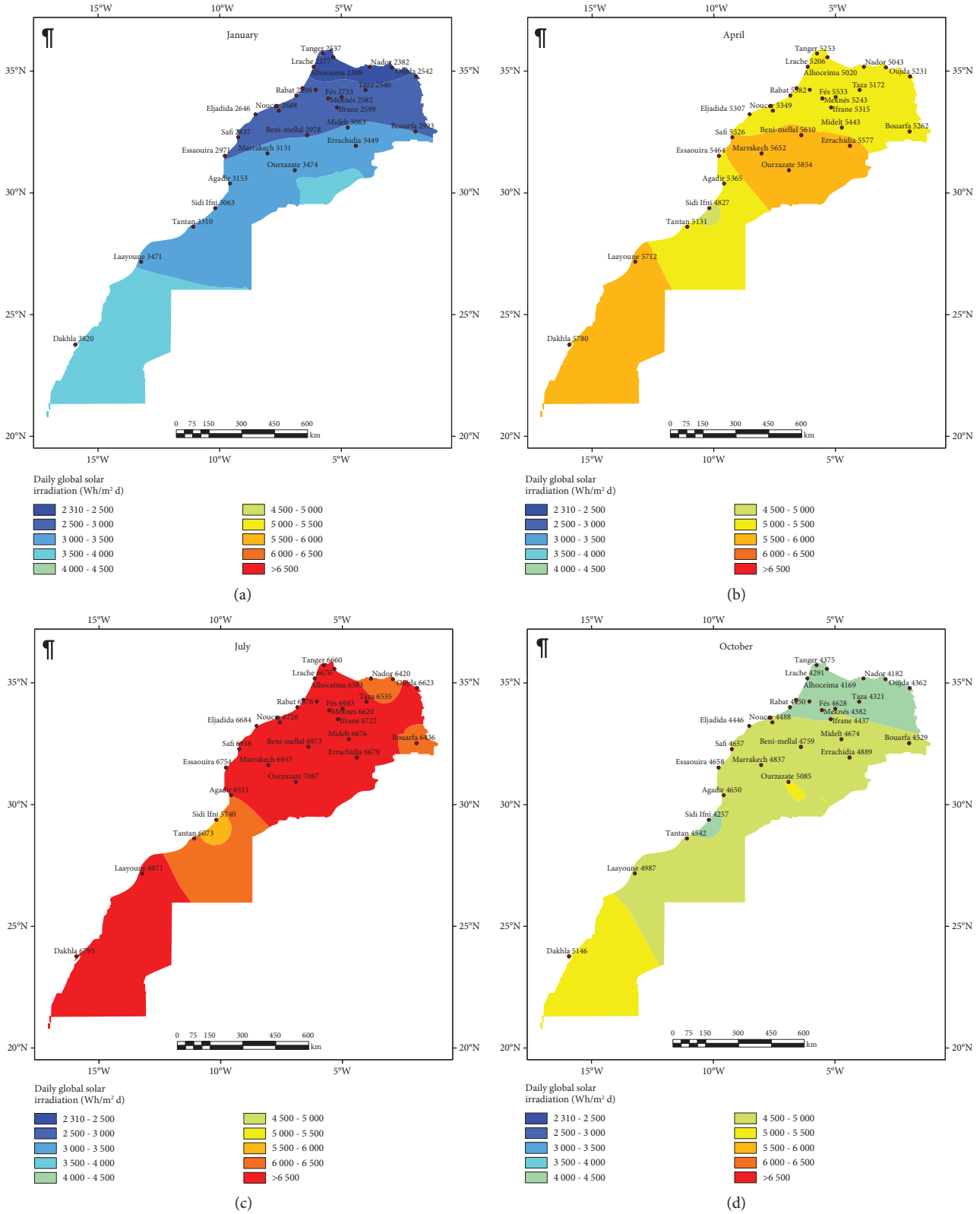

FIGURE 5: Maps of the monthly average values of daily global irradiations on a horizontal plane, coming from Morocco. Maps of global solar radiation on a horizontal plane (a–d).

spectral components of solar radiation, namely, the ultraviolet component (H_{UVT}) which is involved in the study of the atmosphere and the variations in the ozone layer thickness. The photosynthetically active component noted as H_{PAR} (photosynthetically active radiation) intervenes during the photosynthesis process and plant development; knowing the

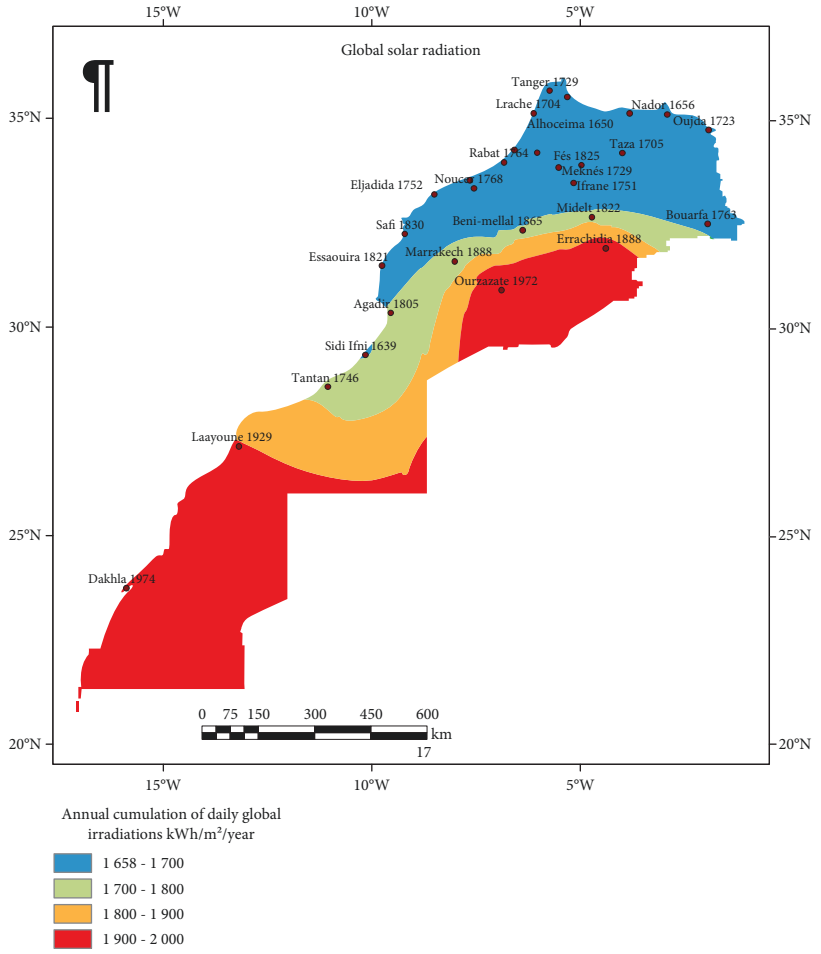

FIGURE 6: Map of annual cumulation of daily global irradiations on a horizontal plane incident in the Moroccan territory. Map of global solar radiation on a horizontal plane.

H_{PAR} value at various sites allows for the appropriate choice of adapted crops. Lastly, the infrared component H_{IR} is used by satellite techniques to determine the total atmospheric column of the water vapor used by meteorology for the climate prediction [50].

Based on one year's worth of measurements of the different components of the solar radiation provided by the National Meteorological Department, we noticed that the variations of the global radiation and the spectral components, functioning in time, have the same rate. As a result, we searched correlation equations connecting the global solar radiation to the spectral solar radiation.

For this, we graphed each spectral component according to the global radiation, which gave us linear equations of the form $y = ax$. To improve the correlation coefficients, we defined three intervals according to the meteorological state of the day characterized by its clearness index K_t [51]. The results are presented in Table 5.

6. Performance Evaluation and Model Validation

To evaluate the quality of the models used to estimate the solar radiation components, we compared the estimated values generated by the different models against the measured values by using the usual statistical indicators such as the relative error (RMBE), the mean absolute error (MAE), the mean absolute percentage error (MAPE), and the mean squared error (RMSE) [34, 38].

$$\begin{aligned} \text{RMBE} &= 100\frac{\sum_{i=0}^{n}(p_i - m_i)}{\sum_{i=0}^{n} m_i}, \\ \text{MAE} &= \frac{\sum_{i=0}^{n}|p_i - m_i|}{N}, \\ \text{MAPE} &= \frac{1}{N}\sum_{i=0}^{n}\left|\frac{p_i - m_i}{m_i} * 100\right|, \\ \text{RMSE} &= \frac{100}{\bar{m}}\sqrt{\frac{\sum_{i=0}^{n}(p_i - m_i)2}{N}}. \end{aligned} \tag{10}$$

6.1. Validation of Energy Component Models. Using the measurements provided by the Solar Energy and Environment Laboratory's station network, we were able to calculate the statistical indicator and validate the estimation models. However, these calculations were effected

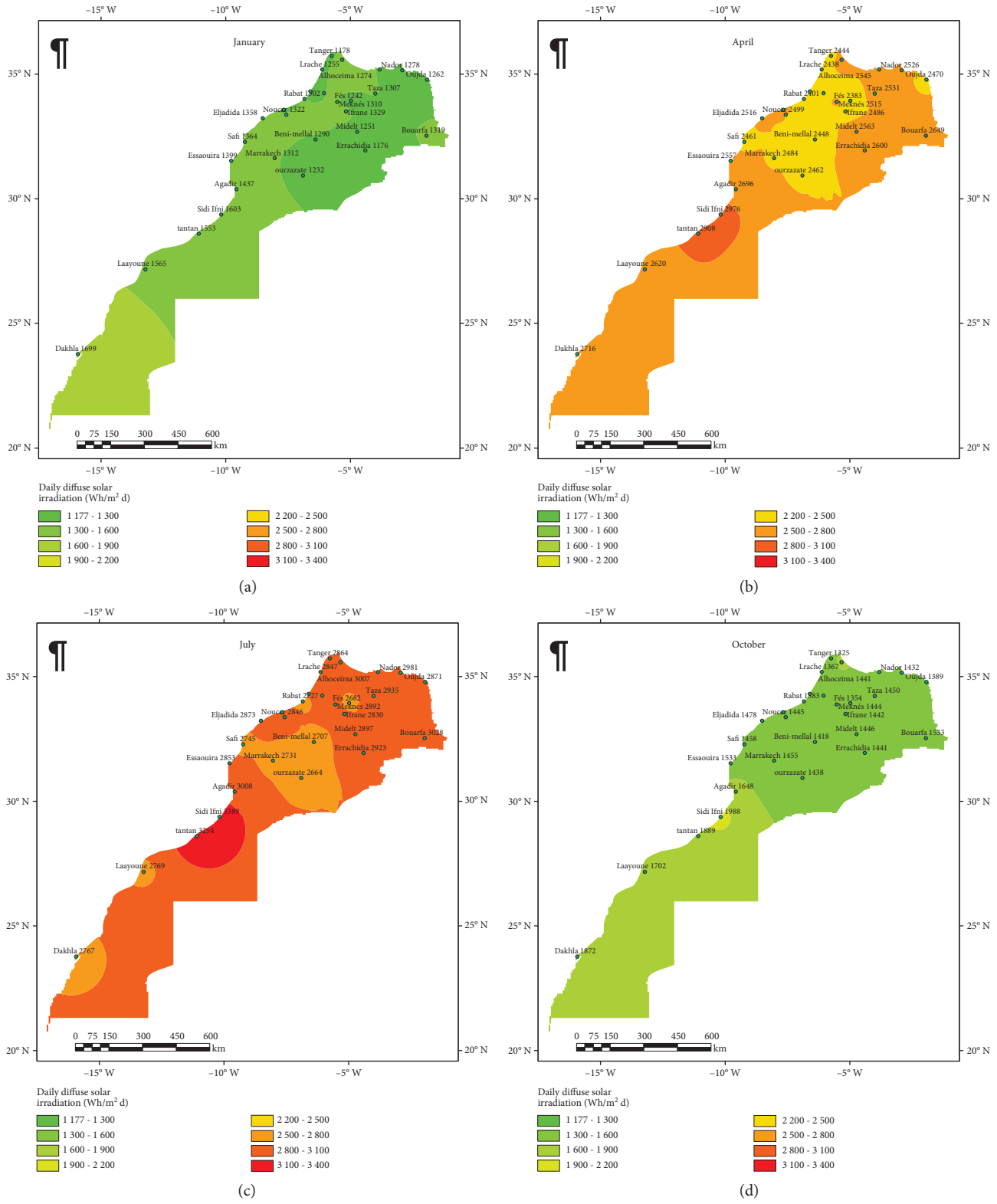

Figure 7: Maps of the monthly average values of daily diffuse irradiations on a horizontal incident plane in Morocco. Maps of diffuse solar radiation on a horizontal plane (a–d).

for all sites previously mentioned. Table 6 and Figures 1–3 are examples of the obtained results for the Rabat Site.

6.2. Validating Spectral Components. The formulas for estimating the spectral components of solar radiation from the measurement of global solar radiation were developed

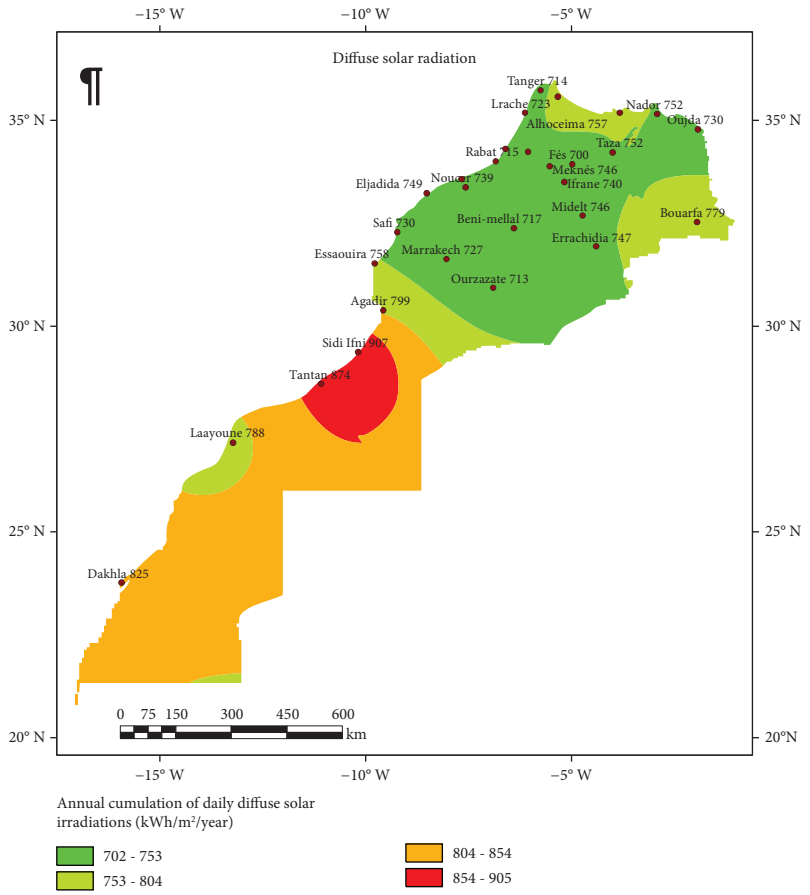

FIGURE 8: Map of annual cumulation of daily diffuse irradiations on a horizontal plane incident in the Moroccan territory. Map of diffuse solar radiation on a horizontal plane.

according to the state of the day characterized by its K_t clarity index. The results in Table 7 revealed that the proposed models estimate the spectral components with remarkable accuracy since the maximum deviations obtained do not exceed 4%.

For all obtained equations, we found that the conditions of the sky (overcast, moderately covered, and clear) have a significant influence mainly on the H_{UV}/H_j fraction. This result is similarly found to the one in Brazil [52]. An estimate of the ultraviolet component that ignores the state of the sky can induce an error of up to 10%. However, the H_{PAR}/H_j and H_{IR}/H_j fractions are less influenced by cloud cover.

7. Application: Building a Ten-Year Database

After having established and validated the extrapolation and correlation equations, we applied them to estimate the different solar radiation components for the different Moroccan sites. The obtained results constitute a solar data bank for all over Morocco for ten years.

Figure 4 represents the flow-chart summarizing all the steps followed for generating all solar components from the site of the Fez.

8. Representative Year

In preproject studies that aimed at sizing solar systems or characterizing the solar radiation potential, it is often necessary to have a minimum of data. Therefore, it is essential to compact the database. Consequently, after having established, for each site, a database for ten years, we were obliged to select a representative year of this database for facilitating the database exploitation.

To determine the representative year, we proceed as follows: for the ten years of estimated values, we calculated an average year. Then, this average year is successively compared to each one of the ten years of estimated values. Consequently, the year with the minimum difference is selected as the representative year.

This work was done for all sites and led us to select 2011 as the representative year for the period between 2009 and 2018.

9. Results

After having established and validated the various components of solar radiation, we created a solar data bank for all over Morocco. Thus, for each city, the obtained results

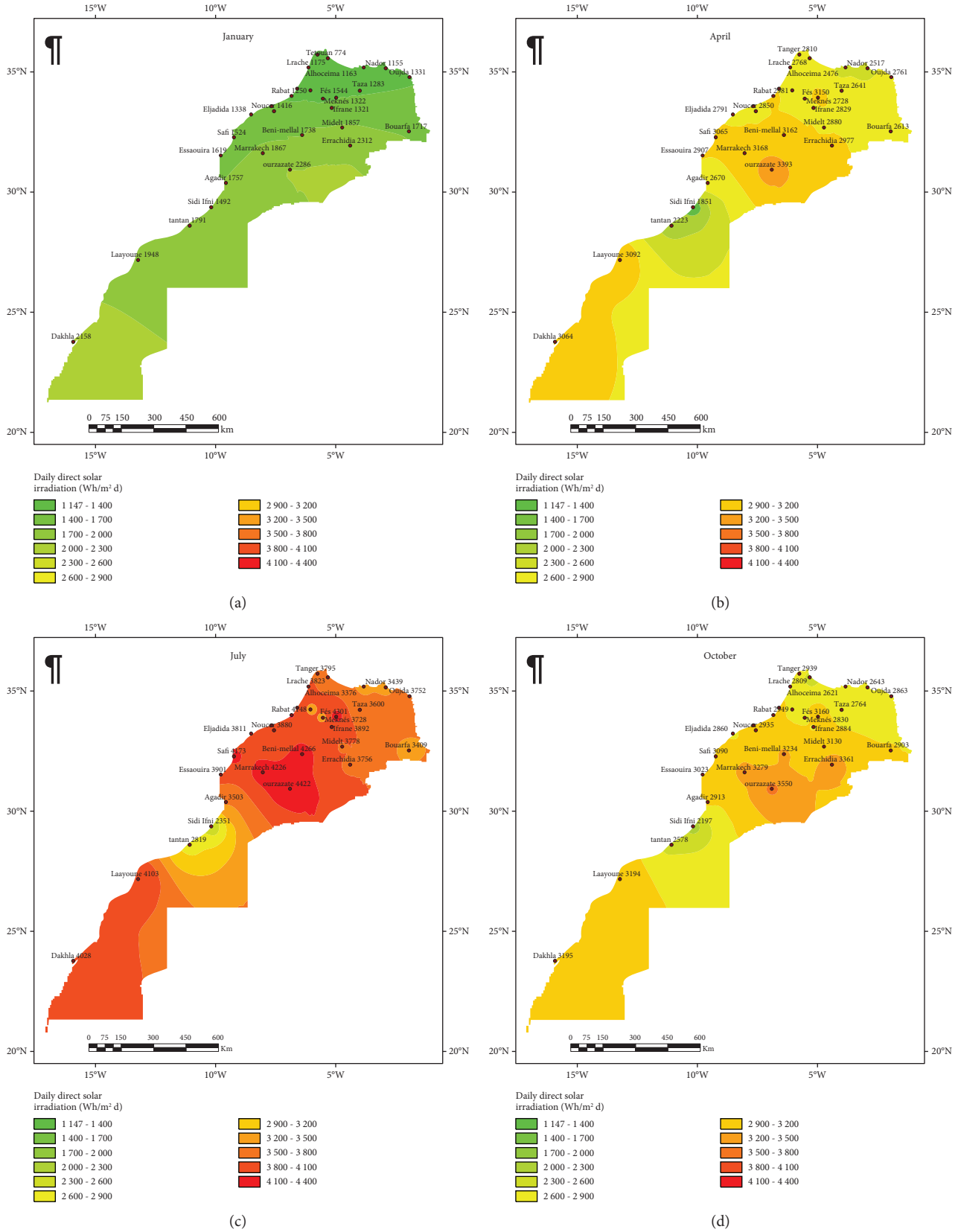

FIGURE 9: Maps of the monthly average daily direct irradiation in the Moroccan territory. Maps of direct solar radiation on a horizontal plane (a–d).

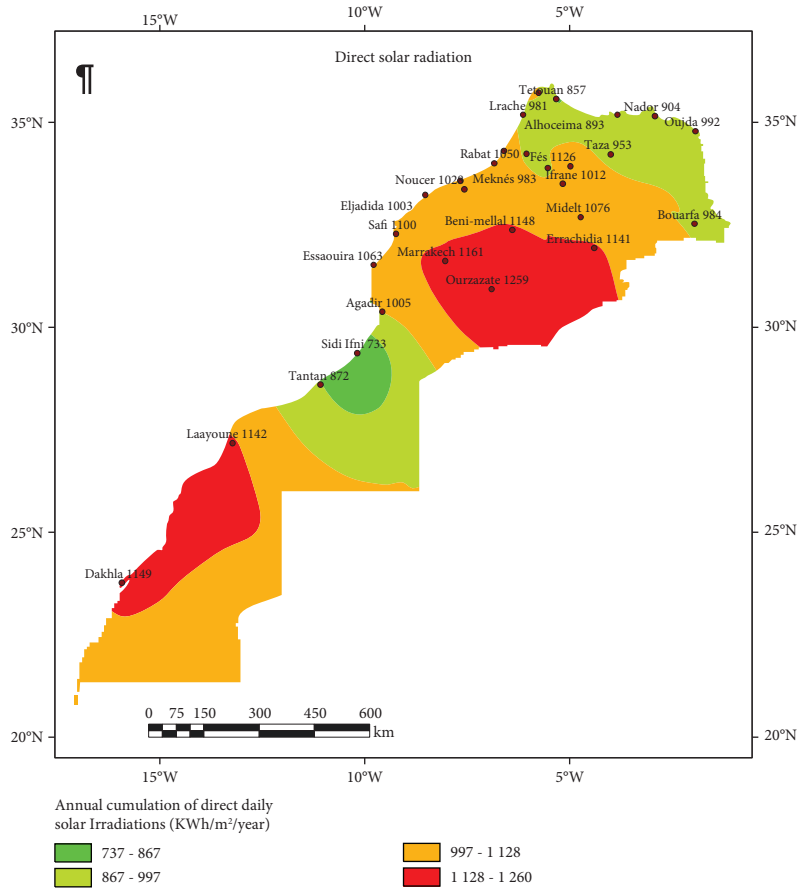

FIGURE 10: Map of annual cumulation of daily direct irradiations on a horizontal plane incident in the Moroccan territory. Map of direct solar radiation on a horizontal plane.

were grouped in two files easily usable; the first one contains the solar components over ten years between 2009 and 2018, and the second contains the solar components of the representative year. However, this second file has the advantage of providing the maximum of climatic information on a site with a minimum of data. This type of file is requested especially for the preliminary project studies.

Table 8 represents a sample data file resulting from different estimations.

In addition, to give an overall view of the results, we projected the obtained values of the solar irradiations on the Moroccan map. Furthermore, In order to reduce the number of figures, we chose to represent only the monthly averages of the daily values of the midseason month of the representative year. Thus, for all cities, we obtained twenty-three maps that gather the various solar irradiations. As a result, for each of the four solar components (global, direct, diffuse, and inclined), we have five maps; four of them represent seasonal values and the last one represent the annual cumulative values. The obtained maps are shown in Figures 5–12. The three spectral components (H_{UVT}, H_{PAR}, and H_{IR}) are shown in Figure 13.

Finally, in order to evaluate the variation of solar radiation components, we calculated, for each solar component, the monthly averages of the daily values (Table 9) and the minimum (Table 10) and maximum (Table 11) daily values for each month of the representative year. Caused by the large number of stations, only the results obtained in Rabat's station are presented in Tables 9–11 (minimum, maximum, and averages of the daily values for each month of the representative year).

10. Discussion

From the obtained results in Tables 6 and 7 and the curves in Figures 1–3, we can conclude that the correlation between the estimated and measured solar energy resources has a good level of precision. This was reflected in the following observations:

(i) The annual average of daily relative errors for energetic components of solar radiation does not exceed 5.42% for global radiation, -3.63% for diffuse radiation, and 2.32% for direct radiation

(ii) The comparative curves show that the measured and estimated values of solar radiation undergo almost the same variations throughout the year and the differences that do not exceed 12.14% for global

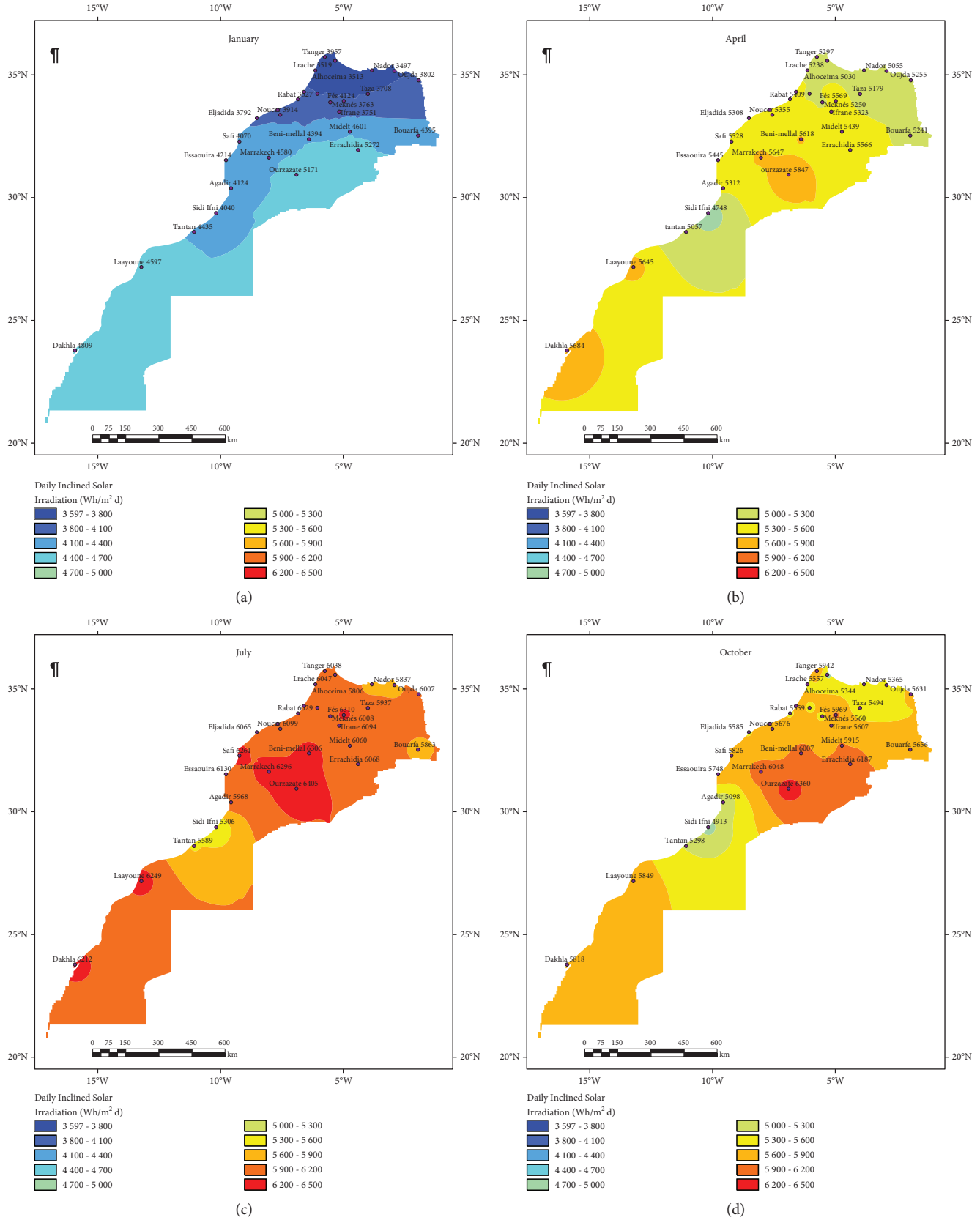

Figure 11: Maps of the monthly average values of the daily global irradiations on inclined planes (β = the site latitude). Maps of the global solar radiation inclined with β = the latitude's site (a–d).

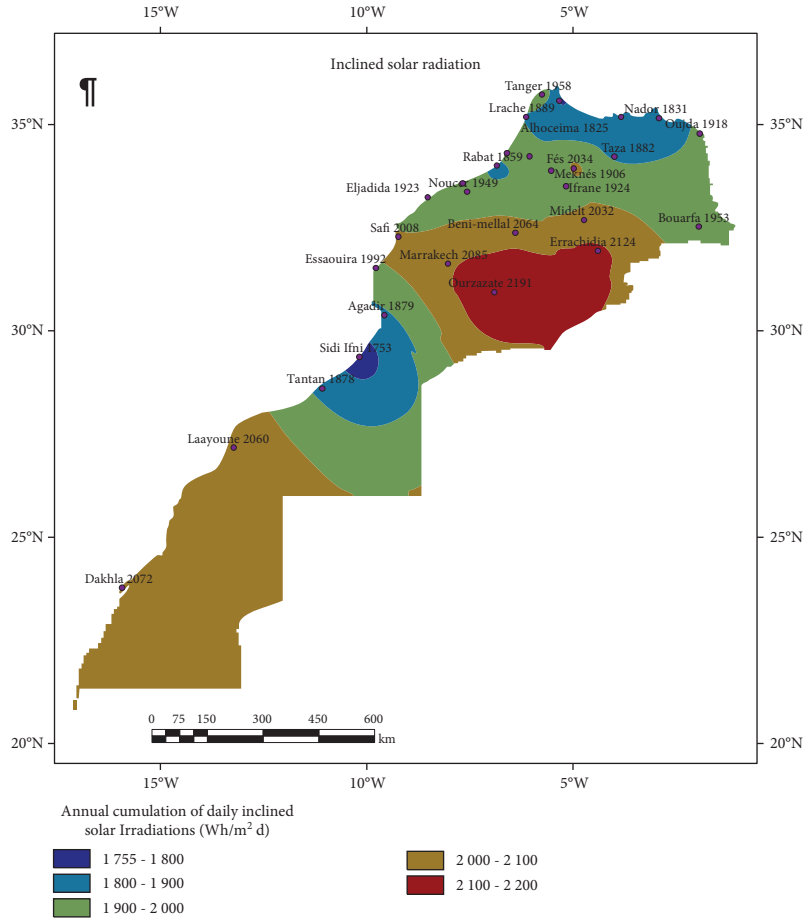

FIGURE 12: Map of annual cumulation of daily global irradiations on inclined planes (β = the site latitude) incident in the Moroccan territory. Map of the global solar radiation inclined with β = thelatitude's site.

radiation, 12.71% for diffuse radiation, and 17% for direct radiation. This result is approved by comparing the cloud of points generated by representing the estimated values in function of the measured values, with the first bisector, which gave almost identical trends

(iii) For the spectral components, the relative errors do not exceed 3.8% for H_{UVT}, 2.4% for H_{PAR}, and 2.2% for H_{IR}

When we compared our results with those obtained by other authors' models, we noticed that our method diminished the differences between estimated and measured values. In brief, the results of this comparison are shown in Table 12.

Regarding the maps in Figures 5–12, we notice that the Moroccan territory receives a very important sunshine during all seasons. However, there is an unequal distribution of solar resources between regions. This inequality is reflected by maximum values of radiation in the south and south-east regions such as Ouarzazate, Er-Rachidia, Laayoun, and Dakhla and by minimum values of solar radiation in the north regions such as Tangier, Tetouan, and the coastal zone between Agadir and Tan-Tan where there is a microclimate.

In addition, the spectral component maps show a similar distribution compared to the global radiation maps, reflected by intense irradiations in the south and south-east regions and low radiations in the north and the microclimate zone. The linear aspect of the estimation equations connecting the spectral components to the global radiation explains this result.

11. Conclusion

Through this work, we have been able to create a database that brings together the different components of solar radiation at daily scale over a period of ten years from 2009 to 2018. This database regroups more than one million daily values (1,058,500 values), which divides into 36,500 values for each site.

To create this databank, at first, we developed a model to estimate the different components of the solar radiation, and then we validated this model by comparing the estimated values with the measurements provided by installed stations. As a result, the validity tests showed that our model presents minimal errors that do not exceed 5.42% for global radiation, 3.8% for H_{UVT}, 2.4% for H_{PAR}, and 2.2% for H_{IR}. In addition, we compared our results with those obtained by other

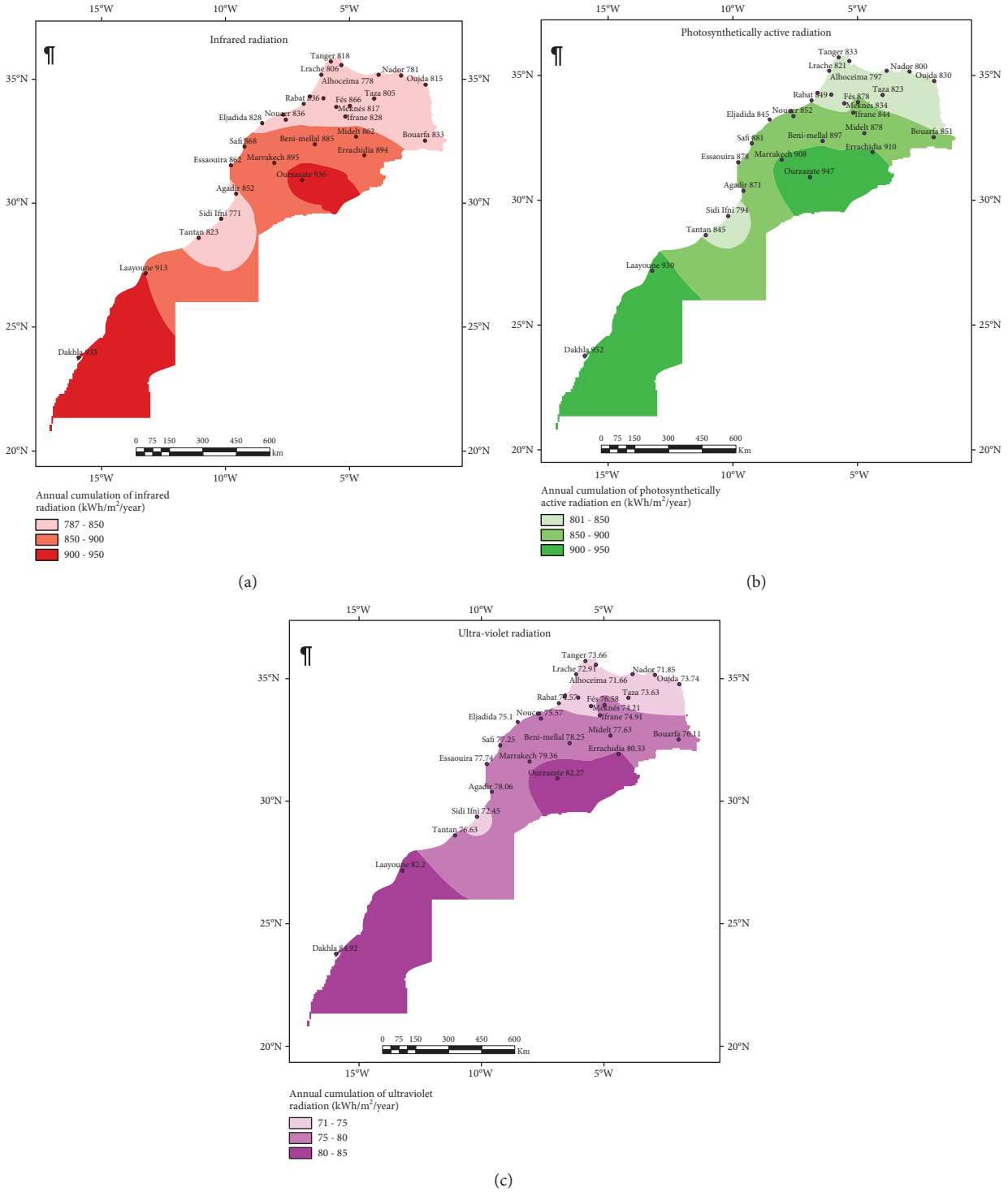

Figure 13: Maps of the annual cumulation of daily irradiations of the spectral components of solar radiation (H_{UVT}, H_{PAR}, and H_{IR}) on the horizontal plane incident in the Moroccan territory. Maps of solar radiation spectral components (a–c).

estimation models developed around the world. The results of this comparison showed the advantage to our model with errors do not exceed 6%.

To get the general idea about the solar radiation distribution over all Morocco and considering the large number of data, we chose to present the obtained results in maps. In order to reduce the number of figures, we chose to represent only the monthly averages of the daily values of the midseason month for the representative year and the annual cumulative solar irradiations for the same year. As a result, twenty-three maps of solar radiation were generated. Consequently, we have been able to complete and to update the various works affected in our laboratory, and we have been able to build a complete, clean, and precise

Table 9: Representative year monthly averages of various solar radiation component daily values (Wh/m^2).

	H_j	H_{dj}	H_{bj}	$H_{\beta j}$ ($\beta = \phi + 20$)	$H_{\beta j}$ ($\beta = \phi$-20)	$H_{\beta j}$ ($\beta = \phi$)	$H_{\beta j}$ ($\beta = 90$)	H_{UVT}	H_{PAR}	H_{IR}
Jan	2552	1302	1250	3772	3072	3627	3252	112	1235	1200
Feb	3881	1471	2409	5271	4556	5223	4247	162	1864	1843
Mar	4493	1966	2527	4718	4848	5075	3273	189	2162	2131
Apr	5382	2401	2981	4704	5511	5409	2822	231	2595	2542
May	5859	2825	3035	4489	5777	5414	2491	251	2825	2769
June	6942	2723	4220	4900	6722	6129	2459	299	3390	3334
Jul	6668	2727	3941	4900	6522	6029	2546	293	3312	3255
Aug	5742	2552	3191	4743	5788	5571	2723	273	3077	3020
Sept	5001	1878	3124	5051	5349	5526	3327	227	2655	2638
Oct	4231	1383	2848	5533	4913	5559	4313	177	2076	2064
Nov	2585	1196	1503	3820	3117	3681	3264	116	1312	1290
Dec	2470	1024	1508	4129	3128	3855	3682	119	1374	1358

Table 10: Representative year monthly maximum values.

	H_j	H_{dj}	H_{bj}	$H_{\beta j}$ ($\beta = \phi + 20$)	$H_{\beta j}$ ($\beta = \phi$-20)	$H_{\beta j}$ ($\beta = \phi$)	$H_{\beta j}$ ($\beta = 90$)	H_{UVT}	H_{PAR}	H_{IR}
Jan	3322	1635	2211	5618	4191	5206	5023	146	1608	1565
Feb	5050	2044	3759	6730	5919	6743	5481	206	2414	2414
Mar	6463	2786	4797	6837	6940	7249	5021	259	3090	3090
Apr	7253	3273	5212	6370	7360	7257	3695	298	3467	3467
May	8140	3570	6084	5837	7962	7312	2922	326	3891	3891
June	8192	3575	5999	5556	7895	7115	2684	338	3916	3916
Jul	7832	3652	5563	5522	7612	6944	2887	337	3833	3833
Aug	7072	3320	4551	5452	7018	6600	3069	312	3683	3683
Sept	5883	2981	4175	6065	6185	6416	4235	276	3303	3303
Oct	5285	2424	3907	6523	6034	6688	5344	224	2659	2659
Nov	3688	1843	2669	5953	4630	5638	5109	163	1946	1946
Dec	3061	1459	2151	5530	4016	5083	4984	139	1583	1583

Table 11: Representative year monthly minimum values.

	H_j	H_{dj}	H_{bj}	$H_{\beta j}$ ($\beta = \phi + 20$)	$H_{\beta j}$ ($\beta = \phi$-20)	$H_{\beta j}$ ($\beta = \phi$)	$H_{\beta j}$ ($\beta = 90$)	H_{UVT}	H_{PAR}	H_{IR}
Jan	1176	1011	59	1051	1185	1167	776	56	574	541
Feb	1884	1074	179	1712	1911	1893	1258	90	919	867
Mar	1114	1103	11	936	1103	1061	672	54	544	512
Apr	886	877	9	741	876	842	531	43	432	407
may	1843	1825	18	1536	1821	1747	1099	89	900	848
June	3303	2193	316	2693	3254	3101	1856	159	1612	1519
Jul	4885	2052	2109	3620	4758	4403	2039	138	1407	1327
Aug	3996	1815	833	3346	3986	3840	2201	173	1904	1853
Sept	2418	1563	171	2265	2494	2502	1592	89	900	848
Oct	2778	801	823	3052	3003	3189	2371	39	395	372
Nov	931	397	315	734	1049	1003	411	19	196	184
Dec	679	616	1	659	702	712	359	30	304	286

Table 12: Relative errors (RMBE) calculated from the values generated by different methods of estimation and the measured values.

Solar components	Our estimation methods	Nfaoui's methods	Lemmini's methods	Bargach's methods	Benkaddour's methods	Zou et al.'s model	Wang et al.'s model
Global solar radiation	5.42%	-11%	-14.7%	-10.6%	14.13%	-17%	
Diffuse solar radiation	-3.63%	12.76%			-8%		11.7%

database covering all Morocco over a period of ten years. This database covers the basic needs of engineers, installers of solar systems, and especially researchers who often need a long-term database.

Nomenclature

H_j: Daily global solar radiation on horizontal surface (Wh/m^2 day)
H_{dj}: Daily diffuse solar radiation (Wh/m^2 day)
$H_{\beta j}$: Daily global solar radiation on tilted surface (Wh/m^2 day)
H_{bj}: Daily beam solar radiation (Wh/m^2 day)
H_f: Daily global solar radiation of Fez's site (Wh/m^2 day)
H_{UVT}: Daily ultraviolet solar radiation (Wh/m^2 day)
H_{PAR}: Daily photosynthetically active radiation (Wh/m^2 day)
H_{IR}: Daily infrared solar radiation (Wh/m^2 day)
H_0: Daily extraterrestrial solar irradiation (Wh/m^2 day)
I_0: Solar constant 1 367 W/m^2
φ: Latitude of the place (°)
δ: Solar declination (°)
R^2: Correlation coefficient (%)
RMBE: Relative error (%)
MAE: Mean absolute error (%)
MAPE: The mean absolute error percentage (%)
RMSE: The mean squared error (%)
K_t: Daily clearness index
K_d: Daily diffuse fraction
σ: Insolation fraction.

Data Availability

The data used to support the findings of this study are available from the corresponding author upon request.

Conflicts of Interest

The authors declare that there is no conflict of interest regarding the publication of this paper.

Acknowledgments

This work was supported by the Arab Fund for Economic and Social Development (AFESD) and Mohammed V University as part of the 2012 emergency plan.

References

[1] J. Fan, L. Wu, F. Zhang et al., "Empirical and machine learning models for predicting daily global solar radiation from sunshine duration: a review and case study in China," *Renewable and Sustainable Energy Reviews*, vol. 100, pp. 186–212, 2019.

[2] L. Feng, A. Lin, L. Wang, W. Qin, and W. Gong, "Evaluation of sunshine-based models for predicting diffuse solar radiation in China," *Renewable and Sustainable Energy Reviews*, vol. 94, pp. 168–182, 2018.

[3] L. Zou, L. Wang, L. Xia, A. Lin, B. Hu, and H. Zhu, "Prediction and comparison of solar radiation using improved empirical models and adaptive neuro-fuzzy inference systems," *Renewable Energy*, vol. 106, pp. 343–353, 2017.

[4] N. S. Chukwujindu, "A comprehensive review of empirical models for estimating global solar radiation in Africa," *Renewable and Sustainable Energy Reviews*, vol. 78, pp. 955–995, 2017.

[5] M. Abdel Wahab and K. S. M. Essa, "Extrapolation of solar irradiation measurements: case study over Egypt," *Renewable Energy*, vol. 14, no. 1-4, pp. 229–239, 1998.

[6] O. Nait Mensour, S. Bouaddi, B. Abnay, B. Hlimi, and A. Ihlal, "Mapping and estimation of monthly global solar irradiation in different zones in Souss-Massa area, Morocco, using Artificial Neural Networks," *International Journal of Photoenergy*, vol. 2017, Article ID 8547437, 19 pages, 2017.

[7] L. Zou, A. Lin, L. Wang et al., "Long-term variations of estimated global solar radiation and the influencing factors in Hunan province, China during 1980–2013," *Meteorology and Atmospheric Physics*, vol. 128, no. 2, pp. 155–165, 2016.

[8] W. Qin, L. Wang, A. Lin et al., "Comparison of deterministic and data-driven models for solar radiation estimation in China," *Renewable and Sustainable Energy Reviews*, vol. 81, pp. 579–594, 2018.

[9] L. Wang, O. Kisi, M. Zounemat-Kermani et al., "Prediction of solar radiation in China using different adaptive neuro-fuzzy methods and M5 model tree," *International Journal of Climatology*, vol. 37, no. 3, pp. 1141–1155, 2017.

[10] J. E. Hay, "Satellite based estimates of solar irradiance at the earth's surface–I. Modelling approaches," *Renewable Energy*, vol. 3, no. 4-5, pp. 381–393, 1993.

[11] A. Mechaqrane, *Contribution à l'étude des images du satellite METEOSAT pour la détermination du gisement solaire marocain*, Thèse de 3ème cycle, Faculté des Sciences de Rabat, 1990.

[12] L. E. Akpabio and S. E. Etuk, "Relationship between global solar radiation and sunshine duration for Onne, Nigeria," *Turkish Journal of Physics*, vol. 27, pp. 161–167, 2003.

[13] E. O. Ogolo, "Estimation of global solar radiation in Nigeria using a modified angstrom model and the trend analysis of the allied meteorological components," *Indian Journal of Radio & Space Physique*, vol. 43, pp. 213–324, 2014.

[14] L. Wang, O. Kisi, M. Zounemat-Kermani, G. A. Salazar, Z. Zhu, and W. Gong, "Solar radiation prediction using different techniques: model evaluation and comparison," *Renewable and Sustainable Energy Reviews*, vol. 61, pp. 384–397, 2016.

[15] C. M. Dos Santos, J. L. De Souza, R. A. Ferreira Junior et al., "On modeling global solar irradiation using air temperature

for Alagoas State, Northeastern Brazil," *Energy*, vol. 71, pp. 388–398, 2014.

[16] F. Oloo, L. Olang, and J. Strobl, "Spatial modelling of solar energy potential in Kenya," *International Journal of Sustainable Energy and Management*, vol. 6, pp. 17–30, 2016.

[17] M. R. Yaïche and S. M. A. Bekkouche, "Estimation du rayonnement solaire global en Algérie pour différents types de ciel," *Revue des Energies Renouvelables*, vol. 13, pp. 683–695, 2010.

[18] M. Koussa, M. Haddadi, and A. MALEK, "Reconstitution des irradiations globale et diffuse en fonction de quelques paramètres météorologiques pour un ciel quelconque," *Revue des Energies Renouvelables*, vol. 10, pp. 75–92, 2007.

[19] T. E. Boukelia, M. S. Mecibah, and I. E. Meriche, "General models for estimation of the monthly mean daily diffuse solar radiation (case study: Algeria)," *Energy Conversion and Management*, vol. 81, pp. 211–219, 2014.

[20] J. C. Lam and D. H. W. Li, "correlation between global solar radiation and its direct and diffuse components," *Building and Environment*, vol. 31, no. 6, pp. 527–535, 1996.

[21] B. Jamil and A. T. Siddiqui, "Generalized models for estimation of diffuse solar radiation based on clearness index and sunshine duration in India: applicability under different climatic zones," *Journal of Atmospheric and Solar-Terrestrial Physics*, vol. 157-158, pp. 16–34, 2017.

[22] F. Cao, H. Li, T. Yang, Y. Li, T. Zhu, and L. Zhao, "Evaluation of diffuse solar radiation models in Northern China: new model establishment and radiation sources comparison," *Renewable Energy*, vol. 103, pp. 708–720, 2017.

[23] H. D. Kambezidis, B. E. Psiloglou, D. Karagiannis, U. C. Dumka, and D. G. Kaskaoutis, "Recent improvements of the meteorological radiation model for solar irradiance estimates under all-sky conditions," *Renewable Energy*, vol. 93, pp. 142–158, 2016.

[24] C. Renno, F. Petito, and A. Gatto, "ANN model for predicting the direct normal irradiance and the global radiation for a solar application to a residential building," *Journal of Cleaner Production*, vol. 135, pp. 1298–1316, 2016.

[25] L. Wang, Y. Lu, L. Zou et al., "Prediction of diffuse solar radiation based on multiple variables in China," *Renewable and Sustainable Energy Reviews*, vol. 103, pp. 151–216, 2019.

[26] A. A. El-Sebaii, F. S. Al-Hazmi, A. A. Al-Ghamdi, and S. J. Yaghmour, "Global, direct and diffuse solar radiation on horizontal and tilted surfaces in Jeddah, Saudi Arabia," *Applied Energy*, vol. 87, no. 2, pp. 568–576, 2010.

[27] A. Ibrahim, A. A. El-sebaii, M. R. I. Ramadan, and S. M. El-broullesy, "Estimation of solar irradiance on inclined surfaces facing south in Tanta, Egypt," *International Journal of Renewable Energy Research*, vol. 1, pp. 18–25, 2011.

[28] L. Feng, W. Qin, L. Wang, A. Lin, and M. Zhang, "Comparison of artificial intelligence and physical models for forecasting photosynthetically active radiation," *Remote Sensing*, vol. 10, no. 11, p. 1855, 2018.

[29] L. Wang, O. Kisi, M. Zounemat-Kermani, B. Hu, and W. Gong, "Modeling and comparison of hourly Photosynthetically Active Radiation in different ecosystems," *Renewable and Sustainable Energy Reviews*, vol. 56, pp. 436–453, 2016.

[30] Z. IHSANE, *Contribution à l'étude du gisement solaire Marocain: Irradiations journalières et horaires, globale, diffuse, et direct, d'un plan horizontal*, Thèse de 3ème cycle. Faculté des sciences de Rabat, 1989.

[31] M. N. Bargach, *Contribution à l'étude du gisement solaire marocain. Application à un générateur photovoltaïque*, Thèse de 3ème cycle, Faculté des sciences de Rabat, 1983.

[32] F. Lemmini, *Etude du rayonnement Global à Beni-Mellal. Rapport interne*, Laboratoire d'énergie solaire Rabat, 1983.

[33] H. Nfaoui, "*Trois années de mesures d'ensoleillement à Rabat. Etude statistique et présentations des données*," Thèse de 3ème cycle. Faculté des Sciences de Rabat, 1986.

[34] M. L. Ben Kaddour, *Etude du gisement solaire au Maroc en vue de son exploitation dans l'habitat*, Travail de fin d'etudes,Ecole Nationale des travaux publics de l'Etat, vaulx-en-velin, France, 1981.

[35] B. Pillot, M. Museli, P. Poggi, and J. B. Dias, "Satellite-based assessment and in situ validation of solar irradiation maps in the Republic of Djibouti," *Solar Energy*, vol. 120, pp. 603–619, 2015.

[36] P. Blanc, *Atlas du potentiel solaire photovoltaïque et thermodynamique en région Paca*, Centre Energétique et Procédés MINES Paris Tech/ARMINES, 2011.

[37] R. M. Yaich and A. Bouhanik, *Atlas Solaire Algérien*, Centre de développement de l'énergie renouvelable, Algérie, 2002.

[38] A. Mefti, M. Y. Bouroubi, and A. Khellaf, "Analyse critique du modèle de l'atlas solaire de l'Algérie," *Revue des Energies Renouvelable*, vol. 2, pp. 69–85, 1999.

[39] J. Almorox, M. Benito, and C. Hontoria, "Estimation of monthly Angström–Prescott equation coefficients from measured daily data in Toledo, Spain," *Renewable Energy*, vol. 30, no. 6, pp. 931–936, 2005.

[40] J. Bahraoui-Buret, M. N. Bargach, and M. L. Benkadour, *Le gisement solaire marocain. Editions SMER*, 1983.

[41] The Eppley Laboratory INC, 12 Sheffield Avenue Newport, RI 02840-1618 USAhttp://www.EppleyLab.com.

[42] B. Ihya, A. Mechaqrane, R. Tadili, and M. N. Bargach, "Prediction of hourly and daily diffuse solar fraction in the city of Fez (Morocco)," *Theoretical and Applied Climatology*, vol. 120, no. 3-4, pp. 737–749, 2015.

[43] M. T. Joutey, *Etude et validité des méthodes d'extrapolation de rayonnement solaire globale. Mémoire de master en physique énergie et technologie des matériaux*, Faculté des sciences de Rabat, 2010.

[44] L. BAHMAD, *Caractérisation de l'état de l'atmosphère à Rabat : transmission, extinction, trouble atmosphérique*, Thèse de 3ème cycle, Faculté des Sciences de Rabat, 1986.

[45] M. Iqbal, *An introduction to Solar Radiation*, Academic press, Canada, 1983.

[46] A. Khtira, *Etude théorique et expérimentale du rayonnement direct à Rabat, Contribution à l'utilisation des images satellite METEOSAT pour la détermination du gisement solaire*, Thèse de 3ème cycle. Faculté des sciences de Rabat, 1984.

[47] C. H. Perrin de Brichambaut and C. H. Vauge, *Le gisement solaire : évaluation de la ressource énergétique. Technique et Documentation*, Lavoisier, 1982.

[48] V. Badescu, *Modeling Solar Radiation at the Earth's Surface*, Springer-Verlag, Berlin Heidelberg, 2008.

[49] B. Ihya, A. Mechaqrane, R. Tadili, and M. N. Bargach, "Optimal tilt angles for solar collectors facing south at Fez city (Morocco)," *Journal of Natural Sciences Research*, vol. 4, no. 10, pp. 120–127, 2014.

[50] S. Lahjomri, *Etude des rayonnements ultraviolets et infrarouges à Rabat*, Mémoire de DESA, Faculté des sciences de Rabat, 2001.

[51] M. Hamatti, R. Tadili, M. N. Bargach, A. Mechaqrane, and B. Ihya, "Evaluation des composantes spectrales du rayonnement solaire à rabat (MAROC)," *Revue Internationale D'Héliotechnique*, vol. 44, pp. 1–6, 2012.

[52] J. F. Escobedo, E. N. Gomes, A. P. Oliveira, and J. Soares, "Modeling hourly and daily fractions of UV, PAR and NIR to global solar radiation under various sky conditions at Botucatu, Brazil," *Applied Energy*, vol. 86, no. 3, pp. 299–309, 2009.

Hindawi
International Journal of Photoenergy
Volume 2019, Article ID 1263480, 8 pages
https://doi.org/10.1155/2019/1263480

Research Article

Line-End Voltage and Voltage Profile along Power Distribution Line with Large-Power Photovoltaic Generation System

Toshiro Matsumura,[1] **Masumi Tsukamoto**,[1] **Akihiro Tsusaka**,[1] **Kazuto Yukita**,[1] **Yasuyuki Goto**,[1] **Yasunobu Yokomizu**,[2] **Kento Tatewaki**,[2] **Daisuke Iioka**,[3] **Hirotaka Shimizu**,[4] **Yuuki Kanazawa**,[5] **Hiroyuki Ishikawa**,[5] **Akimori Matsuo**,[5] **and Hideki Iwatsuki**[5]

[1]*Department of Electrical Engineering, Aichi Institute of Technology, Japan*
[2]*Nagoya University, Japan*
[3]*Tohoku University, Japan*
[4]*Polytechnic University, Japan*
[5]*Chubu Electric Power Co. Inc., Japan*

Correspondence should be addressed to Toshiro Matsumura; matukaze@aitech.ac.jp

Received 6 December 2018; Accepted 6 February 2019; Published 24 March 2019

Guest Editor: Marialaura Di Somma

In recent years, the introduction of the photovoltaic generation system (PV system) has been increasing by promoting the use of renewable energy. It has been feared that the reverse current from the PV system may cause an unacceptable level of voltage rise at the interconnection node in the power distribution system. This paper discusses the effects of the reverse current on the voltage rise and fall characteristics of the interconnection node and the voltage profiles along the power distribution line. When the line current on the circuit is small, the voltage on the line monotonically increases from the sending end to the receiving end. When a relatively large current flows, it causes a voltage reduction near the distribution substation. Furthermore, on the basis of the voltage aspects in the power distribution system with a large PV system, the allowable limits of the line current and the output power from PV system are investigated.

1. Introduction

In recent years, photovoltaic power generation systems (PV systems) have been encouraged and its introduction into the electric power distribution systems is being advanced as a matter of national policy in Japan. Numerous studies on the influence of interconnecting large PV systems on the power quality of the electrical power system have been performed [1–5]. It has been feared that a rise in voltage may be caused by the reverse current from the PV system in the power distribution system [6].

In general, the voltage rise due to the PV system in a distribution system is expressed by the magnitude of a reverse power flow. Several investigations have been conducted on the method of voltage regulation in a distribution system with a PV system. There has been growing recognition that the reactive power control of a PV system is useful in compensating for the voltage fluctuation which results from solar irradiance conditions [7]. The power factor control for distributed generation in a distribution network has been proposed to mitigate the voltage rise due to the active power output from the distributed generation [8]. It was suggested that the magnitude of reactive power injection from a PV system connected to a low-voltage grid was determined by the voltage sensitivity matrix [9]. A static var compensator (SVC) installed in a low-voltage distribution network has been proposed for suppressing the voltage rise due to the reverse power flow from the PV system [10]. A voltage regulator with a tap changer is also useful as a countermeasure against the voltage rise in the distribution

system. It was proposed that multiple line drop compensations controlled the tap position of a load tap changer in the distribution substation for the purpose of voltage regulation [11]. An online control strategy for the tap position has been proposed by using the measurement data of voltage, power, and tap position and the state estimation for the purpose of minimizing the number of tap operations [12].

On the contrary, the voltage reduction in a distribution feeder due to the reverse power flow from large-scale PV systems has been reported [13, 14]. As mentioned above, it is well accepted that the reverse power flow from a PV system causes the voltage rise in a distribution system. In [13, 14], the authors indicated that the voltage in a distribution feeder decreased with the increase in the reverse power flow from the PV system in cases where the reverse power flow is drastically larger than the supply power to the load in the distribution system. We showed from basic circuit theory that the large reverse current from a PV system might cause a reduction in the voltage of the interconnection node in the case of a long distribution line [15]. We also qualitatively and quantitatively indicated the effects of the distribution line length on the voltage rise and fall characteristics at the interconnection node [15].

This paper discusses the effects of a reverse current on the voltage rise and fall characteristics at the interconnection node and the voltage profiles along a power distribution line. Furthermore, the allowable limits of the line current and the output power are investigated on the basis of the voltage behavior in the power distribution system.

2. Distribution System Model

Figure 1 shows a single-phase equivalent circuit of a power distribution system with a large PV system at the receiving end. It is supposed that the distribution substation (sending end) voltage is $V_s = 6.6\,\text{kV}$, the line impedance per unit length is $r + jx$, and the reverse line current is $\boldsymbol{I}$. The total line impedance is $(r + jx)D$ for the whole line length of D.

In Japan, after the introduction of the Feed-in Tariff (FIT) scheme in 2012, large capacities of photovoltaic generators (PV) have been constructed in rural areas. These rural areas are relatively far from load centers where substations are located, and so, large capacities of PV are connected near the end of 6.6 kV distribution feeders. Therefore, no load is assumed in order to fundamentally investigate the influence of only the PV system.

3. Vector Diagram of Voltage

3.1. Vector Locus of Receiving-End Voltage. In this section, our previous paper [15] is briefly reviewed. Figure 2 illustrates the vector diagram among the receiving-end voltage V_r, sending-end voltage V_s, and the inverse current I from the PV system. Here, the power factor is 1 and the whole length of the line is D. The locus of the voltage vector V_r with an increase in I is indicated by a bold solid line. A circle centered on point "o" and having the sending-end voltage V_s as its radius is drawn by a dashed line.

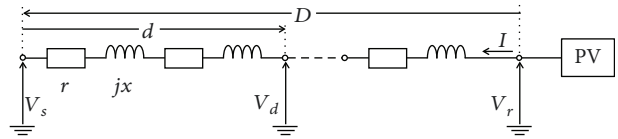

Figure 1: Single-phase equivalent circuit of a power distribution system.

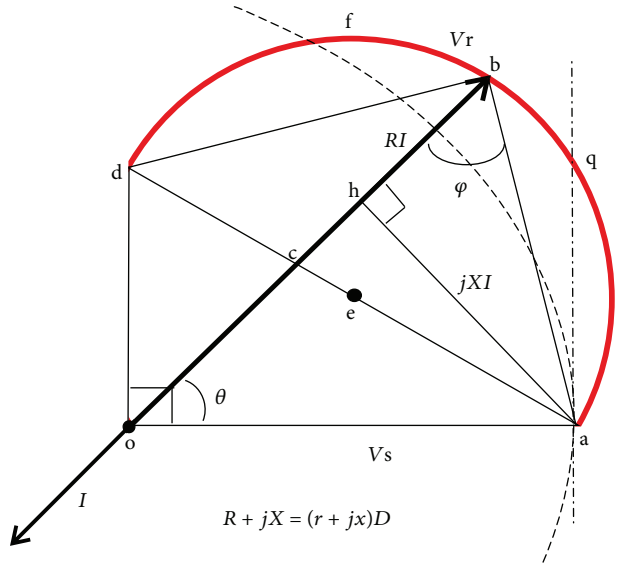

Figure 2: The locus of the receiving-end voltage vector.

The ratio of rDI and xDI is always constant. As the current increases, triangle "abh" consisting of $RI(=rDI)$ and $XI(=xDI)$ becomes similarly large. Triangle "abh" represents the magnitude of the voltage rise at the receiving end due to the line impedance and the reverse current I.

In this case, although the current I is in phase with the voltage V_r, the phase of the current I as well as the voltage V_r is advanced compared to the voltage V_s by the angle of θ. As the current increases, the phase angle θ increases and finally becomes $\theta = \pi/2$.

Angle "dba" is always a right angle regardless of the magnitude of the inverse current I. Therefore, the locus of the receiving-end voltage V_r is drawn with a circular arc whose diameter is shown by line "ad."

The tangent line at point "a" to the circle drawn with a dashed line is shown by a one-dot chain line. Point "q" is the intersection point between the bold solid line and the one-dot chain line. The maximum receiving-end voltage V_{r-max} is given by line "oq."

3.2. Expression of the Receiving-End Voltage. From Figure 2, the magnitude of the receiving-end voltage is expressed by the following expression:

$$V_r(I) = rDI + \sqrt{V_s^2 - (xDI)^2}. \quad (1)$$

Using $V_s^2 - (xDI)^2 \geq 0$ due to voltage stability, the allowable range of the current I is deduced as

$$0 \leq I \leq \frac{V_s}{xD}. \quad (2)$$

The allowable limit of the current I is also represented as

$$I_{\max} = \frac{V_s}{xD}. \quad (3)$$

The magnitude of the maximum receiving-end voltage becomes

$$V_{\text{r-max}} = \frac{V_s}{\sin(\varphi)}, \quad (4)$$

where $\tan \varphi = x/r$.

When $V_r = V_s$, the current I is given by the following expression:

$$I = \frac{2rV_s}{z^2 D}, \quad \text{at } V_r = V_s, \quad (5)$$

where $z = \sqrt{r^2 + x^2}$.

From the abovementioned expressions, the following facts are found out:

(1) With an increase in the sending-end voltage V_s, both $I_{\max}$ and $V_{\text{r-max}}$ become large

(2) Thus, even if the receiving-end voltage V_r becomes higher than the allowable voltage range, V_r could fall within the allowable range by decreasing V_s. However, the decrease in V_s might cause the opposite effect to reduce the allowable limit of the current I

(3) $V_{\text{r-max}}$ is independent of D and I but depends only on the line impedance. When the magnitude of the resistance component of the line impedance becomes relatively smaller than that of the reactance component, $V_{\text{r-max}}$ is suppressed to be low

(4) The allowable limit of the current I, $I_{\max}$, is in inverse proportion to the product of D and x, that is, the whole reactance component of the line. $I_{\max}$ is independent of the resistance component

(5) When the whole length or the reactance component of the distribution line becomes larger, the allowable limit of the current I becomes smaller

(6) Thus, the voltage instability is likely to be caused by an increase in D

3.3. A Case Study on the Receiving-End Voltage as a Function of Line Current. As a case study, the dependence of the receiving-end voltage V_r on the line current is calculated for the line impedance of $0.3 + j0.4\,\Omega$/km and a whole line length of 25 km. Figure 3 shows the receiving-end voltage V_r as a function of the line current $I_L = I/\sqrt{3}$. In this figure,

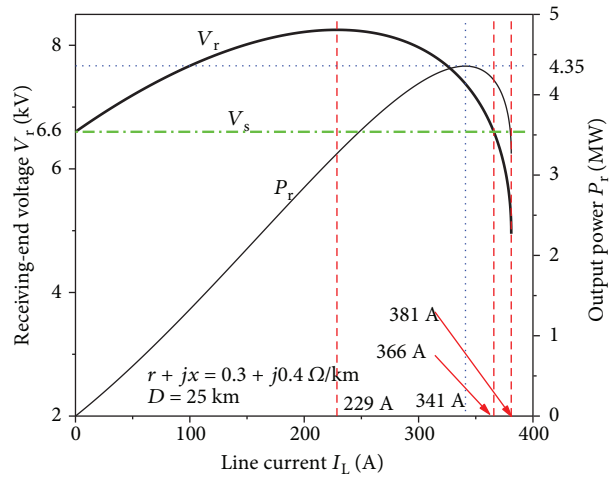

FIGURE 3: Receiving-end voltage as a function of the line current in the case of $r + jx = 0.3 + j0.4\,\Omega$/km and $D = 25$ km.

sending-end voltage $V_s = 6.6$ kV and output power of the PV system, $P_r = V_r I = \sqrt{3} V_r I_L$, are also drawn with a one-dot chain straight line and with a thin solid line, respectively.

In this case, the receiving-end voltage V_r is increased with an increase in the line current until $I_L = 229$ A. After the receiving-end voltage V_r indicates a maximum magnitude at $I_L = 229$ A, the voltage V_r begins to be reduced with an increase of I_L. At $I_L = 366$ A, the magnitude of the voltage V_r becomes the same as that of the sending-end voltage V_s. When the line current increases to more than 366 A, the receiving-end voltage becomes less than the sending-end voltage. The allowable maximum line current is 381 A.

Concerning the output power of the PV system, P_r increases with an increase in the line current until the line current reaches 341 A, where P_r is at its maximum. In the range of $I_L = 229$ A to 341 A, although the receiving-end voltage V_r decreases with an increase in the line current I_L, P_r continues to increase with an increase in the line current I_L because of the small decreasing rate of V_r. When the PV system is controlled to keep the output current constant, the output current from the PV system can be enlarged to larger than 341 A, while the output power must be reduced.

4. Voltage Profile along the Line

4.1. Vector Diagram. Figures 4–8 illustrate the vector diagram of the voltage vector V_d on the line away from the sending end by a distance d.

In Figure 4, triangle "agk" indicates the magnitude of the voltage rise of V_d due to the line impedance. The vector end point of V_d moves on line "ab" with an increase in the distance d because the line impedance is directly proportional to d.

Figure 5 shows the vector diagram where the receiving-end voltage becomes maximum. Line "ab" exists outside of the circle of the one-dot chain line. Therefore, the voltage V_d is always larger than the sending-end voltage, and V_d rises with an increase in d.

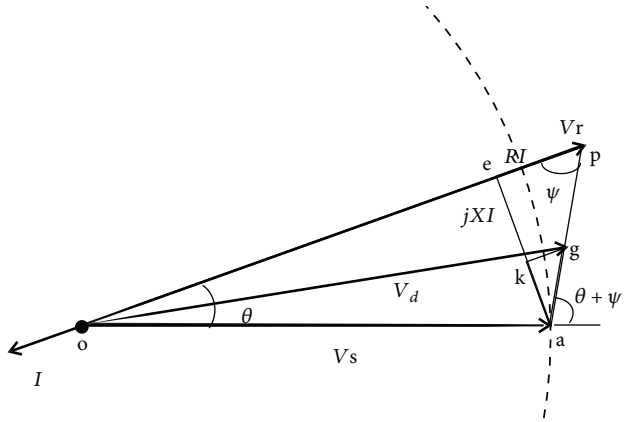

Figure 4: Vector diagram of voltage in the case of a relatively small line current.

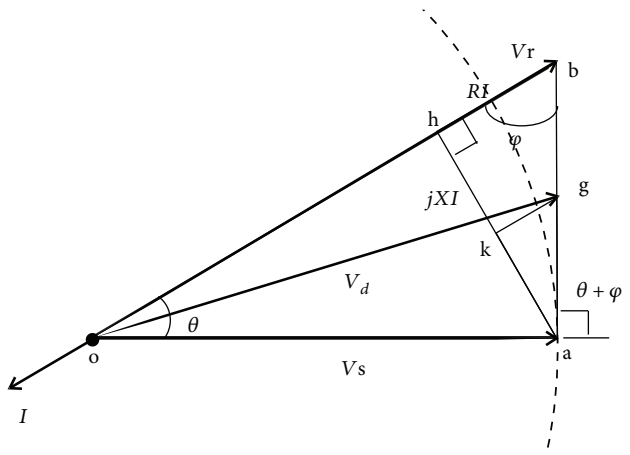

Figure 5: Vector diagram of voltage in the case of the maximum receiving-end voltage.

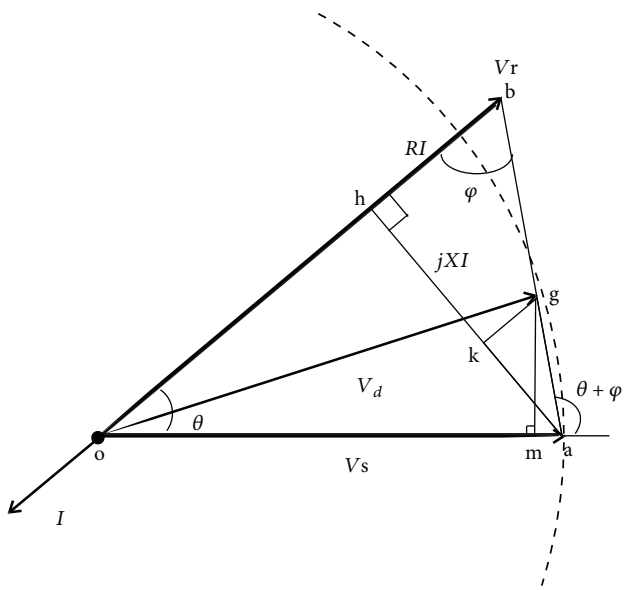

Figure 6: Vector diagram of voltage in the case of a relatively large line current.

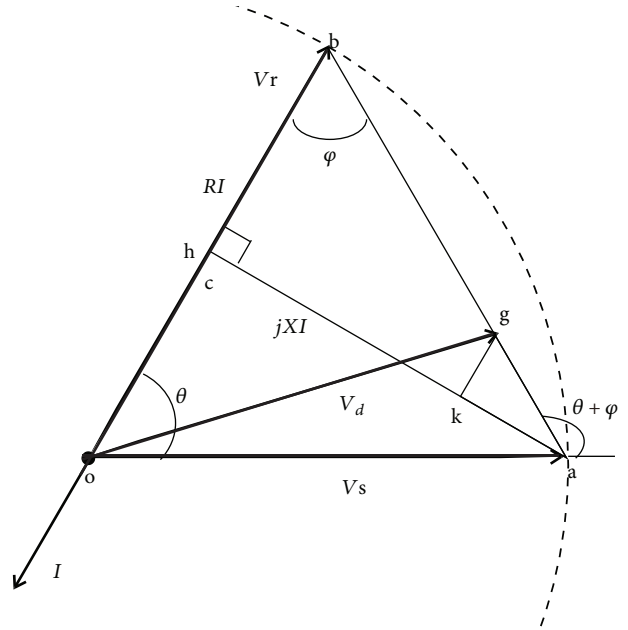

Figure 7: Vector diagram of voltage in the case of $V_r = V_s$.

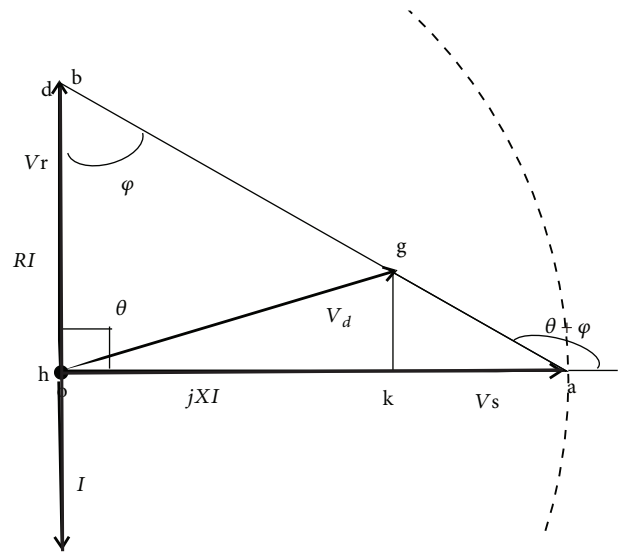

Figure 8: Vector diagram of voltage in the case of the allowable limit of line current.

In the case of Figure 6, line "ab" exists partially in the inner side and the outer side of the one-dot chain line circle. Therefore, the voltage V_d is smaller than V_s near the sending end, whereas V_d is larger than V_s near the receiving end.

On the other hand, Figures 7 and 8 indicate the vector diagram at $V_r = V_s$ and at the allowable limit of the line current, respectively. In these figures, line "ab" is in the inner side of the one-dot chain line circle. Therefore, the voltage V_d is always smaller than the sending-end voltage V_s.

4.2. Expressions of Voltage Profile along the Line. From Figure 6, the voltage V_d at the node far away from the sending end by d is given as follows:

$$V_d = \sqrt{\overline{\mathrm{gm}}^2 + \overline{\mathrm{mo}}^2} = \sqrt{[(zd)I\sin(\lambda)]^2 + [V_s + (zd)I\cos(\lambda)]^2}, \quad (6)$$

where $\lambda = \theta + \varphi$,

$$\sin\theta = \frac{(xD)I}{V_s}. \quad (7)$$

4.3. Dependence of Voltage Profile on Line Current. As a case study, the voltage profile along the power distribution line described in Section 3.2 ($r + jx = 0.3 + j0.4\,\Omega$/km) was estimated as a function of the line current. Figure 9 shows the voltage profiles derived for the line current of 112 A, 229 A, 319 A, 341 A, 366 A, and 381 A. Consequently, the following results were found:

(1) When the line current I_L is 112 A, the voltage V_d increases almost proportionally to d

(2) When I_L becomes 229 A, where the sending-end voltage V_r is at its maximum, the profile of the voltage V_d shows a downward convex waveform. However, the voltage V_d is always higher than the sending-end voltage until the line current is 229 A

(3) When I_L becomes more than 229 A, the voltage V_d strongly shows a similar tendency as stated above so that V_d begins to be lower than 6.6 kV just near the sending end

(4) When I_L is 319 A or 341 A, the profile of the voltage V_d consists of the lower zone near the sending end and higher zone near the receiving end

(5) When I_L reaches 366 A, the voltage at the receiving end coincides with the voltage at the sending end. The voltage V_d is always smaller than the sending-end voltage

(6) When the line current reaches 381 A, which is the allowable limit of the line current, the receiving-end voltage V_r and the voltage V_d are always smaller than the sending-end voltage

(7) In the case of $r + jx = 0.3 + j0.4\,\Omega$/km and $D = 25$ km, the line current at more than 381 A cannot flow safely due to equation (2).

4.4. Dependence of Voltage Profile on Line Length D. In this section, the dependences of the voltage distribution along the line on the whole line length D are discussed for two distribution lines, whose impedances are $0.3 + j0.4$ and $0.15 + j0.4\,\Omega$/km. The latter impedance is one with a wire thicker than that of the former one. In Figure 10, the voltage profiles along the line are illustrated as a parameter of the whole line length D for the line current of 262 A, which corresponds to the output power of 3,000 kW based on the rating voltage of 6.6 kV.

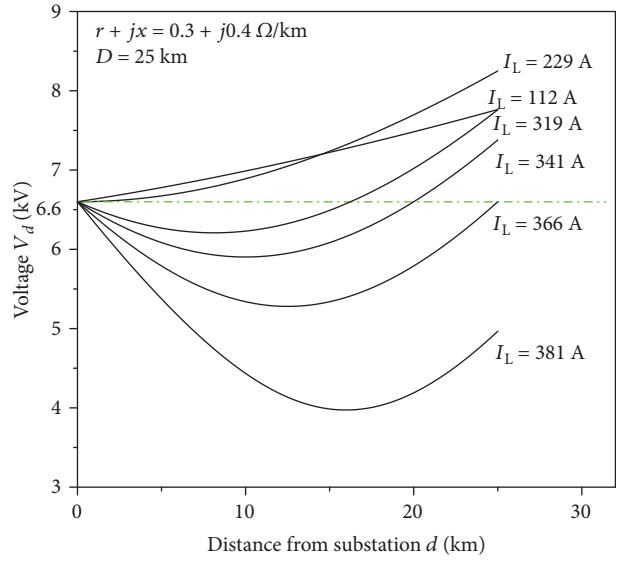

Figure 9: Voltage profiles as a parameter of the line current for the whole line length $D = 25$ km (line impedance of $0.3 + j0.4\,\Omega$/km).

The following results can be pointed out:

(1) In the case of $D = 5$ km, the voltage V_d increases almost proportionally to d

(2) In the case of $D = 10$ km, the profile of the voltage V_d shows a downward convex waveform

(3) When the whole line length D is shorter than 21.8 km for $r + jx = 0.3 + j0.4\,\Omega$/km or 12.8 km for $0.15 + j0.4\,\Omega$/km, where the receiving-end voltage V_r becomes maximum, the voltage V_d is always higher than the sending-end voltage

(4) When D is longer than 21.8 km or 12.8 km, the profile of the voltage V_d consists of the lower zone near the sending end and the higher zone near the receiving end compared with the sending-end voltage

(5) When D reaches 34.5 km or 23.9 km, the voltage at the receiving end coincides with the voltage at the sending end. The voltage V_d is always smaller than the sending-end voltage

(6) When D is larger than 34.5 km or 23.9 km, the receiving-end voltage V_r and the voltage V_d are always smaller than the sending-end voltage

(7) In both cases of $r + jx = 0.3 + j0.4\,\Omega$/km and $0.15 + j0.4\,\Omega$/km, the line current of 262 A cannot flow safely through the power distribution system of which the whole line length D is more than 36.3 km due to equation (2)

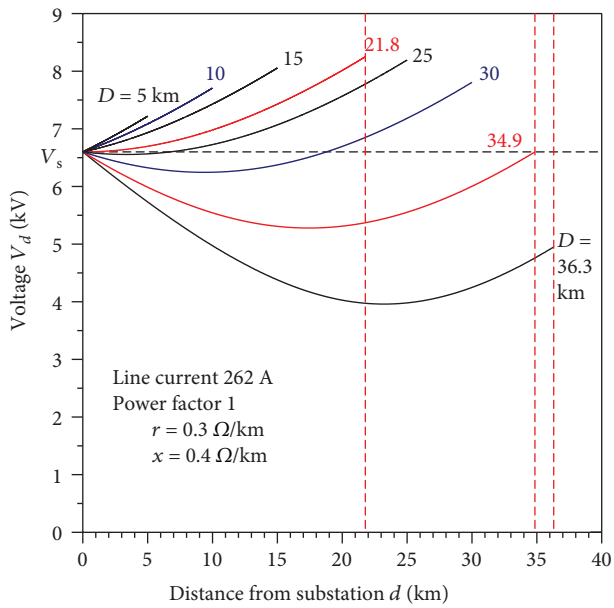

(a) Line impedance of $0.3 + j0.4\,\Omega$/km

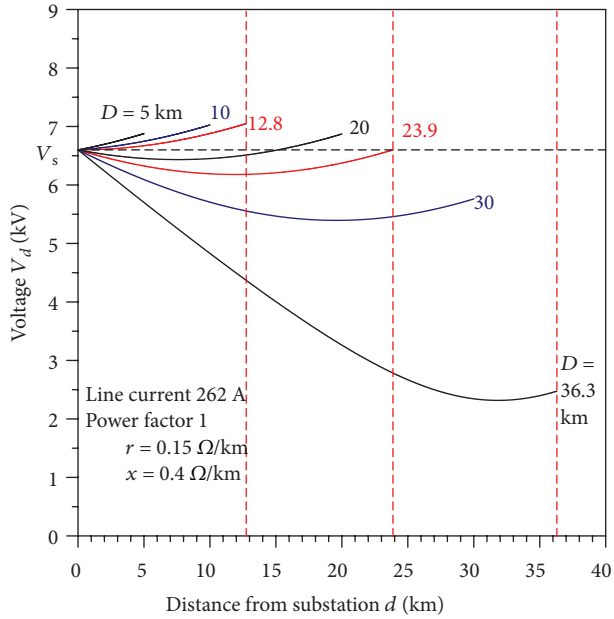

(b) Line impedance of $0.15 + j0.4\,\Omega$/km

FIGURE 10: Dependence of the voltage profile on the whole line length D at a line current of 262 A.

5. Effect of Output Power from PV System

5.1. Voltage Power Characteristics and Allowable Limit of Output Power from the PV System. Figures 2 and 4 give the following expressions:

$$\begin{aligned} (V_r - rDI)^2 + (xDI)^2 &= V_s^2, \\ V_r^2 - 2rDIV_r + (rDI)^2 + (xDI)^2 &= V_s^2. \end{aligned} \tag{8}$$

Using $P_r = V_r I$, equation (8) is reduced as follows:

$$\begin{aligned} V_r^2 - 2RP_r + \left(rD\frac{P_r}{V_r}\right)^2 + \left(xD\frac{P_r}{V_r}\right)^2 &= V_s^2, \\ V_r^4 - \left(2rDP_r + V_s^2\right)V_r^2 + (zD)^2P_r^2 &= 0. \end{aligned} \tag{9}$$

This equation has the following roots:

$$V_r^2 = \frac{\left(2rDP_r + V_s^2\right) + \sqrt{\left(2rDP_r + V_s^2\right)^2 - 4(zD)^2P_r^2}}{2}. \tag{10}$$

Thus, the voltage-power characteristics are represented by the following expression:

$$V_r = \sqrt{\frac{V_s^2 + 2rDP_r + \sqrt{V_s^4 + 4rDV_s^2P_r - 4(xD)^2P_r^2}}{2}}. \tag{11}$$

The real root must exist:

$$V_s^4 + 4rDV_s^2P_r - 4(xD)^2P_r^2 > 0. \tag{12}$$

Consequently, the allowable output power is expressed as follows:

$$0 < P_r < \frac{r + \sqrt{r^2 + x^2}}{2x^2D}V_s^2. \tag{13}$$

This equation suggests the following facts:

(1) The allowable limit of the output power from the PV system is proportional to the square of the sending-end voltage. Thus, the allowable limit can be enlarged by the rise of the sending-end voltage

(2) The allowable limit is inversely proportional to the whole line length D. Therefore, the long power distribution system cannot be allowed to introduce the larger-power PV system compared with the short-line power distribution system

(3) The resistance component of the line impedance becomes the smaller, and the allowable limit of the output power is reduced

5.2. Dependence of Receiving-End Voltage V_r on Output Power P_r from the PV System. The solid line in Figure 11 illustrates the dependence of the receiving-end voltage V_r on the output power P_r derived from equation (13) for the line impedance of $r + jx = 0.3 + j0.4\,\Omega$/km. In this figure, the corresponding line current I_L is also plotted as a function of the output power P_r. The solid lines in this figure show that the maximum magnitudes of P_r and I_L are 4.36 MW and 341 A for $0.3 + j0.4\,\Omega$/km, respectively. In the case of $0.3 + j0.4\,\Omega$/km, V_r is always higher than V_s.

As described in Section 3.3, if the PV system is strongly controlled to keep the line current constant, the line current could be enlarged to more than 341 A by reducing the output

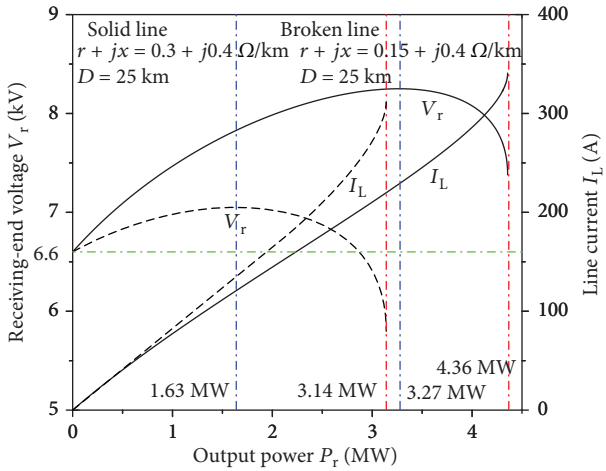

Figure 11: Dependence of the receiving-end voltage V_r on output power P_r for the whole line length $D = 25$ km (line impedances of $0.3 + j0.4\ \Omega$/km and $0.15 + j0.4\ \Omega$/km).

power. However, when the PV system is controlled to keep the output power constant, P_r and I_L are limited to the abovementioned magnitudes.

The dashed lines in Figure 11 shows the ones for $0.15 + j0.4\ \Omega$/km, which is the impedance for the thicker wire compared to the abovementioned wire of $0.3 + j0.4$ W/km. In the case of this line impedance, the maximum magnitudes of P_r and I_L are 3.14 W and 312 A, respectively. These magnitudes are smaller than the ones for $0.3 + j0.4\ \Omega$/km.

It is pointed out that the use of the thicker wire brings about the reduction of the voltage rise, but concurrently the allowable limit of the output power of the PV system must be decreased.

5.3. Dependence of Voltage Profile V_d on Output Power from the PV System P_r. Figures 12(a) and 12(b) show the voltage profiles as a parameter of the output power P_r, the former for $r + jx = 0.3 + j0.4\ \Omega$/km and the latter for $r + jx = 0.15 + j0.4\ \Omega$/km. In Figure 12(a), only four voltage profiles can be seen, which are the same as those of the upper four profiles in Figure 8, because of the allowable range of the output power.

In Figure 12(b), five profiles are drawn. In the case of $0.15 + j0.4\ \Omega$/km, when the output power from the PV system is larger than 2.86 MW, the receiving-end voltage V_r and the voltage V_d are always smaller than the sending-end voltage V_s. However, the allowable limit of the output power is 3.14 MW, which is smaller than that of $0.3 + j0.4\ \Omega$/km. It should be noted that if the thick wire is used as the power distribution line, too much reduction of the voltage might be caused by the large output power of the PV system.

6. Conclusion

The voltage rise and fall characteristics caused by the introduction of large PV systems into a long power distribution system is studied in this work by using vector diagrams of a single-phase equivalent circuit.

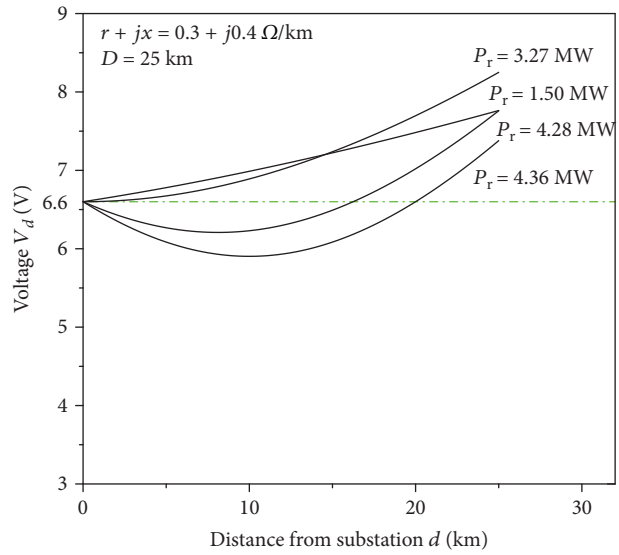

(a) Line impedance of $0.3 + j0.4\ \Omega$/km

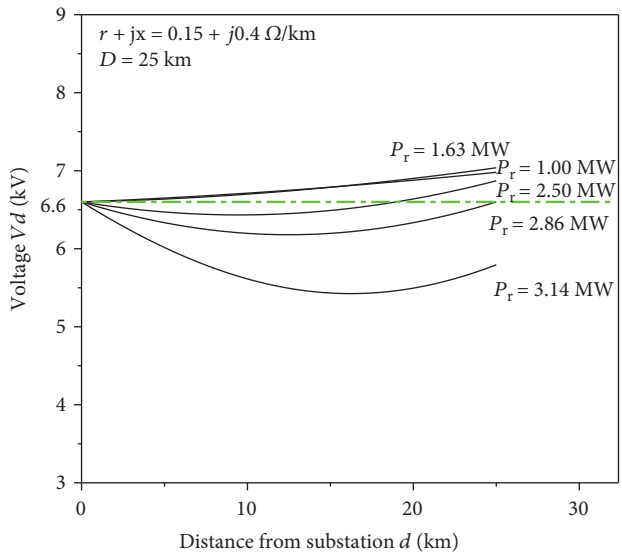

(b) Line impedance of $0.15 + j0.4\ \Omega$/km

Figure 12: Voltage profile V_d as a parameter of output power P_r for the whole line length $D = 25$ km.

When the line current on the circuit is small, the voltage on the line monotonically increases from the sending end to the receiving end. When a relatively large current flows, it causes a voltage reduction near the distribution substation even if no load exists.

The allowable limit of the output power from the PV system can be enlarged by the rise of the sending-end voltage. However, it heightens the receiving-end voltage and the voltage profile. It should be noted that the small resistance component of the line impedance prevents the rise of the voltage and also reduces the allowable limit of the output power.

Data Availability

The data used to support the findings of this study are included within the article.

Conflicts of Interest

The authors declare that there is no conflict of interest regarding the publication of this paper.

References

[1] T. Stetz, M. Kraiczy, and K. Diwold5, "High penetration of PV in local distribution grids," IEA PVPS Task14-2Report, 2014.

[2] dena: dena Ancillary Services Study 2030, "Security and reliability of a power supply with a high percentage of renewable energy. Final report," 2014.

[3] K. Ishikawa, H. Taniguchi, H. Suzuki, Y. Ota, and Y. Mizuno, "Fundamental voltage characteristics in power system with a large penetration of photovoltaic generation," *IEEJ Transactions on Power and Energy*, vol. 134, no. 1, pp. 2–8, 2014.

[4] K. Ishikawa, H. Taniguchi, H. Suzuki, Y. Ota, and Y. Mizuno, "Fundamental study on voltage stability in power system with large penetration of photovoltaic generation considering induction motor dynamics," *IEEJ Transactions on Power and Energy*, vol. 134, no. 7, pp. 568–578, 2014, (in Japanese).

[5] M. Imanaka, M. Machida, J. Baba, and D. Iioka, "Basic study on high penetration of photovoltaics with advanced voltage control and partial voltage boost in distribution networks—1. Analysis of hosting capacity," The Papers of Joint Technical Meeting, PE-16-064/PSE-16-084, IEE Japan, 2016.

[6] C. L. Masters, "Voltage rise: the big issue when connecting embedded generation to long 11 kV overhead lines," *Power Engineering Journal*, vol. 16, no. 1, pp. 5–12, 2002.

[7] K. Turitsyn, P. Sulc, S. Backhaus, and M. Chertkov, "Options for control of reactive power by distributed photovoltaic generators," *Proceedings of the IEEE*, vol. 99, no. 6, pp. 1063–1073, 2011.

[8] P. M. S. Carvalho, P. F. Correia, and L. A. F. Ferreira, "Distributed reactive power generation control for voltage rise mitigation in distribution networks," *IEEE Transactions on Power Systems*, vol. 23, no. 2, pp. 766–772, 2008.

[9] A. Samadi, R. Eriksson, L. Söder, B. G. Rawn, and J. C. Boemer, "Coordinated active power-dependent voltage regulation in distribution grids with PV systems," *IEEE Transactions on Power Delivery*, vol. 29, no. 3, pp. 1454–1464, 2014.

[10] D. Iioka, K. Sakakibara, Y. Yokomizu, T. Matsumura, and N. Izuhara, "Distribution voltage rise at dense photovoltaic generation area and its suppression by SVC," *Electrical Engineering in Japan*, vol. 166, no. 2, pp. 47–53, 2009.

[11] J.-H. Choi and J.-C. Kim, "Advanced voltage regulation method of power distribution systems interconnected with dispersed storage and generation systems," *IEEE Transactions on Power Delivery*, vol. 16, no. 2, pp. 329–334, 2001.

[12] D. Ranamuka, A. P. Agalgaonkar, and K. M. Muttaqi, "Online voltage control in distribution systems with multiple voltage regulating devices," *IEEE Transactions on Sustainable Energy*, vol. 5, no. 2, pp. 617–628, 2014.

[13] D. Iioka, K. Miura, M. Machida et al., "Hosting capacity of large scale PV power station in future distribution networks," in *2017 IEEE Innovative Smart Grid Technologies - Asia (ISGT-Asia)*, pp. 1–6, Auckland, New Zealand, 2017.

[14] S. Kikuchi, M. Machida, J. Tamura et al., "Hosting capacity analysis of many distributed photovoltaic systems in future distribution networks," in *2017 IEEE Innovative Smart Grid Technologies—Asia (ISGT-Asia)*, pp. 1–5, 2017.

[15] T. Matsumura, K. Yukita, Y. Goto et al., "A study on rising and reducing process of receiving-end voltage due to introduction of large PV systems into distribution power system," *IEEJ Transactions on Power and Energy*, vol. 138, no. 1, pp. 23–29, 2018, (in Japanese).